ISBN 978-82-326-1768-5 (printed version)
ISBN 978-82-326-1769-2 (electronic version)
ISSN 1503-8181

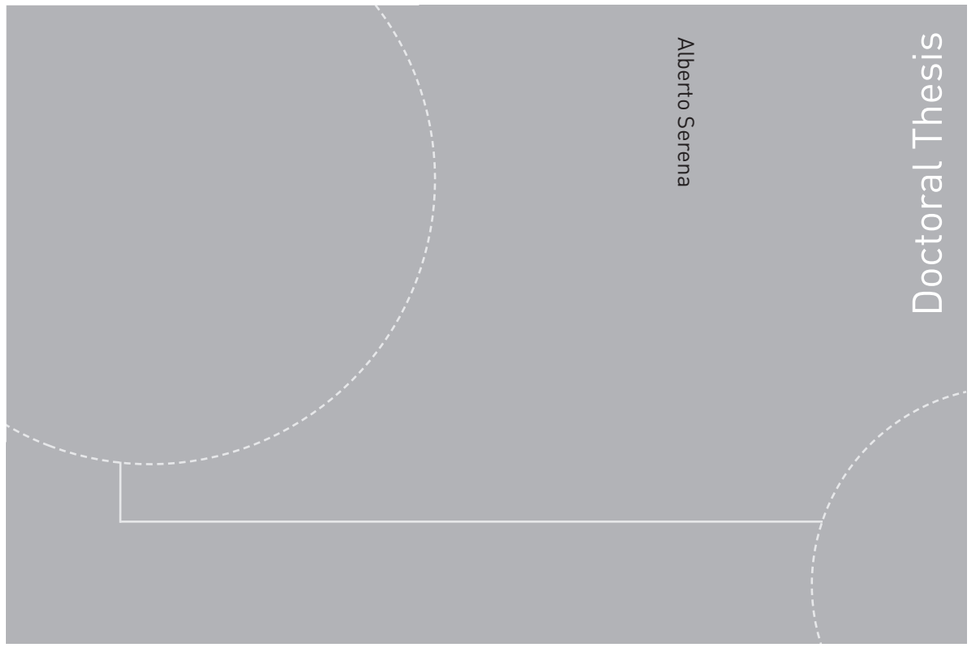

Doctoral theses at NTNU, 2016:215

Alberto Serena

A Multiphase Pump Experimental Analysis

NTNU
Norwegian University of
Science and Technology

NTNU
Norwegian University of
Science and Technology

NTNU
Norwegian University of
Science and Technology
Faculty of Engineering
Science and Technology
Department of Energy and Process Engineering

Doctoral theses at NTNU, 2016:215

NTNU

Alberto Serena

A Multiphase Pump Experimental Analysis

Thesis for the degree of Philosophiae Doctor

Trondheim, May 2016

Norwegian University of Science and Technology
Faculty of Engineering
Science and Technology
Department of Energy andProcess Engineering

NTNU
Norwegian University of
Science and Technology

NTNU
Norwegian University of Science and Technology

Thesis for the degree of Philosophiae Doctor

Faculty of Engineering
Science and Technology
Department of Energy andProcess Engineering

ISBN 978-82-326-1768-5 (printed version)
ISBN 978-82-326-1769-2 (electronic version)
ISSN 1503-8181

Doctoral theses at NTNU, 2016:215

Printed by Skipnes Kommunikasjon as

Contents

Acknowledgment

I would like to express my deep gratitude to all the people who have supported me.
This experience abroad has been the opportunity of meeting people from all over the world, discovering new cultures. I heartily thank those who have welcomed me, inspired, helping me to face with more and more enthusiasm the little and big challenges of this adventure.
I have been pleased to work in close cooperation with many experienced people too.
Special thanks to Prof. Lars E. Bakken for his guidance and suggestions, to Audun Grynning for believing in me, and to the colleagues at NTNU Håvard Rekstad for his encouragement and precious advices, Øyvind Hundseid, Erik Langørgen and Lars K. Sørensen and all the other administrative and laboratory personnel.
I thank the people in the Aker Solutions AS R&D Team for the funding and for contributing with support and interesting technical discussions, especially: Tarjei Larsen, Tarje Olderheim, Magnus Stridh, Christian Høy, Åge Hofstad, Sigmund Rasmussen and Per Rønning. In addition, Åsmund Lerstad from PTM AS for the pleasant collaboration and Andrew Bridges and Shane Kirksey from Photron USA Inc. I have been very pleased to work with the master students during their Project Assignements.

Abstract

This research project focuses on the characterization of the behaviour of a mixed-flow pump under off-design conditions and two-phase operation, in terms of performance degradation and instabilities. The recent multiphase pump models allow to process higher and higher amounts of gas in variable operating conditions. An improved understanding of the fundamental physics is therefore necessary, as, due to the concurrent physics involved and transient phenomena, a proper machine characterization cannot be limited to an overall description of the performance, but rather it needs to rely on advanced analysis tools revealing the local flow phenomena.

Multiphase flow affects turbomachines operation introducing secondary flows, unsteady phenomena and other disturbances in the flow field. Besides influencing the whole system and causing losses, these disturbances introduce additional issues as vibrations and alternating stresses on the rotodynamic components, which can reduce the machine reliability. The detection of the instabilities inception, a proper definition of the safe operation boundaries and the necessary actions to recover stable operation when instabilities appear are of key importance to prevent shut-down events and failures and ensure an extended components life.

The main goal of this investigation consists in the experimental description of the flow regimes in the different performance map zones, aided by flow-visualization; focus is given to the recognition of the flow mechanisms responsible for flow field modifications, which affect the machine stability, and to the relation of the performance and stability variations to the originating phenomena in the hydraulic channels.

In order to accomplish these objectives, a novel multiphase pump laboratory has been specifically designed and built. An extensive literature review of the two-phase flow in turbomachines has helped to include room for the necessary investigations and carefully assess their feasibility. The laboratory facility allows a complete optical access to the pump channels and fine adjustments in the inlet configuration and the tip clearance gap. Tests are performed over a wide range of machine, flow and fluid composition parameters.

As to the investigation tools employed, local measurements of the main flow parameters and a high-speed camera provide an interesting insight into the unsteady and transient flow phenomena. The numerical tool capability is evaluated under single-phase conditions, while a thorough study of the available two-phase flow simulation models and their experimental validation will be the subject of future studies.

The influence of the operating parameters - pump speed, flow rates, mixture composition, suction pressure - on the machine performance and operating range has been extensively studied and the test results confirm most of the expected trends.

The original contribution of the current work has been the understanding of the flow mechanisms and their connection to the outer measurements; this is very useful for a future development of a control strategy in real machines.

On a further stage of the research, it is desirable that the analytical description of the bubble flow and the correlations describing the switch among different flow regimes be validated experimentally for this specific application.

Two-phase flow, especially at unsteady conditions, introduces additional challenges which make the use of advanced visualization techniques require a preliminary assessment, which is the object of future studies. Along with image based metrology, these ones promise to provide a qualitative description of the flow field.

The Doctoral Thesis is based on five research papers which present the main outcomes of the study and are enclosed in the Appendix section. This report provides the necessary background, starting from the literature study which has led to the choice of the research approach, together with a presentation of the testing rig design and building, the experimental facility and procedure description, the test results and the characterization of the main flow mechanisms involved. It should be noted that, as the main focus is set on the flow visualization, the measurement of the pump efficiency has not been prioritized. A preliminary assessment of the numerical simulation tool is performed on single-phase operation. The Conclusion section presents a summary of the findings accomplished within the timeframe of the current work, along with the suggestion of further analyses and investigations for a deeper understanding of the flow phenomena and machine behaviour.

Nomenclature

Symbols

C_D	[-]	Drag Coefficient
c_s	[m/s]	Speed of Sound
d_b	[m]	Bubble Diameter
f	[Hz]	Frequency
$f_{\Delta p}$	[-]	Pressure Increase Multiplier
f_ψ	[-]	Isothermal Head Multiplier
$Eö$	[-]	Eötvös Number
Fr	[-]	Froude Number
g	[m/s^2]	Gravitational Acceleration
Mo	[-]	Morton Number
n	[rpm]	Rotational Speed
p_i	[bar(a)]	Suction Pressure
q^*	[%]	Fraction of Nominal Flowrate
q_g	[m^3/s]	Gas Volumetric Flowrate
q_l	[m^3/s]	Liquid Volumetric Flowrate
q_t	[m^3/s]	Total Volumetric Flowrate
R	[J/(kg K)]	Universal Gas Constant
Re	[-]	Reynolds Number
Ro	[-]	Rossby Number
S	[-]	Slip Ratio
u	[m/s]	Flow Tangential Velocity
u_g	[m/s]	Gas Velocity
u_l	[m/s]	Liquid Velocity
u_s	[m/s]	Phase Slip Velocity
u_{sg}	[m/s]	Superficial Gas Velocity
u_{sl}	[m/s]	Superficial Liquid Velocity
v	[m/s]	Absolute Flow Velocity
w	[m/s]	Flow Relative Velocity
We	[-]	Weber Number
x	[%]	Gas Mass Fraction
y^+	[-]	Dimensionless Wall Distance
$Y_{isot,SP}$	[J/kg]	Single-Phase Isothermal Specific Work
$Y_{isot,TP}$	[J/kg]	Two-Phase Isothermal Specific Work
α	[-]	Void Fraction
β	[rad]	Local Angle Streamline ∠ Circumferential Unit Vector
γ	[rad]	Local Angle Radial Unit Vector ∠ Stream Plane Inclination in the Axial Direction

δ	[rad]	Deviation Angle
δ	[-]	Liquid to Gas Phases Density Ratio
Δp_d	[bar]	Diffuser Pressure Recovery
Δp_i	[bar]	Impeller Pressure Increase
Δp_t	[bar]	Stage Pressure Increase
λ_{cr}	[µm]	Critical Wavelength
ρ_g	[kg/m^3]	Gas Density
ρ_l	[kg/m^3]	Liquid Density
ρ_m	[kg/m^3]	Mixture Density
σ	[N/m]	Surface Tension
φ	[-]	Flow Coefficient
ψ	[-]	Head Coefficient
ω	[rad/s]	Rotational Speed
ω_s	[-]	Dimensionless Specific Speed

Abbreviations

AVI		Audio Video Interleave
BEP		Best Efficiency Point
BPF	[Hz]	Blade Passing Frequency
CFD		Computational Fluid Dynamics
ESP		Electrical Submersible Pump
FFT		Fast Fourier Analysis
fps	[s^{-1}]	Frames per Second
GLR	[%]	Gas Liquid Ratio
GVF	[%]	Gas Volume Fraction
LDV		Laser Doppler Velocimetry
LE		Blade Leading Edge
LES		Large Eddy Simulation
NPSH	[m]	Net Positive Suction Head
PIV		Particle Image Velocimetry
PMMA		Poly(methyl methacrylate)
PS		Blade Pressure Side
SAS		Scale Adaptive Simulation
SS		Blade Suction Side
SST		Shear Stress Transport
TE		Blade Trailing Edge
TLV		Tip Leakage Vortex

Overview of the Presentations and Publications

The study performed to accomplish the scopes of this research project has resulted in the presentations and publications listed below.

Design of a Multiphase Pump Test Laboratory Allowing to Perform Flow Visualization and Instability Analysis
Proceedings of the ASME 2015 Power and Energy Conversion Conference, June 2015, San Diego, California
Paper no. PowerEnergy2015-49769
This research paper presents the general challenges of multiphase pumping, the research approach chosen by the authors and the consequent design of the test facility. The expected trends are outlined.

Experimental Characterization of the Flow Instabilities of a Mixed-Flow Multiphase Pump Operating Air and Water Through Local Visualization and Analysis of Dynamic Measurements
Proceedings of the ASME 2015 International Mechanical Engineering Congress & Exposition, November 2015, Houston, Texas
Paper no. IMECE2015-50396
In this research article a study of the flow unsteadiness which characterizes the surging condition under part-load operation is presented. The tools employed are high-speed imaging and the frequency analysis of the fast-response pressure measurements.

Investigation of the Blade Tip Clearance Effects on Performance and Stability of a Mixed-Flow Pump: High-Speed Camera Recordings of the Flow Structures, Local Measurements and Numerical Simulation
Proceedings of the ASME 2015 International Mechanical Engineering Congress & Exposition, November 2015, Houston, Texas
Paper no. IMECE2015-50398
The main focus of this technical paper is given on the effects the tip leakage flow causes on single-phase operation, both on performance and stability. The rotating stall phenomenon, detected through fast-response measurements and related to visual observations, is responsible of unsteady flow field modifications which might be the originating cause or enhance the irregular flow at surging and two-phase operation.

Experimental Study of the Influence of the Operating Parameters on the Performance and Capability of a Mixed-Flow Multiphase Pump
Proceedings of the ASME 2016 Turbomachinery Technical Conference and Exposition, June 2016, Seoul, South Korea
Paper no. GT2016-56576

This technical paper reviews similar researches that have considered the operating parameters effect on multiphase pumps, with regard to performance and stability. Tests are performed over a wide range of machine and flow parameters and the results are presented as performance maps and specific curves showing the effect of the individual setting. The main flow regimes corresponding to the different zones in the performance curves are presented.

Flow Visualization of Unsteady and Transient Phenomena in a Mixed-Flow Multiphase Pump
Proceedings of the ASME 2016 Turbomachinery Technical Conference and Exposition, June 2016, Seoul, South Korea
Paper no. GT2016-56581
This research paper covers the most demanding aspects of multiphase pumping, unsteady flow mechanisms and transient operation; the approach starts from the study of high-speed movie recordings; the mechanisms responsible for performance degradation, flow unsteadiness and the switch among different flow patterns, are identified.

MultiBooster Model at NTNU
Technical presentation at the Annual Technical Seminar of the Norwegian Association of Thermal Fluid Machines, March 2016, Trondheim

Experimental Study of the Unsteady Flow Mechanisms Causing Performance Degradation and Originating Machine Instabilities on a Multiphase Pump by Means of Flow Visualization
Technical presentation at the International Symposium of Rotating Machinery – International Symposium of Image-Based Metrology, April 2016, Honolulu, Hawaii

Chapter 1
Introduction

Pumping and processing fluids with different properties have revealed to be among the major challenges in the last decades.
Multiphase boosting of oil and gas plays a key role in enhancing production and marginal fields exploitation; especially in the range of 50 to 90% gas volume fraction (*GVF*) it covers an energy-intensive production segment. It promises to reliably and profitably handle unpredictable and untreated flows, making it possible to extend life of dying fields and give access to the exploitation of fields in harsh locations.
This technology reduces pollutants and CO_2 emissions, minimizes the environmental impact, avoids leakages of gas or crude oil. The energy before required for transportation or lost through flaring can now be saved. After Paris COP 21, the *Zero Routine Flaring by 2030 Initiative* has been endorsed by 45 oil companies, governments and others, representing potential CO_2 savings of 100 million tons a year.

Potential fields of applications in two-phase flow turbomachines, which take advantage of this research, comprise [1]:

- combined reinjection of sour gas and water produced by hydrocarbons processing
- wet gas compression
- vapour-liquid streams processed in the liquefied natural gas industry
- increasing energy recovery from existing process units through the development of small two-phase flow turbines to replace choke/let-down valves, improving also the cooling duty, and liquid recovery
- biochemical and pharmaceutical industries: processes requiring aeration of the process medium; examples: single cell protein production from raw materials, microbiological fermentation, biological waste water treatment
- paper industry: deinking of recycled paper through air injection in deinking cells into the pulp slurry
- processes in manufacturing of plastics and elastomers

However, limited research efforts have been invested, specifically in laying down the thermodynamic and flow fundamentals of rotodynamic multiphase pumps.

The design and modelling of a pump operating a multiphase flow is a very challenging task, due to the concurrent physics involved (phase separation, stratification, differential phase kinematics, turbulence, rotational effects, curvature, secondary flows, etc.) and transient phenomena, both linked to the intrinsic unsteadiness of a multiphase flow through a rotating machine (bubble formation, coalescence or breakdown, gas locking) and to variable inlet flow composition (e.g. slug flow). Furthermore, during real operation, these pumps have to cope with highly variable flow rates and fluid properties.k

The phenomenon of multiphase head degradation is not only due to the decreasing mixture density, but also to additional and complex loss mechanisms; the degree of head deterioration varies from mild performance reduction to operating problems as surging and gas locking.

1.1 Historical evolution

The needs of different industrial fields have stimulated the research on multiphase flow in turbomachines. The first studies, dating back to the 1960-1970s, focused on centrifugal pumps operating condensable water and vapour flow, mainly for the nuclear industry; over a very low threshold value of the gas content, the pump blocked due to air accumulation at the inlet. As a first improvement, inducers to homogenize the incoming flow were installed. However, only the processing of limited amounts of gas was allowed. The industry focus, therefore, turned to positive-displacement concept-based models, as the twin-screw and progressive cavity pumps.
The necessity of machines handling with increasingly large amounts of gas and variable operating conditions, along with higher and higher flow and power levels, and costs and reliability issues too, have made the rotodynamic concept be reconsidered for high amounts of gas too. This has required a specific hydraulic design, featuring very long blade channels with an extremely low blade aspect ratio, in order to prevent vertical secondary flows, and progressively varying blade angles, to avoid phase separation. In addition, in order to obtain considerable differential pressure levels, multistage pumps are needed. The number of stages can be over 20 for the Electrical Submersible Pump models. Considerations on the design flow and pressure ratio across each of the single stages have to be included in the design procedure, along with an accurate evaluation of the rotodynamic balancing of the whole assembly.

1.2 Overview of the existing concepts

The design of the helico-axial concept started in the late 1980s; the main goal was producing a multiphase pump capable of processing up to 95 % *GVF* under continuous operation, and it successfully proved to handle with 100 % gas fraction under specific tests. The hydraulic design featured axial impellers with 3 to 5 blades followed by vaned diffuser stages, which provided some pressure recovery and accommodated the flow to the following stage. The outer diameter is constant through the stages, while the inner one increases between the inlet and outlet, following also the gas compression. The blade aspect ratio is low and the blade angles reduced, approaching the very low values characteristic of inducers. Efficiency is affected by the large wetted areas, velocity slip and thermal non equilibrium, as described in [1].
Extensive tests under transient conditions [2] have proved the installation of a buffer tank ahead of the pump is desirable as it improves the equipment reliability when subject to varying conditions.

Electrical Submersible Pumps, extensively studied at the Tulsa and Texas A&M Universities [3-9], provide an alternative solution. In this case, many stages are stacked to build up a significant differential pressure. The single stage comprises a small diameter centrifugal pump with a vaned diffuser. Different design improvements, both for the impeller and the diffuser, have been

proposed, in order to improve the gas-handling capability. The most relevant one for the current research is the Split Vane impeller design [9], which introduces a recirculation path fostering phase interaction and possibly delaying the formation of a gas pocket in the channel.

A broad literature is available for these two specific models; the individual contributions on the different topics will be presented in the corresponding chapters.

1.3 Status

An extensive literature review has shown that previous experiences have focused on:

- Experimental research programs on two-phase flow through centrifugal pumps, performed on small-scale model pumps operating at low pressure and with an air-water mixture as the fluid; test reports on machines operated at realistic conditions lack flow visualization
- Semi-empirical models based on curve fitting of test data sets
- Analytical models solving one-dimensional equations for the two phases.

Empirical or semi-empirical models and libraries of performance data are available, but they are unfortunately valid only for particular pump and flow operating conditions and reveal large discrepancies in performance predictions as they are referred to different parameters. For the range between medium and high pressure boosting the fundamentals are even more lacking.

However, this research field takes advantage of previous researches at the University which have tried to gain an insight into the fundamental mechanisms of wet gas compression and pumps operating with high *GVF*; knowledge transfer from the nuclear industry is available too, although these studies focused on single-stage, high-diameter pumps.
Transfer of theoretical knowledge on flow patterns and phase transition is more fruitful from pipe two-phase flow, study area in which a much higher effort has been put in the last decades, but centrifugal and Coriolis forces have to be considered in addition to friction and gravity, even though this last component is not so relevant in these fast-rotating machines. A suitable way to take advantage of these methods and results is the definition of equivalent quantities taking into account these additional phenomena, as, for example, the inclusion of the centrifugal and Coriolis forces in the definition of the Froude number.

1.4 Challenges

Extensive analyses are needed to optimize and improve the design of these machines, through experimental data collection and processing, numerical tools and analytical prediction models.

The main challenges are related to the complexity of the two-phase flow through a rotating machine, presenting intrinsically unsteady mechanisms as turbulence, rotor-stator and gas-liquid interactions. These phenomena involve a broad range of temporal and spatial scales, which complicate the analytical and numerical analyses. Therefore, the approach chosen for this research starts from the visualization of the real flow phenomena in the hydraulic channel and of transient events, and their relation to the machine outer measurements.

Besides causing performance degradation and instabilities, multiphase flow, in addition, introduces further challenges due to the alternation of the compressible gas phase and liquid films on the measurement sensors. Some characteristic flow perturbations, as those occurring during rotating stall, are dampened by the air compressibility.

1.5 Objectives

The research consists in the study of a multiphase pump stage, provided by Aker Solutions AS, in a laboratory setup, testing its ability to handle multiphase flows with a broad range of gas-liquid compositions. In order to allow this, a specific test rig has to be designed and commissioned.

This research takes advantage of the joint efforts of industry and university, the former contributing with its experience and dynamism and the latter with its theoretical approach and connections with other international research centres.

The main objectives are:

- a detailed literature review of similar applications, in order to study the expected trends and evaluate which investigation tools and analyses can be conveniently included
- the design and construction of a test laboratory allowing to perform the proper analyses
- a complete mapping of the multiphase performance of a one-stage Multibooster® pump
- a deeper understanding of the flow mechanisms responsible for performance degradation and instabilities.

These findings promise to increase the knowledge of the fundamental flow phenomena and their relation to the pump design and the outer machine behaviour, and to assess the validity of the analysis tools used to recognise the inception of instabilities and improve the design.

Chapter 2
Two-Phase Flow in Pumps

In this chapter, after the presentation of the terminology and symbols adopted in the Thesis, a brief explanation on the modifications of the single-phase flow pumps theory by two-phase flow operation is given. A literature review of previous researches on the key aspects - flow visualization in the pump channels, performance tests outlining the influence of the operational parameters, modelling attempts and finally the machine behaviour at unsteady operating conditions – has been performed to decide the main research approach which promises to gain a further understanding on the flow phenomena causing performance deterioration and instabilities.

Depending on the layout and the balance between desired flow rate and energy transfer, a general pump classification comprises radial, mixed-flow and axial machines, with shrouded, semi-open or open impellers and vaned or volute diffusers.

Figure 1 presents the circumferential and meridional views of a representative multiphase pump open impeller.

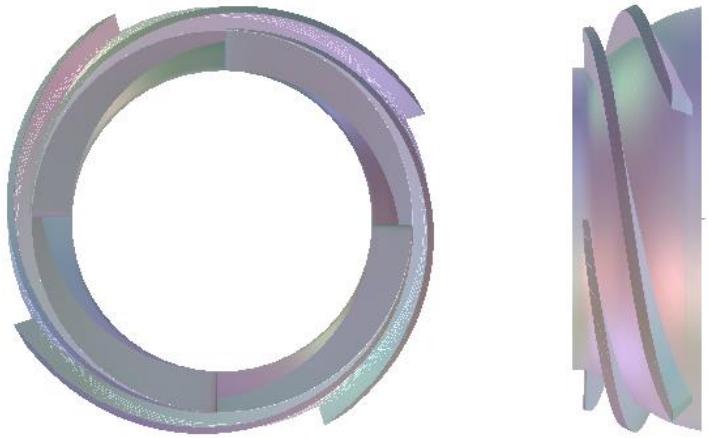

Fig. 1 – Circumferential and meridional views of a representative multiphase pump impeller

The hub and the shroud constitute the inner and outer hydraulic channel walls respectively, while the blade pressure side (PS) is the wall leading in the direction of rotation, followed by the blade suction side (SS); the leading (LE) and trailing (TE) edges refer to the front and rear ends of the blades, in the streamwise direction.
The Eulerian monodimensional theory lays its foundation on the hypothesis that the flow path follows an ideal streamline parallel to the blades, which is drawn at the design stage in order to accomplish the inlet and outlet angles necessary to give the desired work transfer.

The study is performed considering the flow velocities in the static and rotating reference systems, obtaining the absolute (v) and relative velocities (w), respectively. u are the tangential velocity components. Typical velocity triangles are shown in Fig. 2. $\beta_{2\infty}$ is the outlet flow angle according to the Eulerian theory.

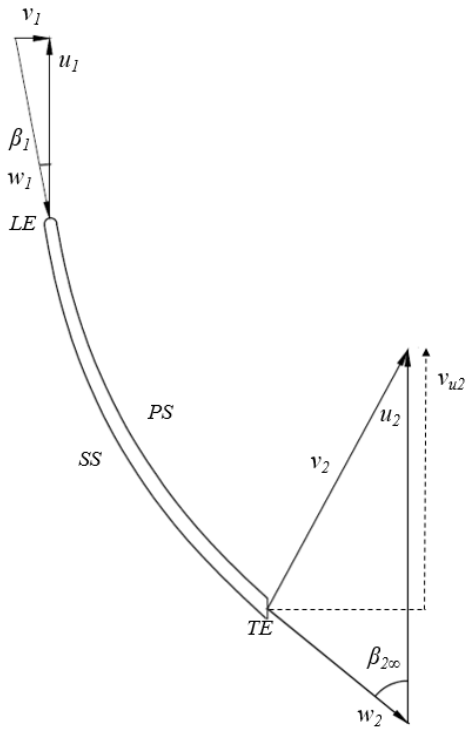

Fig. 2 – Velocity triangles

These conditions could be fulfilled only if the rotor had an infinite number of blades. However, blades are needed to transfer the mechanical work to the fluid, and the space among the blades, widening towards the outlet, allows blade and Coriolis forces to act on the flow, deviating it from its ideal trajectory. In addition, in its path through the hydraulic channels, the flow encounters obstructions, sharp edges and sudden turnings, which cause energy losses and modify the velocity field locally and the pressure field over the whole machine.

Away from the best efficiency point, additional phenomena as recirculation will further enhance flow deviation. In addition, severe part-load conditions might feature rotating stall, resulting in uneven sucking conditions too.

The main effect is the decrease of the relative flow angle, reducing the tangential component of the absolute velocity at the outlet ($v_{u2} < v_{u2\infty}$), which is strongly related to the head production.

This is usually quantified by the deviation angle δ, shown in Fig. 3, expressed as the difference between the theoretical flow angle $\beta_{2\infty}$ and the effective relative flow angle β_2.

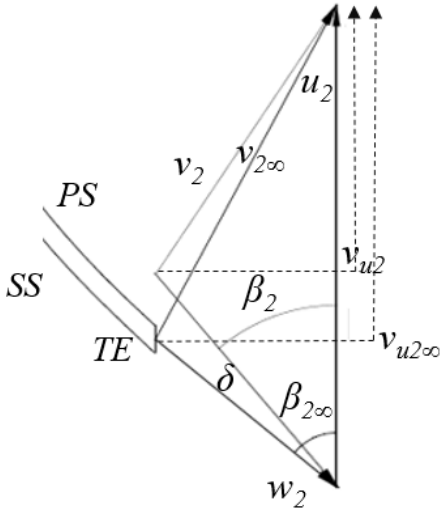

Fig. 3 – Flow deviation at the impeller outlet

As reported by Gülich [10], the main mechanism inducing this phenomenon is the different flow velocity across the blade surfaces, due to the work transfer, which acts in the triangular section at the outlet, especially for backward curved blades; for radial blades, the major cause has to be identified in the Coriolis force, driving the fluid towards the pressure surface.
Correlations are available to quantify the reduction in the circumferential component of the outlet velocity; however, the large channel width in this specific design allows a very uneven outflow profile, which, with recirculation, complicates the analysis.

In case of two-phase flow, the phase slip (different relative velocities between the phases) acts in a similar way, modifying the velocity triangles at the outlet, thus affecting the pump capability. The flow deviation, also enhanced by air accumulation on the suction side of the trailing edge, and phase slip effects add. The liquid phase acceleration modifies the outlet triangle; this effect is accounted for in a similar fashion by [11] and [12].

Many challenges are introduced in turbomachines analysis, as not only each of the phases responds differently to the forces in the hydraulic channel, but also the mechanical and thermal interaction among the phases has to be taken into account. In addition, multiphase flow affects turbomachines operation introducing secondary flows, unsteady phenomena and other disturbances in the flow field. Many of these features present an unpredictable behaviour.

The general investigations usually comprise the study of:

- bubble size and shape variation, coalescence and breakup processes
- different response of the individual phase to the forces in the hydraulic channels
- flow field steady state modifications by gas accumulation
- typical flow patterns and flow regime transitions
- specific phenomena as alternating channel obstruction and the accumulation and release of gas pockets, presenting a mechanism similar to bubble formation.

In addition to these fluid-dynamics issues, the machine characterization involves the evaluation of the performance degradation, compared to single-phase operation, and the identification of the stable working range, in order to define, later, a control strategy to keep the machine away from unstable conditions and recover normal operation in case of sudden variations in the operating parameters.

2.1 Definitions

Hereafter, the definitions of the machine, flow and fluid parameters used in this Thesis are presented.

- Machine
  - Truly dimensionless pump specific speed, ω_s [-]
    Specific speed numbers are usually employed to indicate how the overall machine design prioritizes the desired head production or the flow rate, this affecting the pump layout.
    The single-stage, mixed-flow pump considered in this study presents a dimensionless specific speed number 0,56. It is calculated as

$$\omega_s = \frac{\omega\, Q^{0,5}}{(g\, H)^{0,75}}$$

    with the values of Q and H taken at the nominal point and expressed in m^3/s and m, respectively.

  - Rotational speed, n [rpm] or ω [s^{-1}]
    Usually expressed in revolutions per minute (rpm), its proper unit when used in calculations is radians per second. Along with the machine outer diameter, it defines the term used to express the mechanical work transfer from the blades to the fluid. To improve the energy intensity of a machine, the rotational speed is increased. According to the single-phase pump similitude theory, variations in the rotational speed affect the head production with a factor proportional to ω^2, while the flow rate is directly proportional to ω.

  - Blade tip clearance [µm]
    In rotating machinery, the flow tends to escape from the main passages, finding a possible path through the gaps; seals are designed to avoid this. However, performing flow visualization inside the pump channels requires the removal of the shroud: due to the pressure difference across the blades, a considerable tip leakage occurs, affecting the performance and

introducing disturbances. The tip gap has, therefore, to be set at a minimum value, limited by the shear stress on the outer casing and the rotor total indicated runout.

- Geometrical design parameters:
    - outer and inner machine diameters at inlet and outlet: the considered model has an outer diameter of 320 mm
    - number of impeller and diffuser blades: the studied pump features a four-bladed impeller and a vaned diffuser
    - blade height, chord and thickness; aspect ratio, defined as span/chord
    - blade angles β - the inlet defined by the necessity to match the machine with the incoming flow, the outlet one linked to the desired work transfer and particularly affecting the machine behaviour and the performance curve shape
    - γ angle, defining the inner and outer radii evolution as the axial coordinate increases between inlet and outlet.

    These last two angles are shown in Fig. 7, in the Analytical Models Section.

The set of these parameters defines the machine hydraulic design, which, for the machine considered in this study, is proprietary and is, therefore, not reported explicitly. However, a discussion on the design goals and considerations on the impeller channels layout and the main values are reported in Ch. 3.

Experimental and numerical investigations are performed on a given design, the Aker Solutions MultiBooster®, so the main focus is set on the effect of operating parameters as rotational speed, relative flow rate, gas content, tip clearance, suction pressure, rather than the hydraulic design; in a further stage of the project, after the understanding of the fluid mechanisms and the reliability of the analysis tools is improved, design modifications can be considered.

In general, design guidelines comprise [13]:

- high solidity blade rows are required to generate gradual blade forces
- fluid deceleration is controlled by appropriate impeller-hub and shroud contours shapes
- leakage flows in open impellers reduce the differential pressure across the blade tip
- to increase the maximum flow rate, usually bounded by choking:
    - reduction in the relative velocity at the inlet, through prerotation, using guide vanes or rotating devices
    - widening of the inlet throat area

- Energy
    - Specific Work, Y [J/kg]

      This parameter expresses the amount of work transferred per unit of mass flow, and corresponds to the useful enthalpy rise.
    - Head, H [m]

This value, named also *Total Dynamic Head*, expresses the energy independently of the fluid density. It is related to the specific work by $Y = g\,H$.

- Flow
  - Volume Flow Rate, Q [m^3/s]
    This parameter is directly linked to the flow velocity and is measured separately for both the phases. Since the gas phase is compressible, reference should be made to the conditions it is calculated at. Gas and liquid volume flow rates are distinguished.
  - Mass Flow Rate, m [kg/s]
    This parameter is referred to the amount of fluid flowing for unit of time.
  - Total Volumetric and Mass Flow Rates, Q_t [m^3/s] and m_t [kg/s]
    They depict the total flow processed by the machine and are calculated as the sum of the individual phase flow rates.
  - Reference value for the flow rate
    At the design stage, a reference value is defined; usually, the nominal or the best efficiency point (BEP) values are taken. In this specific case, the nominal flow rate is taken when the inlet flow matches the blade angles (no incidence losses condition).
  - Relative flow rate, q^* [%]
    This value is calculated as the ratio between the actual total volume flow and the reference flow rate and expresses how much the flow velocity is reduced compared to the reference case. It is the main parameter involved in the off-design grade definition and especially the part-load operation.

Non-dimensional coefficients

- Flow Coefficient, φ [·]
  This number expresses the ratio among the meridional and the tangential components of the flow velocity, and is used for non-dimensional plots of the machine performance.
- Head Coefficient, ψ [·]
  This parameter expresses the ratio among the work transferred to the fluid and the machine kinetic energy at the outlet section – the rotational speed and the outer diameter are the machine parameters involved.

Two-phase flow involves fluids in a different state of the matter; if the phases do not consist of the same chemical substance, the flow is named two-phase and two-component, as the air-water mixture considered in this study.

- Void Fraction, α [·]
  It is defined as the ratio of the cross-sectional area occupied by the gas phase to the whole area available for the flow, and expresses the portion of the flow area available to the gas phase.
- Superficial phases velocities, u_{sl} and u_{sg} [m/s]

These parameters, also called volumetric fluxes, are calculated dividing the phase velocity by the total flow area, and are related to the phase velocities by the void fraction.

- Phase velocities, u_l and u_g [m/s]
  These are calculated dividing the volumetric flow rate of the phase by the cross-sectional area that specific phase is flowing through.
- Slip Velocity, u_s [m/s]
  This variable expresses the velocity difference among the phases.
- Slip Ratio, S [·]
  It is the ratio between the gas- and liquid- phase velocities and plays a major role in the flow-regimes characterization.
  Only when the slip ratio is 1, the gas volume fraction and the void fractions are equivalent. In practical applications, this occurs when the flow regime is homogeneous and the dispersed phase travels at almost the same velocity of the continuous one.

Non-dimensionless numbers provide an insight into the governing forces and physical phenomena and help to identify comparable conditions where the leading physics are maintained while the operating parameters are varied. The most relevant for this application, which can be object of further study, are the following ones:

- Rossby Number, *Ro*
$$Ro = \frac{U}{Lf}$$
  In a rotating system, this number relates the inertial to the Coriolis forces. U, L and f are the characteristic velocity, length and Coriolis frequency.
- Bubble Reynolds Number, Re_b
$$Re_b = \frac{\rho_l u_r d_b}{\mu_l}$$
  It expresses the ratio between inertial and viscous forces. A proper knowledge of the relative phase velocity and a representative value for the bubble size is needed.
- Eötvös Number, *Eo*
$$Eö = \frac{g {d_b}^2 (\rho_l - \rho_g)}{\sigma}$$
  It relates the buoyancy with the surface tension force.
- Froude Number, *Fr*
$$Fr = \frac{u_r}{\sqrt{g d_b \frac{(\rho_l - \rho_g)}{\rho_l}}}$$
  This number measures the relative importance of inertia compared to buoyancy forces.
- Weber Number, *We*
$$We = \frac{\rho_l {u_r}^2 d_b}{\sigma}$$

The Weber number, important to determine the bubble shape and regime, relates inertia and surface tension forces.

- Morton Number, *Mo*

$$Mo = \frac{We^3}{Fr^2 Re^4} = \frac{g\mu_l{}^4(\rho_l - \rho_g)}{\rho_l{}^2\sigma^3}$$

This number relates the previous ones and it is exclusively a function of the fluid properties.

The identification of representative temporal and spatial scales, along with fluid properties, is required.

Although the typical transition values have been originally obtained for specific experimental cases, these numbers, if adapted properly, are useful to describe the balance between the different mechanisms acting on the fluids in the hydraulic channels of rotating machinery.

- Fluid
  - Gas Volume Fraction or Volumetric Quality, *GVF* [·]
    This parameter has a key value in multiphase pumping, expressing the ratio of the volumetric gas fraction to the total one.

$$GVF = \frac{Q_g}{Q_g + Q_l}$$

  - Gas Mass Fraction or Quality, *x* [·]
    It is calculated as the ratio between the gas phase and the total mass flow rates.

$$x = \frac{m_g}{m_g + m_l}$$

2.2 Physics of the entrained bubble

In this paragraph, a brief presentation of the main bubble features and forces is given with the main goal of showing how many real phenomena would affect a simplified analytical treatment, thus justifying the choice of the research approach, which starts from flow visualization. An exhaustive and comprehensive treatment is beyond the scopes of the current Thesis, and can be found in specific books.

The bubble motion description requires the identification of a characteristic bubble size; its shape and the surrounding flow regime represent the other parameters involved in the fluid-dynamic analysis, which is, however, complicated by the mutual interaction between the flow and the particle and by the fact that the bubble size and shape vary along the path and cover a broad distribution, depending on the very local flow field values and balance of forces. Phenomena as coalescence and breakup, in addition, occur continuously.

2.2.1 Main particle shapes and regimes

The fluids and flow characteristics influence the motion of particles; in order to describe it, corrective factors are related to how their irregular shapes deviate from some reference ones, presenting a simplified geometry, which eases the study.
Ideal particles are usually classified in groups, according to [14].
An important feature is the presence of axes of symmetry; with regard to this, bubbles can be:

- axisymmetric – spheroids or ellipsoids of revolution, generated by the rotation of an ellipse around its axes: oblate if minor, prolate if major; the aspect ratio is equal to the length on the axis of symmetry divided by the maximum diameter orthogonal to the axis
- orthotropic – have three mutually perpendicular planes of symmetry; an axisymmetric particle is orthotropic if it has a plane of symmetry normal to the axis.

Concerning the shape, it is defined making use of parameters as volumetric shape factor, sphericity, circularity.

When it comes to bubble regimes, external forces and the continuous flow field deform the fluid particle; normal and shear stresses at the interface counteract these sources, preventing sharp variations in the particle shape.
In order to perform this study, some basic cases are usually identified. The role of the additional forces in the rotating channels are highlighted later.
Starting from the basic case of gravity causing free rise or fall, particles in free motion can be:

- spherical, if interfacial tension and viscous forces are much higher than inertia forces
- ellipsoidal, if oblate with a convex interface – usually featuring shape fluctuations
- cap, presenting a flat base

Figure 4 shows the characteristic map relating the bubble regimes to the non-dimensional numbers.

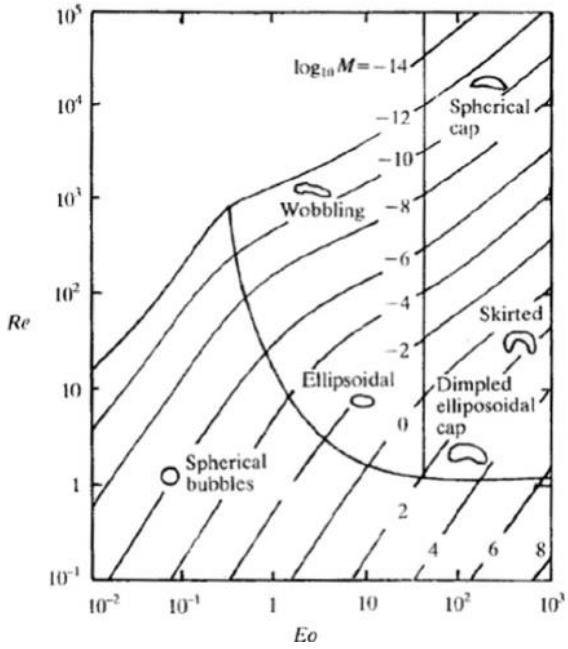

Fig. 4 - General graphical correlation in terms of Eo, Re and Mo, for an estimation of the shape regime (taken from [15])

Two different rotational motions can occur: if the axis is normal to the relative motion, the resulting movement is called top-spin and is related to the generation of a lift force, while, if the axis is aligned with the direction of motion, screw motion occurs.
Only in the ideal case the net drag force is parallel to the direction of motion; for the other cases, through a drag ratio, the force is related to the reference case of an equivalent sphere. A non-symmetrical particle experiences translations and rotations resulting in irregular motion and spiral patterns. Second-order tensors determine the force and torque:

- resistance to translation expressed by a symmetric translation tensor
- rotations through a symmetric rotation tensor
- torques from translation and drag from rotation by an asymmetric coupling tensor

Secondary motions, probably due to wake shedding, comprise rigid body movements and shape dilatations, and further complicate the flow-dynamics analysis.

In correspondence to a threshold value of *Re*, the vorticity generation is no longer balanced by diffusion and convection; periodical low-frequency oscillations of the wake fluid are shed, resulting in the phenomenon of wake instability.
Internal recirculation in case of air bubbles in a water flow, due to the very low viscosity ratio, delays the flow separation and wake formation in the external fluid – this has suggested an

interesting method of delaying the separation of the boundary layer, making the solid surface move the same way as the shearing flow.
The effect of surfactants, reducing the surface tension, is to dim the internal motion, thus affecting the wake structure.

2.2.2 Formation and breakup

Bubble formation constitutes a complex phenomenon as it involves a sequence of mechanisms.
In general, for sufficiently large bubbles, the dominant forces promoting fission are the shear, while the ones resisting are due to surface tension.
Breakup occurs for a variety of phenomena, depending on the main physics involved:

- If the heavier fluid lays on top, the interface between the fluids experiences increasing Rayleigh-Taylor instabilities, which are limited by surface tension and viscous forces; however, these last forces cannot keep pace with the disturbance if the wavelength overcomes the critical value:

  $$\lambda_{cr} = 2\pi \sqrt{\frac{\sigma}{g\Delta\rho}}$$

  which can't overcome half the circumference, obtaining the maximum stable diameter

  $$(d_e)_{max} = 4 \sqrt{\frac{\sigma}{g\ \Delta p}}$$

- Resonance between the natural frequency of the particle and the eddy oscillation
- When particles flow in a velocity gradient zone, tension forces cannot oppose the shear stresses, and this results in breakup; as the surrounding flow accelerates, the particle experiences a stretching in the flow direction and starts oscillating; this movement is dampened by viscosity and surface tension; before breakup, it reaches an ellipsoid shape with an aspect ratio determined by the fluid properties and the acceleration. Intense velocity field variations, generating strong local shear stresses, stretch the bubble which separates generating two ellipsoids.
- Turbulence complicates the analysis; Hinze [16] proposed a scale for turbulent fragmentation;
  - The total local shear stress should overcome the surface tension and viscous forces inside the particle.
  - Turbulent eddies smaller than the bubble diameter are responsible for breakup, while the other vortices only move the particle; it should be noted that there are difficulties in measuring the energy spectrum – often homogeneous and isotropic turbulence is assumed, with eddies in the inertial subrange.

  The breakup mode under the main action of turbulence is more irregular.

Most of the breakup occurs close to the pipe walls, under the action of spatial velocity gradients, while, when the flow is accelerating over time, breakup happens in the center, due to pressure pulsations.

More recent studies have included additional effects, as the reciprocal interaction between the bubbles and the turbulent field, the lift force, different bubbles regimes; furthermore, while the particle inertia is very little, the added mass term is not negligible. Spelt and Biesheuvelt [17] have studied the influence of isotropic homogeneous turbulence on the ascending motion of small bubbles, under the assumption of spherical shape and high-Reynolds number regime. The analysis is restricted to low turbulent intensities compared to the bubble rise velocity; as the turbulence intensity increases, the acceleration reaction forces reduce the bubble diffusivity, restraining it from adapting to the surrounding main flow path.
Magnaudet and Eames [18] have reviewed the effects of drag, added-mass force, and shear-induced lift experienced by spheroidal bubbles moving in inertia dominated, time-dependent, rotational, non-uniform flows. The characteristic motions at path instability are discussed.

2.3 Bubble motion models applied to the study of multiphase pumps

Earlier studies on centrifugal pumps, as in [19], focused on the description of the forces on a single bubble which cause the air phase to follow a specific trajectory. The same authors have related the observed bubble size to the characteristic channel size and flow velocity, using a modified Weber number. Improved results were presented by Furuya [11]. However, these models were limited to low gas contents, both for the assumption of no interference to the main flow, and to the fact they simplified phase interaction. In addition, proximity to the walls or enlarged bubbles adhering to them require different boundary conditions: the flow is no longer uniform and modified interfaces have to be considered. When the bubble diameter reaches a threshold value, the channel diameter becomes the controlling length affecting the particle shape and velocity; a so-called slug forms, and presents a rounded front region – its shape depending on local flow characteristics – and a long cylindrical section flowing in an annular liquid film.

In general, due to their different physical properties, the liquid phase behaviour is dominated by the effect of body forces and inertia, while the gas phase by buoyancy and secondary flows. As a direct consequence, the liquid phase is more prone to separation migrating towards high-radius zones, while the gas bubbles, which can't overcome the pressure gradient due to the insufficient drag, will evolve from coalescence to the formation of a gas pocket, finally leading to blockage. The entity of this phenomenon is strongly affected by the bubble size.

In [10], a detailed explanation of the physical mechanisms influencing the mixture behaviour and affecting the overall pump performance can be found.

Sterrett [20] described the kinematics of a single bubble passing through a centrifugal pump impeller considering a logarithmic spiral and a radial vane design. A strong influence of the bubble diameter is reported; a critical size is found; over this value, the bubble is no longer able to exit the impeller. This behaviour is explained by the different dependence on the bubble diameter of the

two dominant forces: the adverse pressure gradient increases more significantly, favouring the formation of the gas pocket and strongly affecting performances.

As explained in the paragraph presenting the theoretical treatment of bubble dynamics, a comprehensive analysis of the forces and mutual effects has been performed by other researchers; however, thanks to the improved hydraulic design, multiphase pumps handle with very high gas fractions. Under these conditions, flow structures as vortices, bubbles, and mechanisms as bubble-bubble interaction, bubble-turbulence interaction, moving and deforming interfaces, present a rapidly varying character and cover a broad range of spatial scales; so, it is not yet possible the analytical description of the overall flow evolution.
The flow regime experiences a deviation from the ideal homogeneous path as soon as the gas fraction becomes progressively higher, or the flow velocity is reduced, the former causing increased bubble sizes and accumulation of gas pockets, the latter promoting coalescence – for the longer residence time - and phase separation. The last phenomenon is enhanced at atmospheric inlet pressure operation, when the density ratio between the phases is maximum. In this case, the bubbles migrate towards the low-pressure regions, as the vortices cores and wakes.
In addition, local geometrical variations as curvatures and obstructions before and after the stage, along with the unsteady contribution of the flows through gaps and seals, can significantly affect the machine stability.

2.4 Flow patterns and gas locking

Multiphase flow morphology is usually described making use of a flow patterns classification. Difficulties are due to the mutual dependence of flow values and flow geometry. The transition between flow patterns occurs when the processes are no longer balanced; it is often accompanied by intensified flow instabilities.
The void fraction presents both an overall mean value and an intermittency. Similarly, Brennen [21] classifies the flow patterns based on the degree of separation and the level of void fraction intermittency.
On a mathematical perspective, a fully dispersed flow requires the particle size to tend towards zero, and the homogeneous flow assumption requires no velocity slip – i.e. relative motion between the phases, guaranteed by the infinite drag. In many practical applications the flow is well dispersed and the particle diameter much smaller than the representative channel dimension, but, still, a certain velocity slip exists. In the studied multiphase pump, the flow pattern presents these features only around nominal flow conditions: as soon as the flow rate is reduced, cross-streamline motions arise, promoting separation and intermittency.
The tendency towards dispersion or separation is studied identifying the dominant processes enhancing each of the trends and comparing the phases relative motion velocity with a characteristic velocity of the mixing motions in the continuous phase; the flow pattern boundary occurs when these two velocities are balanced, as discussed in Brennen [21]. Processes promoting

separation depend on the density ratio between the phases and buoyancy forces due to the gravitational acceleration or the Lagrangian fluid acceleration, while hydrodynamic forces counteract this tendency: turbulence and the shear created by unsteady velocities lead to dispersion. At very high *Re*, segregation occurs when the bubble relaxation time is comparable with the typical time of the turbulent flow motion.
The traditional cases of horizontal and vertical pipes are well covered in the scientific literature; in the hydraulic channels of a rotating machine, however, a more complex system of forces acts on the flow and the channels present varying forms and shapes. The gas phase would tend to flow back driven by the pressure gradient, while the air bubbles get compressed in the streamwise direction. The typical flow structures in a multiphase pump channel can be distinguished in Fig. 5.

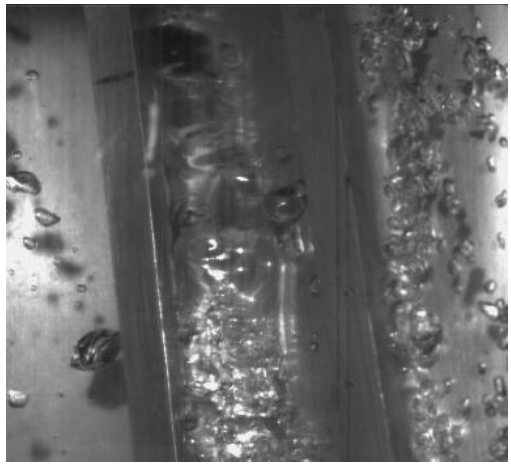

Fig. 5 - Main flow structures and bubbles evolution in the hydraulic channel, from flow visualization on the analyzed pump

Turbulence and shear around the leading edge fission the bubbles determining their size. As the *GVF* is increased or the rotational speed reduced, the bubble size increases and the air phase forms gas-filled wakes on the impeller blade suction side, close to the trailing edge, deviating the flow leaving the impeller; this is the main explanation of performance degradation at nominal operating conditions.
When the flow velocity is limited and the gas fraction increased, the air phase eventually forms a gas pocket which adheres to the blade pressure side. The interface with the high velocity water stream becomes very unstable: waves form and a higher intermittency flow regime results. Buoyancy, the Bernoulli effect and surface tension are now the main forces promoting or opposing stability.

2.5 Previous investigations and experimental campaigns

2.5.1 Flow visualization

As presented in the previous paragraphs, the pump geometry highly affects the two-phase flow patterns. The study of the forces balance and the tendency to stratification helps defining some trends, but accurate flow visualization provides the most suitable tool for the understanding of the flow phenomena.

Figure 6 presents an overview of a typical impeller-diffuser pump stage, with the nomenclature used further in the description.

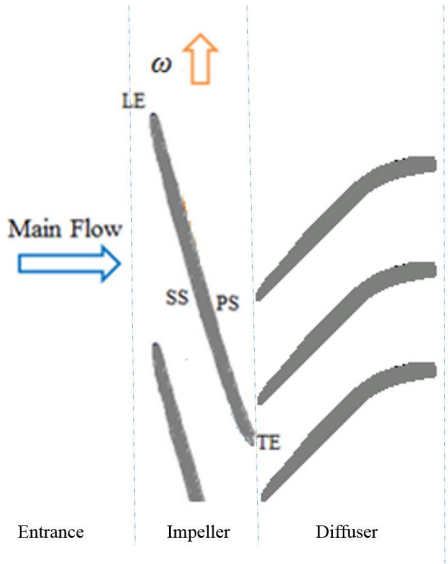

Fig. 6 - Overall view of the flow channels of the impeller and diffuser stages

A summary of the main outcomes of the most interesting experimental results from tests and visual observations performed on pumps operating a two-phase flow is reported in Appendix I. The researches [19,22-32] studied the accumulation zones and the performance breakdown phenomena on radial machines; limited values of the gas-handling capabilities are due to the centrifugal pump design. Analyses of the helico-axial model [33-34] covered a broader range of *GVF*, as the machine considered in this Thesis. The studies reported in [5-6,8] focused on an Electrical Submersible Pump. The authors report different locations of the recirculation zones and a different pump behaviour when the main influencing parameters (mixture composition and flow rate) are varied.

2.5.2 Performance and the influence of the operating parameters

Detailed two-phase performance maps, covering the pump operating zones at different speeds and gas contents, are useful to predict the region of unacceptable pump performance, determine the safe operating areas and study the surging behaviour and its control.

Hereafter, a brief summary of the previous experimental performance investigations with the main observations reported by the respective authors.

Cappellino et al. [35] reported the experimental investigation on impellers of several diameters and representative of different specific speed groups; a discussion on the effects of suction pressure, tip clearance and solidity is included: impellers with fewer vanes, presenting larger channels and a broader turbulence spectrum, are less susceptible to blockage. It was suggested the use of some devices to prevent gas accumulation and locking, as an inducer in front of the pump stage. A transparent casing allowed flow visualization.

Turpin et al. [36] related the head characteristics of centrifugal pumps with the gas content and inlet pressure. Three different impellers are compared; air and water and gasoline and carbon dioxide are the working fluids. Intermittent gas-locking and severe low-frequency head oscillations, as experienced in the current research, are reported as the gas content is increased. In the water and air case, detachment from the reference curve occurs at 7% gas content, and intermittent gas locking at 11%; the head oscillation period is about 1-2 s. Operation with gasoline and CO_2 resulted in an increased gas-handling capability. A relation to predict the region of unacceptable pump performance at given gas content and inlet pressure is presented; however, its capabilities, at high gas-content and low suction pressure, were limited.

Chan [37] performed an experimental investigation on a vertical, single stage, double volute centrifugal pump. Test data were obtained measuring mass flux and local void fraction at the pump suction, and the effect of inlet flow conditions on performance characteristics were taken into account. Performance degradation was strongly dependent on the suction temperature.

Cooper et al. [13] presented different design approaches for helico-axial multiphase pumps, depending on the desired operating range, in function of *GVF* and inlet pressure. The use of a preliminary inducer is suggested in order to reduce the bubble size. Choking and shock losses might occur when operating at low suction pressure, due to the reduced speed of sound.

Korenchan [38] presented a head-loss ratio to correlate experimental data from a scaled coolant pump; the use of correction factors to relate data referred to the upstream or average void fractions in the pump stage was suggested. The effects of the system pressure and condensation are considered. Head degradation dependence on scale needs to be determined in order to consider the results valid for the full-scale pump. The correlation found is pump-specific, being strictly related to pump efficiency, geometric scale, inlet piping configuration, pump specific speed.

Leporcher and Taiani [39] presented the outcomes of performance, sensitivity and endurance tests on a helico-axial pump; the effects of rotational speed and suction pressure are included. Reference values for the operational parameters are: n = 1800 – 6600 rpm, GVF = 50 – 100 % at suction, p_i = 2 – 23 bar. Transient tests comprised:

- closure of the pump discharge, which resulted in a very low suction pressure increase with lower flow rates, even at high rotational speed
- modification of the suction flow rate at constant speed: at part-load, vibrations and difficulties in controlling the discharge pressure were experienced
- speed increase at a given flow rate, resulting in a suction pressure reduction
- processing of liquid slugs.

Vangen et al. [40] presented a review of the Poseidon pump installation and operation; reference tests are performed to qualify the equipment. The thermodynamic and fluid properties impact on capability and performance has been taken into account too: they report slightly better efficiencies and higher capacity for offshore tests compared to the onshore water-air tests. The booster presented a certain self-adaptive ability to GVF variations.

Poullikkas [29] performed experimental and visual investigations on different centrifugal shrouded and unshrouded impellers. A thorough definition of two-phase head degradation was presented, including the effects of gas compressibility and the contribution of the individual phases. The effects of low suction pressure were discussed too. High-speed video recordings helped the analysis of unshrouded impellers instabilities.

An accurate review of the state of the art of the helico-axial technology was performed by Falcimaigne [33], including the main analyses and methodologies, making use of advanced techniques: experimental (laser Doppler anemometry), design (optimization by neural network and genetic algorithm), computational calculations.

Ramberg [41] analyzed the performance and transient behaviour of a multiphase pump; for the performance degradation formulation, the mixture is treated as a single component flow with suitable average properties, the homogeneous equilibrium bubbly flow in this case. The influence of the fluid viscosity is taken into account. Concerning transient tests, the pump showed a damped response to the variation in the operating conditions.

Beltur et al. [42] and, more in general, studies from the TUALP consortium [3-8], performed extensive tests on a multistage Electrical Submersible Pump, including the effect of fluids with different properties, the stage number, the suction pressure, over a broad range of rotational speeds and mixture compositions. In [3], map boundaries of surging and gas locking are presented. At high GVF, a peculiar behaviour is observed: the curve changes its slope twice and a minimum performance zone is recorded before gas locking. The hydraulic power delivered to the fluid is calculated separately for the liquid and gas fractions; in this last case isothermal and adiabatic behaviours are compared.

Barrios [4] performed a visualization study, focusing on the bubble size and surging mechanisms. Gamboa and Prado [7] reviewed the surging inception conditions and studied the effect of the test procedure. It is reported an asymptotic evolution of the critical *GVF* as the suction pressure is increased, and the evolution of the performance deterioration rate, which is constant before surging inception, and then dependent on the flow rate.

Morrison and the research team at Texas A&M University, as reported in [9], performed experimental tests on an Electrical Submersible Pump with a Split Vane Impeller design, installed in a closed loop where the two phases are directly derived from a pressurized separator. The main effects considered having an influence on the performance and gas handling capability are the rotational speed and suction pressure; the former seems to be the most affecting.

Similar investigations were performed on a test facility at the University of Beijing, as reported in [43-44]. An accurate study of the inlet flow regime helped the evaluation of the installation of a buffer tank at the inlet. Four different flow regimes are identified and linked to the zones in the performance curves; the effect of *GVF*, rotational speed and relative flow rate is discussed.

The investigations reported in [3-8], [29], [35], [36] and [43-44] featured a similar test loop arrangement as the one considered in this research, with a booster pump for the liquid phase.
It should be noted that, in some of them, data are presented in relation to the liquid phase flow rate, and not the mixture volume flow rate, as in this study. This is justified by the fact that the single-phase liquid flow rate corresponds to a real measurement which remains constant throughout the stage, while, due to the gas phase compressibility, the gas volume flow rate varies along the channel. On the other side, when presenting the data in terms of liquid flow rates, curves are taken at varying values of *GVF* and total volume flow – in this case there is no correspondence between measurement and local flow field property. The current choice involves a different meaning, as when the gas amount becomes significant, the main mechanism is no longer constituted by a water flow carrying on air bubbles, but rather a complex mixture.

The test results reported in the available literature analyze the effects of different fluid and flow parameters, and explore the machine gas-handling capabilities. When tests are performed at increased suction pressure, a major difference is whether the inlet flow is provided by a pressurized tank or, alternatively, an additional booster pump, as in this research. When test points are taken in the negative slope zone of the performance curve, the device providing the desired suction pressure is not influencing the pump behaviour; however, when the unstable operating zone is approached, the presence of a booster installed in series can significantly counteract the characteristic pressure and flow pulsations, while a pressurized tank would dampen them; in this case, how the booster or tank responses affect the overall system behaviour should be carefully considered. Finally, experimental tests have shown that, after the instability onset is hit, some air remains trapped in the hydraulic channels; if enough overpressure is provided by the devices installed upstream (in this case the centrifugal pump), the flow can still circulate. These test points, however, do not present the necessary repeatability to be included in performance curves, as different gas

accumulations can occur. After the maximum *GVF* is hit, air gets trapped in the pump stage and the available flow area in the hydraulic channels is strongly reduced; the air occupies the lower span ring, while the limited water flow rate flows along the outer annulus, in a similar fashion as annular flow. The pump still works, delivering very limited values of flow and head.

2.6 Modelling

2.6.1 Semi empirical models

The first performance modelling attempts, due to the difficulties in the description and modelization of the multiphase flow and lack of local visualization and measurements in the pump channels, focused on the overall performance degradation, starting from simple empirical and semi-empirical correlations. This approach is based on correlations from experimental data. The performance deterioration has usually been specified through head- and efficiency- multipliers and losses factors, taking into account the performance degradation due to the presence of gas bubbles and accumulations. Quasi-isothermal or in alternative a polytrophic compression approach (no longer neglecting heating effects) can be considered.

You will find a report of the main experiences which have set the milestones in the performance deterioration modelling attempt in Appendix II. [45], [36] and [38] are on centrifugal pumps, while [41] on the helico-axial concept.

2.6.2 Analytical models

Fundamentals

These models can provide a correct insight into the forces that drive the fluid. The fundamentals of a pump analytical model are the following:

- Hyphotheses, assumptions and simplifications:
    - gas compressibility can be assumed or neglected
    - gas thermodynamic transformation: isothermal or adiabatic
    - interfacial momentum transfer term can be modelled as a source of losses
    - phase mixing effects due to turbulence and recirculation are usually neglected
    - mass transfer between the phases is usually neglected
- Basic equations
    - mass conservation
    - momentum balance
    - energy equation - simplifications are usually made: internal power losses contribute to heat generation, which is absorbed by the liquid phase; thus, phases are in thermal equilibrium and the fluid behaviour is considered isothermal; this allows to skip the need of an energy equation.

- Constitutive equations requiring correlations or modelling
    - interfacial friction force. The dependence of the drag coefficient on flow regime and of the bubble size on pump speed has to be taken into account
    - virtual mass force
    - wall friction force
- Additional terms, describing specific phenomena, can be included to improve the modelling adherence to the real physics
    - shock (inlet) and sudden expansion (outlet) losses
    - deflection of the flow angle
    - phenomena in the transition between the bladed channel and unbladed zones
    - bubble size correlation, mainly as a function of the void fraction and pump rotational speed

Due to the difficulties in measuring each phase properties and the complications a two-phase model introduces in an analytical expression, to simplify the study, the first attempts have focused on treating the mixture as a homogeneous, equilibrium flow, with the assumption of absence of phase velocity slip, which is, however, one of the main factors causing degradation in the pump behaviour.

The homogeneous model lays its foundations on the assumption that pump performance under two-phase flow can still be described with the same formal expression used for single-phase liquid flow, adopting the mixture density. This approximation is valid only for the operating range of very limited *GVF* and close to nominal q^*, thus covering the zone away from the instabilities the investigations of this study are addressed to. It can, however, still be used as a comparison.
As a result, especially in the analytical performance prediction, the homogeneous models which were usually adopted give good results only at rather low gas fractions.

One-dimensional models have acquired good prediction capabilities with the two-fluid model, taking into account the different phase velocities.

A further improvement has been the inclusion of liquid viscosity (through the friction term), gas compressibility (equation of state), virtual mass term (particularly important since the density ratio is very high), non-spherical (ellipsoid) elongated bubble shape; these, expressing the mutual interaction between the phases, require an iterative procedure, to refine the calculation at each cell boundaries.

Additional corrections, CFD based or through correlations from experimental data, are needed to improve the accuracy of the predictions and account for phenomena as shock at the inlet, flow deviation at the outlet, end losses, leakages and recirculation, this last playing a key role when operating away from the nominal flow rate.

The general scheme of an analytical performance model comprises the following steps:

- Channel geometry description, streamline approach and discretization

  The three-dimensional pump geometry is usually described and specified through the angles β and γ and the coordinates r and z.

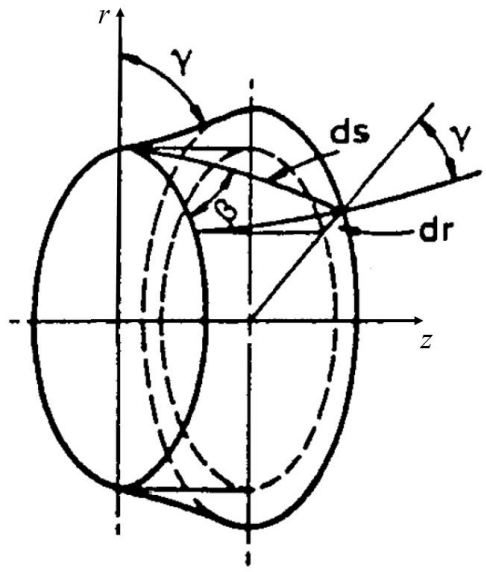

Fig. 7 - Geometrical specifications (adapted from [46])

To analyze the flow behaviour in the impeller channel, the use of a local coordinate system allows to make a sort of monodimensional study of the evolution of pressure, void fraction and phase velocities along the streamline coordinate s, and to express secondary flows in the normal n (between blade pressure and suction surface) and local vertical o (between casing and rear shroud) directions, these causing separation, recirculation and bubble accumulation. The geometric relation between the two coordinate systems can be obtained composing two rotations in series, as in Fig. 8, from the local cylindrical one (r, ϑ, z).

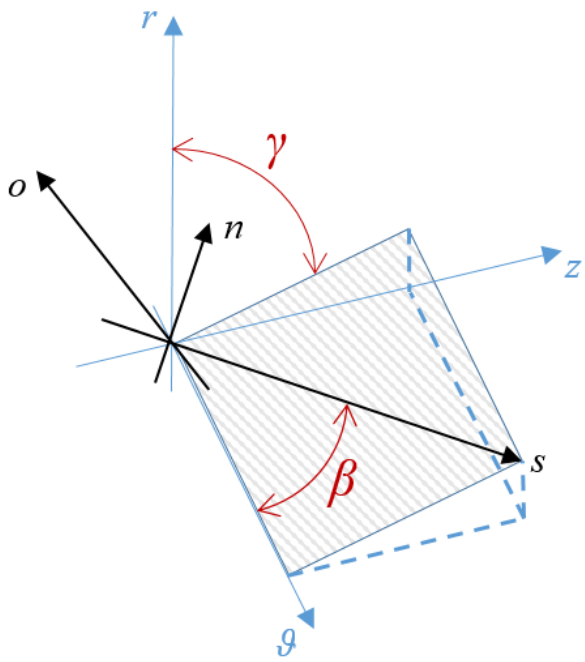

Fig. 8 - Coordinate system transform

In the streamline approach the trajectory of the bubbles is assumed to be equal to that of the liquid, so a control volume bounded by two streamlines can be used. This assumption is realistic only around the nominal operation point.
The considered volume is limited by the streamline coordinates, the normal coordinate *n* and a unit stream thickness.

- Body forces and pressure gradient balance in the blade channel

  The forces acting on the flow which need to be considered are inertia, pressure gradients, body forces (due to centrifugal, Coriolis, channel curvature accelerations). The resultant momentum equations are solved in the three directions. An optimal flow requires balance between the pressure gradients and the resultant of the body forces, both in the blade-to-blade and spanwise directions. If this condition is not accomplished, secondary motions occur.
  In case of two-phase flow, the pressure gradient drives the gas phase towards lower pressure zones (acting as the buoyancy force), while body forces (proportional to the fluid density) lead the liquid phase
  Some parameters are defined to describe the resultant trend:
    - Rossby number: ratio between the centrifugal and Coriolis acceleration components

- Froude number: ratio between inertia force and buoyancy (adapted from free surface motion). A modified Froude number, relating inertia and the resultant of body forces, can be used to predict flow stratification.

- Void fraction and pressure evolution along the pump

  The liquid phase and the particle momentum equations are merged in order to eliminate the pressure gradient term. The phase velocities are now expressed in terms of the mass flow rates, the densities, the flow areas and the void fraction, and substituted in the previously obtained equation. A final expression for the void fraction evolution along the streamline is obtained; the only variable is $\alpha(s)$. This prediction, even if neglecting some phenomena affecting the flow, can help defining a general trend.

- Phase slip

  The slip between the liquid and gas phase is one of the key phenomena responsible for a degradation in the performance. Two-fluid models allow for the calculation of different phase flow fields, but an accurate experimental validation is needed.

- Sensitivity analysis

  Once the model is implemented in a computer program, the input parameters can be varied and the effect of bubble size, rotational speed, flow rate, density ratio can be rapidly studied. A careful evaluation of the boundaries setting the validity of the considered physics is needed. In addition, it is desirable the knowledge of the bubble size in the different operating conditions.

The estimation of the void fraction distribution and slip ratio is of key value.
Mechanisms as phase separation, stratification, differential phase kinematics depend on operational conditions and impeller geometry.

Two-phase head degradation

As stated before, multiphase flow impairs pump performance for a variety of phenomena. In [19] a detailed analysis of the phenomena causing head degradation is performed. Results are altered by the definition of the density average, which is called mass- or momentum- depending on the weights.
In the head degradation expression, also considered in [11], the separate contributions of liquid acceleration, slip velocity and void fraction variations can be distinguished. The values describing the velocity and void fraction distribution at the outlet can be either obtained from the analytical model or numerical simulations.

$$\Delta H_{TP} = \frac{p_2 - p_1}{\rho^*_{TP} g} + \frac{v_{2l}^2 - v_{1l}^2}{2g} \cdot (1-x) + \frac{v_{2b}^2 - v_{1b}^2}{2g} \cdot x$$

$$\Delta H_{TP} = \Delta H_{SP} - \Delta H_w - \Delta H_s - \Delta H_\alpha$$

$$\Delta H_{SP} = (1-x) \cdot \frac{v_{u2l}^{1\phi} u_2 - v_{u1l}^{1\phi} u_1}{g} + x \cdot \frac{v_{u2b}^{1\phi} u_2 - v_{u1b}^{1\phi} u_1}{g}$$

$$\Delta H_w = (1-x) \frac{\Delta v_{u2l} u_2}{g} + x \cdot \frac{\Delta v_{u2b} u_2}{g}$$

$$\Delta H_s = (1-x) \cdot \left\{ \alpha_2 \cdot \left(\frac{w_{2b}}{w_{2l}} - 1 \right) \cdot \frac{w_{2l}^2 - u_2^2}{2g} - \alpha_1 \cdot \left(\frac{w_{1b}}{w_{1l}} - 1 \right) \frac{w_{1l}^2 - u_1^2}{2g} \right\} + x \cdot \left\{ (1-\alpha_2) \cdot \left(\frac{w_{2l}}{w_{2b}} - 1 \right) \frac{w_{2b}^2 - u_2^2}{2g} - (1-\alpha_1) \cdot \left(\frac{w_{1l}}{w_{1b}} - 1 \right) \frac{w_{1b}^2 - u_1^2}{2g} \right\}$$

$$\Delta H_\alpha = \frac{1}{\rho^*_{TP} g} \int_1^2 \left(\rho_l \frac{w_l^2 - u^2}{2} - \rho_b \frac{w_b^2 - u^2}{2} \right) \frac{d\alpha}{ds} ds$$

Furuya, in [11], proposes a different formulation for the calculation of the mixture density in case of separated flow.

An alternative decomposition was proposed by Poulikkas in [29]:

Total two-phase head = Liquid kinetic energy head + Gas kinetic energy head - Compression head loss

As also noted by Poullikkas [29], it should be observed again that in order to calculate the quantities ΔH_w, ΔH_s and ΔH_α in the previous equations, detailed data for the relative velocities for both gas and liquid should be known as well as the void fraction along the path of blade through flow.

Previous models

In Appendix III, a summary of the main analytical models [11,19,46-51] based on the streamline approach is reported. Focus is given on the original contribution of each author, along with the main settings and modelling validity.

Analytical models, despite providing acceptable accordance between predictions and experimental data, still present complexity and dependency on empirical closure relationship.

In [52], a combined approach to the impeller design is presented: quasi-3D inverse method and direct viscous flow analysis are employed. Several performance curves obtained from an experimental validation test are then commented. A theoretical method to design the blade geometry is desired. The inverse methods start from the required flow field features to calculate the blade geometry, under the simplification of neglected viscosity: quasi-3D vs fully 3D alternatives are possible. In the combined approach employed (Q3D inverse computation + direct

3D viscous flow analysis) the mixture is assumed a homogeneous pseudo-single-phase medium and, in steady state, the influence of compressibility and the *GVF* variation within a pump stage are neglected.

It should be noted, in addition, that at the design stage it is important to study and account for all the secondary effects of losses, as they can be used as a design improvement; end-wall losses, clearance leakages, disk friction, incidence effects, despite affecting efficiency at nominal conditions, can improve the pump handling capability at a wider range of flow rates and compositions, providing recirculation and causing gas pocket breakage, and affect the machine behaviour at instabilities.

2.7 Performance curves

Hereafter, the typical curves used to characterize the multiphase pump behaviour, showing the effect of operating parameters and the operating zones and boundaries, are presented (Fig. 9).

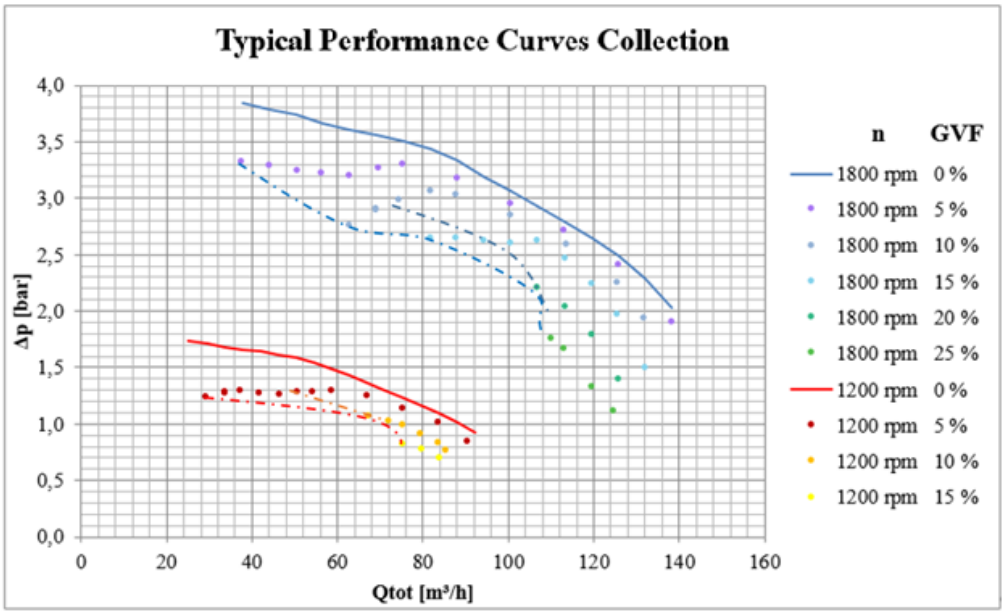

Fig. 9 - Typical performance curves (at p_i = 1 bar, clearance level II, as defined later), showing the effect of flow rates, pump speed and the operating domain

Performance maps are bounded by four characteristic lines, defining the operating range or envelope:

i) Single-phase performance

ii) Critical gas content, corresponding to a full loss of priming
iii) Surging line, marking the onset of the unsteady operating conditions
iv) Choking line at over-load

In Fig. 9, *i)* are the continuous lines, while the *ii)* and *iii)* are dashed. Surging, as later defined, has been observed, in the current research, only between a relative flow rate range of 45 to 75 %, depending on the actual operating conditions.
Since the main focus of this study is on the pump performance degradation and part-load behaviour, the identification of the chocking line, corresponding to the right boundary, is not of primary interest.

The main design objectives are:

- moving the loss of priming line to higher *GVF* values
- minimizing head degradation and losses with decreasing q^*
- broadening the operative range and increasing the efficiency.

Several performance maps and boundaries have been identified and proposed in the past decades, but a lack of theoretical basis to predict surging onset still exists.

The main parameters affecting the pump behaviour and performance are: *GVF*, suction pressure, rotational speed, gas bubbles distribution and dimensions, thermodynamic behaviour of the fluids, impeller geometry. The study of the effect of most of these parameters has been included in the test matrix and will be presented later in Ch. 6.

2.8 Instabilities at low flow

Turbomachinery operational principle is based on the modification of the flow field and a work transfer from the blades to the fluid. A specific operating range is considered at the design stage in order to make the flow and machine angles match. Operation at part-load is characterized by a more complex combination of mechanisms, covering a broader range of phenomena and disturbances, which result in the coexistence of very fine bubbles, due to the high shear in the boundary layers of the tip gap, and a larger gas pocket on the blade pressure side. Even though these ones are not necessarily negative, as specific flow mechanisms like recirculation at part-load can improve the pressure production and increasing turbulence levels widen the two-phase handling capability, off-design operation introduces a broad range of secondary flows together with disturbances and losses which cause irregular stresses and vibrations on the mechanical components; an alternating thrust will lead to higher shaft stresses and bearings and seal problems, these last representing a particularly delicate aspect in subsea applications, where reliability is a major concern.

One of the main goals of the current research is to relate the machine outer measurements, implemented in condition monitoring, to the originating flow mechanisms; this can provide very useful information for an improvement of the hydraulic design.

2.8.1 Surging definition and onset detection

A broad literature is available on part-load phenomena in compressors; these machines, run at constant speed, experience aerodynamic instabilities (rotating stall and surge) when the volume flow is progressively reduced, limiting their operating range. Different stall structures exist, and can be detected through frequency or time-frequency analyses of the pressure oscillations and vibrations.
In analogy with surge in centrifugal compressors, instabilities in pumps restrict the stable operation zone.
For single-phase pumps, as a criterion to guarantee stable hydraulic operation and limited recirculation, a minimum stable flow is considered; according to the API 610 Standard, two definitions of minimum continuous flow exist:

- Thermal flow, *maintaining the liquid temperature below that at which* $NPSH_a = NPSH_r$
- Stable flow, *allowing operation without exceeding the noise and vibration limits imposed by the Standard*

The proper minimum requirement corresponds to the second definition, being a function not only of the *NPSH* margin available, but also the energy level of the pump, the hydraulic design of impeller and casing and the characteristic of the fluid being pumped (correction factors for hydrocarbons operations minimum flow are available).

For a pump operating a two-phase flow, both the shape and location of the surging line are influenced by the actual operating condition, specifically the density ratio and gas volume fraction. The mechanism initiating the surging and causing pump-head breakdown is still unknown, due to the lack of ground knowledge and measured data as phase fractions, velocities, pressure and bubble size. The models predicting this transition are of empirical nature, thus strongly dependent on the pump geometry.

Hereafter, the contribution of the other authors:

- Lea and Bearden [28]: the surging point corresponds to the onset of the intermittent gas-locking regime; pump instability coincides with surging
- Sachdeva [48]: surging occurs when the gas velocity becomes zero; the used 1D model requires a closure relationship (ratio of C_D to bubble size in this case)
- Cirilo [53]: pump instability is related to intake conditions (pressure increases improved the surging behaviour), pump speed (analogue effect as increasing p_i) and number of stages. A correlation for the maximum gas fraction, as a function of the suction pressure, is provided
- Turpin [36] and Romero [54]: correlations to determine the limiting flow under which surging occurs are provided
- Minemura and Uchiyama [55]: the initiation of surging point is caused by a transition from a bubbly flow to slug-flow-like flow pattern; the critical *GVF* at which surging occurs is a function of q_l; in addition, reversed flow is observed

- Estevam [32]: from a visualization study, a correspondence between surging onset and a transition of the flow regime is found; at surging initiation, the bubbles present a critical size
- Pessoa [3]: surging is a phenomenon involving cycling fluctuations of the system pressure; gas locking is similar to the loss of prime condition, while during gas blocking a severe gas accumulation reduces the head but the pump still works
- Prado: the initiation of the surging point is related to the bubble size and the forces acting on bubbles: bubbles of a certain size cannot run away from the impeller as an equilibrium is reached between the buoyancy and drag forces; a bubble larger than the critical size will flow back and eventually coalesce, forming the gas pocket, which initiates the surging condition
- Barrios [4]: surging is triggered by bubbles reaching a radial equilibrium position at the inlet of the impeller channel. An equation for the critical *GVF* leading to surging is proposed, based on the radial equilibrium position of a bubble in a rotating field and relating the critical *GVF* to machine speed, liquid density and surface tension, inlet radius and critical bubble size at surging; others have later proved that this equation under-predicts by orders of magnitude the real critical value
- Gamboa [7]: surging is associated to gas pocket formation or, more in general, to the transition between a homogeneous regime and either a stable gas pocket or a segregated gas regime at low liquid flow rate; the gas pocket behaviour depends on q_l: unstable over the BEP (reaching stability only at high *GVF*, when it is segregated at the top shroud, as stratified flow in pipes), stable below
- Zhang [34]: fluctuations in the pressure, flow rate and power are related to the appearance of a gas pocket flow pattern, characterized by irregular ellipses shaped bubbles, closely gathered to eventually form a gas pocket at the hub; the chordwise location of the gas pocket and its size varies in the following stages, mainly due to gas compressibility.

Each of these hypotheses will be verified and commented, for the studied case, in Ch. 7.

2.8.2 Test procedure

The testing procedure, strictly linked to the way instability zones are approached, can affect the quality of the prediction, due to transient phenomena and different curvatures of the performance characteristics. The exact identification of the inception requires a very careful approach, progressively varying the operating parameters at small steps or continuously (transient test), this last needing a proper control system and instrumentation with a short response time.

As reported in [10] too, the switch in the flow pattern occurs at different values of reduced flow rate, depending on whether the flow rate is reduced or increased. A hysteresis due to the flow pattern switch can exert a major influence on the axial thrust and constitutes an important issue for the mechanical equipment safe operation and duration.

Two main different test procedures are followed:

- Mapping test: at constant gas volume fraction, the total volume flow rate is reduced. The local flow speed is varied and this causes phase mixing and gas accumulation; in addition, recirculation and cross-flows develop.
- Increasing *GVF* test: keeping the same total volumetric flow rate, the normalized gas flow rate is progressively increased; the local flow velocity (besides slip, playing a major role at high gas contents) is maintained constant, while instabilities and performance degradation occur due to gas blocking.

Prado et al. [7] pointed out that the determination of the surging onset is more difficult in this second case as it corresponds to operating conditions where the curve curvature changes.

2.8.3 Parameters and measurements

The accurate characterization of the surging condition will provide the necessary relation between the originating flow mechanisms, including their inception and evolution, and the resulting variations in the flow field variables, which can be measured both locally and over the whole machine.
The main parameters, in mean values and variations, are: pressure increase, pressure ratio, liquid and gas flow rates, inlet pressure, pump rotational speed.
The main instabilities effects are pressure pulsations, resulting in oscillations in the delivered head, eventually leading to performance breakdown, flow rate and torque fluctuations, vibrations, recirculation and secondary flows through gaps and seals.
Therefore, the detection of the related physical phenomena might involve the measurement of the liquid layer at high *GVF*, the maximum bubble size, increased pressure pulsations and a discontinuity in the performance curve. If the hydraulic channels are optically accessible, an indicator is the observation of a flow pattern change.

To detect flow pulsations, fast-response dynamic pressure sensors (installed in static and rotating locations) coupled with a high-sampling rate acquisition system are employed, to provide a temporal and spatial reconstruction of the flow field. However, the impact of multiphase flow is expected to alter the response of the transducers, as the alternation of liquid film and bubbles causes additional pressure pulsations, making the identification of the instability onset more difficult. The additional measurement of other parameters affected by the instabilities is, thus, required to overcome these uncertainties.

2.8.4 Previous studies

According to Esson and Cohen [56], the helico-axial concept is the least prone to develop instabilities and presents a broader stable flow domain, compared to Electrical Submersible Pumps [4] or centrifugal pumps [13,28]. The studies in [41] and [57] have provided interesting observations and made use of techniques which might be taken into account for a further analysis of the pump considered in this specific research. The authors in [7-8] extensively studied the effects of the different operating parameters on the surging phenomenon; a correlation for the surging

onset and a very interesting map, as shown in Fig. 10, summarizing the performance characteristics transitions, are obtained. A summary of each author's original findings is reported in Appendix IV.

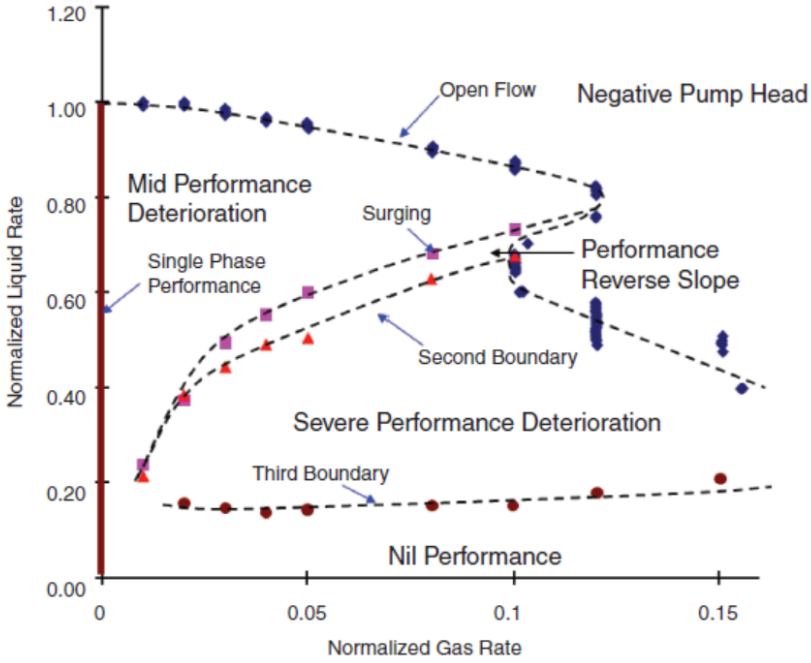

Fig. 10 - Electrical Submersible Pump operating regimes (taken from [7])

In relation to the current research, it should be noted that the particular operating range tested in this specific study (low suction pressure and limited rotational speed) enhances the instabilities: their onset appears earlier and their evolution is quicker. The proper capture of the surging inception and behaviour finds a limit in the relatively long response time of the static instrumentation installed on the machine (pressure and flow sensors).

2.9 Conclusion

The available literature has been carefully reviewed, with regard to these main topics: flow visualization, performance testing, modelling, part-load instabilities. Previous researches managed to cover successfully some of the issues of multiphase pumping. However, they present limitations as they are strongly dependent on the pump geometry and hydraulic design. Therefore, the analyses needed to understand the flow phenomena originating performance degradation and instabilities have to be performed on the specific pump model.

This study has, however, provided a very valuable insight into the analyses and methodologies previously adopted; the opportunity of including the most relevant ones is taken into account in the design of the new test rig, which has to allow to perform the necessary investigations.

Chapter 3
The MultiBooster® Project

3.1 Objectives

The research consists in the study of a multiphase pump stage performance in a laboratory setup, testing its ability to handle multiphase flows with a broad range of gas-liquid compositions. In order to allow this, a specific test rig had to be designed and commissioned.
The candidate has been led by and has coordinated the centres in Tranby - Oslo and Trondheim.

The main contribution within the collaboration with the company is providing a complete mapping of the multiphase performance of one stage of a scaled version of the Aker Solutions AS Multibooster® pump along with an increase in the knowledge of the flow mechanisms fundamentals. On the characteristic map, performance regimes and flow pattern transitions are linked.
The commercial MultiBooster® is a multistage pump, with semi-axial shrouded impellers and vaned diffusers; the hydraulic design is progressively adjusted to accommodate the volume flow reduction due to the gas-phase compression.

For an optimal flow behaviour, sudden accelerations, strong pressure gradients, sharp geometry variations, have to be limited. This results in very long blade channels with progressively varying blade angles, and an inner to outer diameter ratio which is quite high, this to reduce the occurrence of radial motions.

The full-scale pump installed at the Tranby - Oslo manufacturing and test facility comprises 8 stages and is operated at high-speed in a closed pressurized loop; the main result of this testing has been obtaining a detailed performance curve and validating CFD predictions under realistic operating conditions, featuring high values of rotational speed, suction pressure and volumetric gas content.

3.2 Design considerations

In order to perform the necessary analyses, convenient design modifications are required.
The following three key aspects have been the main topics of discussion.

I. Visualization in the pump channel

The study of multiphase flow phenomena inside the impeller requires an accurate visualization and the investigation of the whole hydraulic channel. This is usually done through the installation of pressure sensors on the impeller blades surfaces and on static locations as casing wall and diffuser, and flow visualization making use of high-speed imaging and advanced techniques.

A compromise among costs, mechanical resistance issues and disturbances introduced on the flow is necessary and imposes a spatial discretization of the analysis probes locations.

The installation of pressure sensors on blades surfaces alone would not provide a proper description of the typical features as flow patterns, bubbles formation, coalescence and breakdown and the pump blockage phenomenon. This requires, in addition, the recording of images through a high-speed acquisition camera, to trace the pressure pulsations origin – from local transients or multiphase phenomena.
These techniques, already adopted on water turbines, if performed on a shrouded impeller, rotating at high-speed and relatively high pressure, would introduce challenges and limiting constraints in the pump construction, mainly linked to the difficulty of making appropriate PMMA windows, presenting limited resistance at high pressure, properly lightning the dark, thin channels and gaining access to small areas, where the camera can be placed. Therefore, the initially considered shrouded impeller, mounted in a metallic casing, tested at high-speed and real operating pressure in a closed and pressurized test-loop, has been abandoned: in this case visualization would have only be available at the inlet and on the diffuser. Even the construction of an impeller with see-through windows on the shroud would not allow to have a proper visualization of the impeller channel, due to the long-thin blades, which would require multiple cameras locations, weakening the mechanical structure, and finally the presence of leakages and vortices in the shroud – casing clearance, making it difficult to get a clear visualization of the impeller flow.
A fully axis-symmetric construction has been chosen, to avoid fluid- and roto- dynamic unbalances.

II. Pump layout

For the scaled model, an overhung design has been chosen, to ease the access to the impeller and its eventual disassembly.
According to the considerations above, the construction of an unshrouded impeller and a plexiglass casing has been decided, in order to achieve the desired objectives. This is tested at a wide rotational speed range (from low to medium, 600 – 2500 rpm) and low pressure; visualization in the pump is possible all along the flow path using a high-speed camera focused on different zones. The tip vortices forming due to the absence of the shroud will affect the flow and the pump performance. This pump set-up will allow to improve the blade design and conceive new concepts.
In a following stage of the project, the impeller can be shrouded and installed in a metallic outer casing, to improve the mechanical strength and allow tests at medium to realistic rotational speed range (1800 – 4000 rpm). In this case, the shroud hinders any recirculation path across the blade tips.
The installation of dynamic pressure sensors on the impeller blades will be considered in a following stage of the project; as the installation of the signal transmission system on the shaft affects the rotor balance, a thorough preliminary feasibility analysis is required.

III. Overall test facility arrangement

In an open loop layout, the operating parameters can be varied very rapidly, allowing to perform tests over a wide range of parameters values at small steps, and transient tests too. In addition, the influence of the overall system on the pump behaviour is reduced. However, tests at increased

suction pressure, as performed later in this research, require both the gaseous and liquid phases to be supplied at higher pressure values by additional devices, with a supplementary energy consumption. The air is derived by the building pressurized air system, available at 8 bar (a), while the water flow is provided through a centrifugal pump, which was already in place and with the necessary capacity (P = 160 kW, Q_{max} = 200 m^3/h, p_{max}= 16 bar).

3.3 Test planning

An accurate test plan is scheduled in order to cover the main research topics and accomplish the desired objectives. Initially, the machine and test rig capabilities are explored; afterwards, a comparison with the real machine in terms of curves shapes and performance degradation has been performed. The effects of the reduced values of flow and machine parameters and the disturbances introduced by the top-shroud removal have been investigated. Finally, some characteristic operating conditions have been thoroughly studied, focusing on their origin and evolution, through the aid of flow visualization.

A Gantt chart with the milestones is included in Appendix V.

3.4 Expected results

To achieve one of the main research objectives, experimental data gathered from several tests carried out over a wide range of operating conditions are recorded under performance curves and show the effects of variations in tip clearance, suction pressure, flow rate, mixture composition and pump speed.

According to available literature data, a broader operating range, when the pump rotational speed and inlet pressure are increased, is expected; higher values of the rotational speed reduce the maximum possible bubble diameter, while the inlet pressure affects the density ratio, limiting separation effects. Testing at very low suction pressure will go through cavitation problems, especially with regard to the rotational speed upper limit, and reduced gas-handling capabilities, at low rotational speeds, resulting in a very narrow operating range.

The joint collaboration with the company is expected to result in a better understanding of the fundamentals but at the same time to produce technically and economically feasible solutions, suitable to be implemented in a real world context.

Chapter 4
Test Rig Design, Building and Testing

As stated in the previous chapter, a considerable amount of time of this doctoral study has been devoted to the design and construction of a test facility allowing to perform extensive analyses on the machine performance and stability, and detailed and local visualization of the flow mechanisms, with room for future installation and application of advanced analysis techniques.
Hereafter, the design procedure is reported.
The preliminary discussion has involved the industrial partner and the pump equipment construction has been commissioned to PTM Norway AS. The laboratory team has assisted the mounting and connection of the whole test rig.
In order to allow the study of the inlet flow and ease the assembly unmounting, an overhung design has been chosen. The pump shaft is oversized in order to handle with the alternating stresses caused by the surging and transient conditions. This issue is particularly critical since the impeller is running with a very low tip clearance inside a PMMA® outer casing. A preliminary rotodynamic assessment has provided the overall sizing of the pump – bearings assembly. The double-row angular contact and the roller bearings are mounted in a hub which can be axially moved inside an outer pedestal. The tuning of the whole rotor axial positioning allows to precisely vary the impeller tip clearance, which has proved to play a major influence on pump performance. This value has been initially taken at a relatively high level (around 1,5 mm) when the initial tests were performed, in order to assess the rotodynamic behaviour and preserve the delicate casing. This first testing was successful, and the rotor has been progressively moved resulting in a reduction in the tip clearance down to 410 μm, which allows a satisfactory flow visualization, reducing the influence the tip leakage flow exerts.
In order to keep the costs and power requirements limited, only a single stage pump has been considered.
The hydraulic design reproduces the Aker Solutions AS MultiBooster®, but the removal of the top shroud has been necessary to allow flow visualization. The impeller and diffuser stage are scaled at 80 % of their original value. This allows to reduce the components sizing (the flow rate, directly influencing the whole system and instrumentation sizing, becomes 0,51 times the original value, while the power requirement only 0,33 times). An additional constraint on the system sizing is given by the pressure resistance it has to guarantee.
The rated operational values for the full-size pump are p_i = 10 - 50 bar and n = 3000 - 6000 rpm. Safety issues impose to limit the operating pressure, which is also linked to the sizing of the separator tank. An open loop scheme has been chosen, with the air phase coming from a high-capacity pressurized reservoir, which was already available at 8 bar (a) and its pressure is regulated through a valve, and the water, stored in an open tank, flowing through a centrifugal pump, which provides the desired inlet conditions. An overall view is shown in Fig. 11. When transient tests are performed, a bypass line can exclude this pump and the water flow is derived directly to the pump

inlet, thus excluding the response this component gives, which might affect the multiphase pump stability.

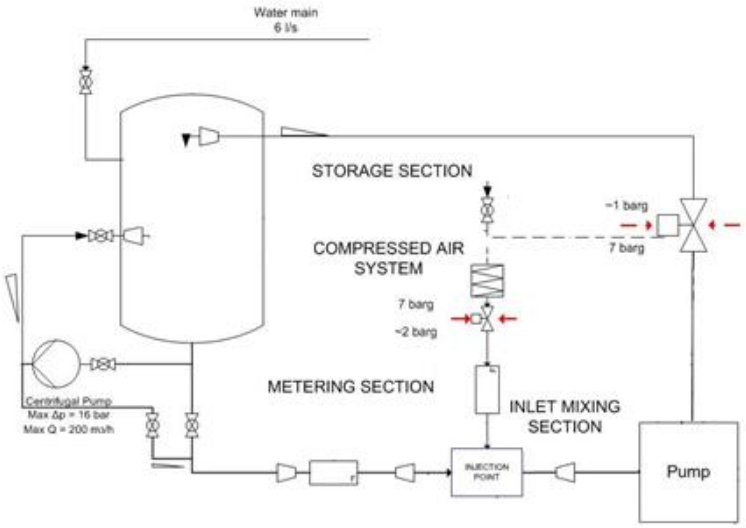

Fig. 11 – Test rig layout

The initial orientation was towards a metal casing with just a small window where to install the high-speed camera and lighting system; however, a different design has been decided, featuring a full 360º thick PMMA casing all around the rotating and static stage. This provides an easy access to the hydraulic channels, a more homogeneous lighting, and room for the implementation, in a further stage of the project, of advanced visualization techniques. The casing is made of two shells which are held by a strong metallic barrel; some metallic elements installed in the barrel arms provide room for the sensors placement. Figure 12 shows the construction. The non-metallic casing limits the equipment rated pressure, which is set at 8 bar (a).

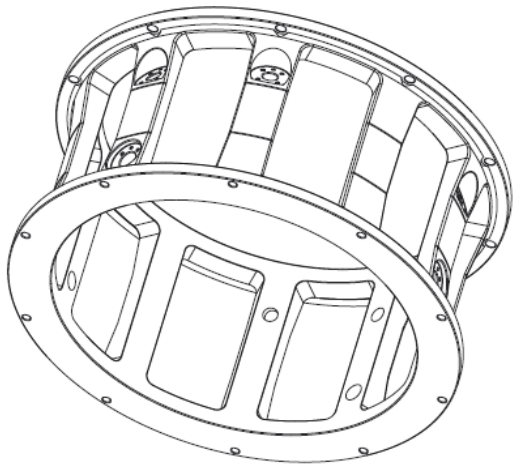

Fig. 12 - Metallic outer barrel holding the transparent casing; the locations where the pressure sensors are installed are visible

The rated values for the electric motor are: n = 1465 rpm, P = 30 kW, V = 230 V, I = 97,5 A, cos φ = 0,85.

The motor is driven by a frequency converter which can vary the voltage and thus increase the shaft rotational speed up to 4000 rpm. The Variable Speed Drive rated power is P = 56 kW.

The design pump speed is, as a first attempt, limited to 2500 rpm, taking into account the shear stresses which could wear the casing and the pressure production, limited by the equipment rated pressure.

It is known that lower turbulence intensities and higher density ratios enhance phase separation; the operational window is reduced and instabilities are expected to appear earlier. How the different sets of operating conditions affect the performance curves shape, the surging line location and the flow physics, is one of the subjects of the research study.

Once the main size and pump layout is chosen, focus is given on the inlet section arrangement, with the water injection apparatus, and the volute and mechanical coupling with the electrical motor. The pipes lengths are chosen so as to provide a regular flow through the flow-meters; a particular importance, especially in determining the system response to pump surging oscillations, presents the length between the pump volute outlet and the choke valve: moving it further away from the pump increases the pressure fluctuations amplitude, while if moved closer, it dampens the pulsations amplitude, which are further reduced and dissipated by turbulence in the valve.

As to the operating fluids, fresh water and air are selected as the liquid and gas phases, respectively. The main advantages they present are linked to safety, environmental and costs issues.

4.1 Layout

Figure 13, obtained from the 3D modelling tool used for the design, shows the final test rig layout. The Piping and Instrumentation Diagram is enclosed in Appendix VI.

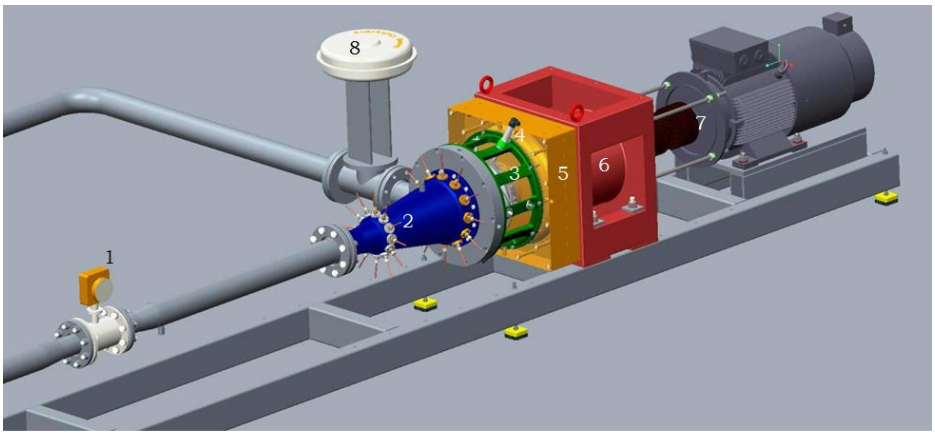

1 - Water Flow Meter
2 - Air Injection Section
3 - Pump Transparent Casing
4 - Local Instrumentation
5 - Volute
6 - Bearing Pedestal
7 - Coupling and Motor
8 - Choke Valve

Fig. 13 - Lab overview

4.2 Main components

4.2.1 Air injection section

Pressurized air is derived from the building reservoir and filtered. The pressure upstream the injector is regulated through a valve, according to the desired test suction pressure. When a high gas flow rate is required, the injection pressure can be increased.

For the injector, different alternatives have been considered; this device should provide a good mixing with the minimum possible pressure loss.

The first design consisted in injection holes drilled in the inlet section blade-profile shaped supports; this solution would allow having a constant flow cross section towards the inlet, avoiding sudden pressure variations and providing a symmetrical flow-pattern before the inlet.

A simpler and cheaper alternative is placing multiple nozzles in the inlet pipe: these devices are symmetrically mounted in the pipe wall, in order to avoid obstruction and pressure losses in the main flow, and inclined towards the flow direction to provide a homogeneous phase distribution in the cross section. Their depth can be varied screwing the nozzle, as it is visible in Fig. 14.

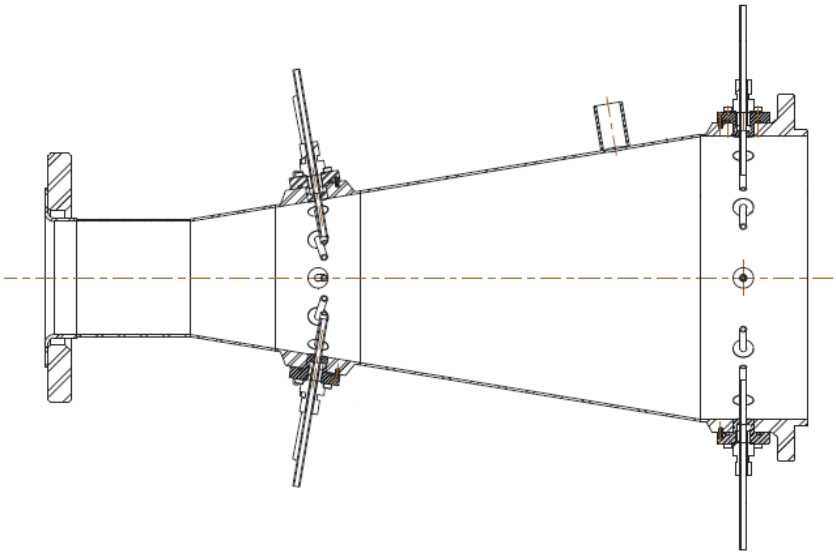

Fig. 14 - Sectional view of the injection section

If stratification is observed before the inlet, due to the low pressure, just some nozzles can be used. Furthermore, air injection only from periodically chosen locations can help performing stall and stability tests.
Air is injected through nozzles of different sizes, depending on the desired amount of gas. The first injection section, located 500 mm upstream of the impeller inlet, is preferred, helping the phases to mix properly. A comparison between the use of nozzles of different sizes and at different reservoir pressures, to obtain the same flow at the inlet, has shown no impact on the differential pressure production and no relevant variations in the bubble size distribution and regularity. However, it should be mentioned that it is difficult to compare the last parameter, as coalescence and breakup occur continuously in the inlet pipe.

4.2.2 Pump inlet

In the current design, the bull nose can be either static, held by eight NACA-profiled supports, or rotating, when directly attached to the impeller. In Fig. 15 the assembly mounted in the static configuration is shown.
In a further stage of the project, variable pitch inlet vanes will be considered, in order to investigate the effect a pre-rotation component can have on pump performance (increasing the absolute velocity without varying the pump speed) and stability at different flow rates.

However, while the introduction of an inducer-like device could be beneficial, according to previous researches and experiences [10], it is expected a negligible influence of the inlet flow regime for this type of pumps.

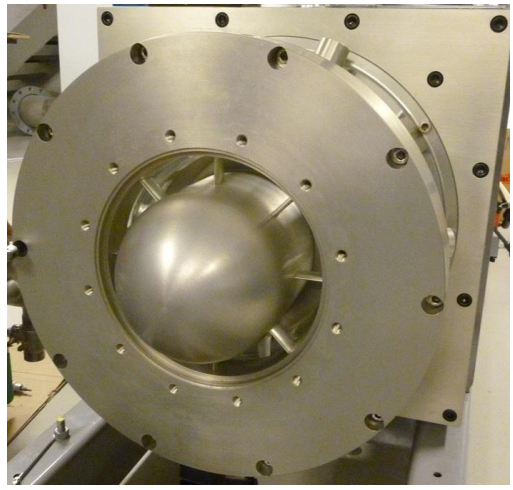

Fig. 15 - Pump inlet

4.2.3 Pump scaling

A compromise needs to be made among the operational parameters, as the pump scaling mainly affects the flow rate, and therefore the overall system size and equipment costs, while the rotational speed and suction pressure affect the fidelity to the real machine; finally, some limitations are imposed by safety issues, especially on the operating pressure.
In single-phase phenomena, the similarity theory requires similar velocity, temperature and pressure fields. In addition, multiphase flow requires the knowledge of the density (or of the void fraction) distribution.
The bare geometrical similarity does not guarantee the involved hydrodynamic and thermodynamic physics to be respected, as the non-dimensional numbers impose different constraints on operational and design parameters. Respecting simultaneously all the non-dimensional numbers is not possible; no comprehensive scaling laws are available for two-phase flow, so, usually, a prevalent physics is chosen to be prioritized after carefully assessing the importance of the different physics involved, this leading to the so-called “distorted-models”.
Ishii [58], performed a perturbation analysis based on the one-dimensional drift-flux model to obtain the similarity groups. Sterrett [20], performing tests on a centrifugal pump operating a two-phase flow, reported discrepancies between a scaled model and the full size one.

In this specific case, the main costs and safety constraints have determined the final scaling; the study starts from the current equipment; the operating parameters are progressively increased towards the highest values to define the main trends.

4.2.4 Centrifugal pump

An already available centrifugal pump, rated at P = 160 kW, Q_{max} = 200 m^3/h, p_{max}= 16 bar, is connected in series to the multiphase pump when tests at higher suction pressure need to be performed.

4.2.5 Bearing cooling system

A bearing cooling system is designed to maintain the bearings balls and rollers well lubricated and cooled. The inlet and outlet oil temperatures are constantly monitored and the cooling water flow is adjusted so as to maintain the desired oil temperature. Details of the cooling loop are reported in the P&ID, included in Appendix VI.

4.3 Instrumentation

The choice of the suitable instrumentation needs to take into account different aspects; instruments transform the variation of a physical quantity into a signal, and are based on different principles; once the desired range is determined, a special care in the choice is given to:

- accuracy, repeatability, reliability
- response time has a key importance for the pressure sensors involved in providing data for the time-frequency analyses
- the evaluation of how much the sensor affects the flow field
- costs.

Resistance to harsh environments is not an issue in this application, as the main fluids are not dangerous; however, water might cause corrosion and some particles are present in the pressurized air coming from the main reservoir. A filter is installed upstream of the air conditioning section.
A certain straight length of unobstructed manifold is usually required both up- and down- stream of the flowmeters.
If possible, instruments with the widest turndown (ratio of the maximum and minimum flow rates which can be measured within the instrument accuracy range) should be chosen.
The location of the sensors is presented in Fig. 16.

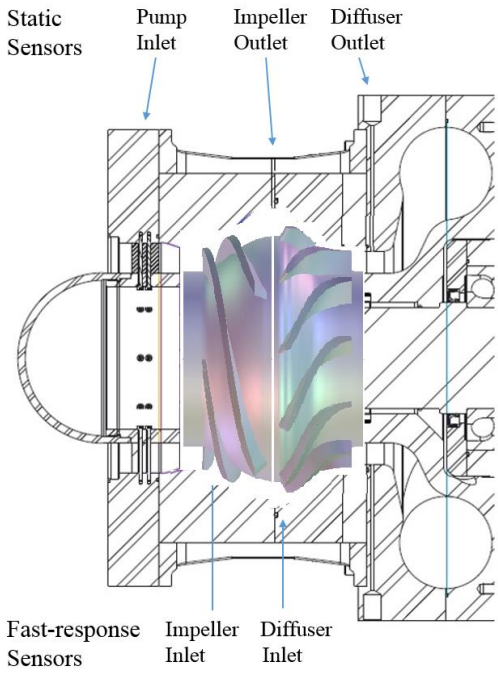

Fig. 16 - Pressure sensors location

In addition to the usual desired features, the fast-response pressure sensors present specific requirements: a high resonant frequency, a low rise time, and low-frequency response. A summary of the main parameters of these instruments is reported in Tab.1, while their flush-mounting on the casing is shown in Fig. 17.

Manufacturer	PCB Piezotronics
Model	113B28
Operating Principle	quartz piezoelectric element
Measurement Range	344.7 kPa
Sensitivity (±15 %)	14.5 mV/kPa
Maximum Pressure	6895 kPa
Resolution	0.007 kPa
Resonant Frequency	≥500 kHz
Rise Time	≤1.0 μ sec
Low Frequency Response (-5 %)	0.5 Hz
Non-Linearity	≤1.0 % FS

Table 1 – Specifications of the fast-response pressure sensors

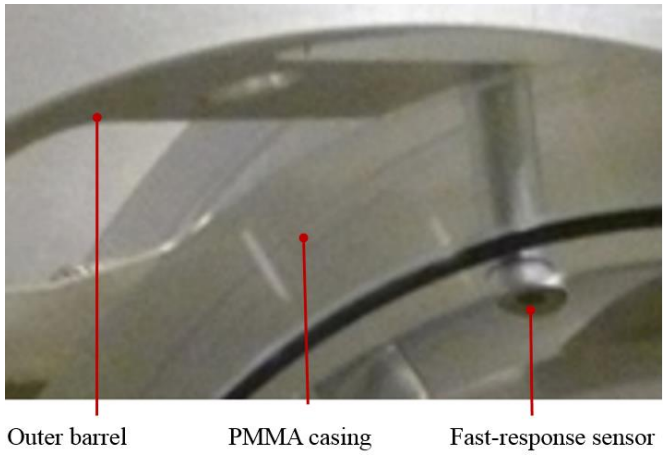

Fig. 17 - Particular of the fast-response pressure sensors installation

Table 2 reports the main features of the instrumentation installed on the test bench.

Parameter	**Instrument Uncertainty**	**Working Principle**	**Manufacturer**	**Range**
Pressure	± 0,1 %	Piezoelectric	Aplisens	0 – 7 bar(a)
Water Flow	± 0,4 %	Electro-magnetic	ABB	0 – 200 m^3/h
Air Flow	± 0,5 %	Thermal	Bronkhorst	0 – 200 m^3/h at normal conditions
Motor Speed	± 0,15 %	Encoder	NPN	0 – 10000 rpm
Temperature (flow)	± 0,3 %	Thermo couple	Aplisens	0 – 60 ^oC
Temperature (bearings oil)	± 0,1 %	RTD	Endress+Hauser	0 – 150 ^oC

Table 2 – Details of the instrumentation

4.3.1 Standards

The permissible values of measurement uncertainties are within the ranges specified in the Standard ISO 9906 (reported in Tab. 3); in addition, when performance points are recorded, the fluctuations of the measurand are taken into account too. Reference is made to grade 1. It is remarked that this has, however, to be taken as a guideline, as it is referred to single-phase operation. In addition, the different Standards present different requirements, related to efficiency or power. The development of a thorough performance calculation procedure, involving the polytrophic calculation for the two-phase flow, is therefore desirable and will be considered later.

Parameter	Instrument Uncertainty	Permissible Overall Uncertainty	Permissible Amplitude of Fluctuations
Pressure	± 1,0 %	± 1,5 %	± 2 %
Water Flow	± 1,5 %	± 2,0 %	± 2 %
Air Flow	± 1,5 %	± 2,0 %	± 2 %
Motor Speed	± 0,35 %	± 0,5 %	± 0,5 %

Table 3 – Uncertainties of the instrument and permissible overall uncertainty and fluctuation from the ISO Standard 9906

4.3.2 Calibration

The instrumentation suppliers provided a calibration certificate in the desired range. Corrective factors are used when the test conditions differ from the calibration rated values.

4.4 Equipment pressure rating and testing

As usually done with pressurized equipment, the main loop section has been tested at 10 bar (a) and the leakages and pressure drop recorded over one hour.

4.5 Data acquisition system

A complete data acquisition system is installed; it features a National Instruments C-Rio 9068 platform, on which the specific boards are placed, and where all the necessary signal conditioning is performed. The flow, low-frequency pressure and temperature sensors are connected to an analog current, 4-20 mA, input board; the choke valve, pneumatically actuated, is governed by an analog current output signal, while the vibration and fast-response pressure sensors provide a voltage output, amplified by a dedicated device.
This system is connected to the control PC, where the specific program in LabVIEW® allows the user to control the test rig. From the main monitor, reported in Fig. 18, the user can command the motor and valves, log the files and monitor the values in real-time.

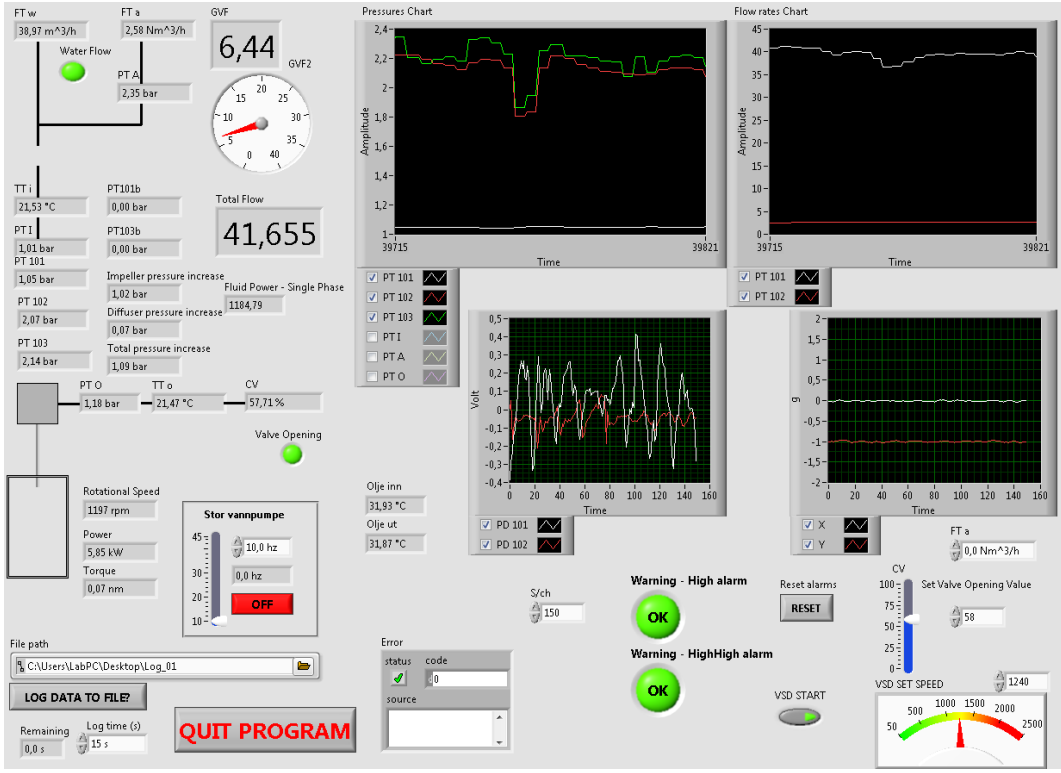

Fig. 18 - Visual interface of the user's monitor

4.6 Data processing

The data acquired in LabVIEW are stored in log files. Depending on the desired analysis, they can be processed in different ways. When performance curves need to be obtained, the raw data are processed in a MathWorks Matlab® script, which performs the statistical analysis. DIAdem®, from National Instruments, is used when the time evolution of the different parameters needs to be investigated or to obtain the Fourier transform, thanks to the fact this software allows to easily create numerical channels useful to compare data acquired at different frequencies.

4.7 Risk assessment

A careful risk assessment has been performed, in compliance with the Standards in force.
The test rig is divided into main nodes: water and main pump loop, air supply, bearings oil cooling pump, centrifugal pump. All the possible sources of risk, events and faults are identified and an assessment is given considering a combination of the probability of occurrence and the

consequences. A formal test procedure, including the necessary care, has to be signed and followed each time the test rig is operated.

4.8 Conclusion

The design process has carefully taken into consideration the desired objectives: the possibility to perform flow visualization with the minimum possible modifications of the original design and the inclusion of room for the installation of additional sensors. It has resulted a very flexible laboratory suitable to test a good combination of the operating parameters; the current capabilities allow to investigate the lower- to mid- range of rotational speed, suction pressure and gas volume fraction. A solid design of the rotodynamic components allows to test at a very reduced value of the impeller tip clearance, limiting the disturbances on the flow and improving flow visualization. Tests at higher gas contents, for performance evaluation purposes, will be planned in a future test campaign. Further updates of the current equipment will follow the needs of future investigations – tests with different fluids, use of tracers and implementation of PIV, closed loop, among others.
The test rig is designed to allow future detailed analyses of the pump response to varying inlet flow composition, ranging from water to almost gas, and transient conditions as closing pump discharge, flow rate modification at constant speed, speed increase at given flow rates. This will also allow evaluating the necessity of a buffer tank or devices to prevent gas accumulation and locking.

Chapter 5
Investigations

The main focus of this study is to relate the pump behaviour and instabilities to flow phenomena in the pump channels, and study the influence of operating parameters (pump speed, flow rates and pressure, mixture composition) on the machine performance and operating range. In a further stage of the project, when advanced visualization techniques are implemented, some typical parameters used to characterize multiphase flow interaction, as the bubble size and liquid film thickness, will be investigated in order to validate the prediction models.

The initial objectives have been:

- To explore the machine capability, corresponding to the ranges in which it provides stable operation, forming the pump operational envelope
- To characterize the performance at different conditions; these ones include machine settings (tip clearance, rotational speed), fluid characteristics (mixture composition) and inlet flow field (flow rate and pressure).

Afterwards, specific flow phenomena are studied, making use of high-speed imaging aided by the analysis of the pressure signals.

5.1 Test procedure

Single-phase testing initially allows to validate the manufacturer's curves and CFD predictions; reference values are obtained for q and Δp, then used to make performance data become non-dimensional.

The two-phase performance tests involve a progressive reduction in q_{tot} at constant n and GVF; a characteristic set of (q^*, GVF) corresponding to surging onset, is detected. All these curves define the operational envelope as later presented to the customer.

The two-phase increasing GVF tests are performed at constant n and q_{tot}, while the GVF is progressively increased until the maximum value at which pump blockage occurs is reached. The GVF is usually varied at steps of 2 or 5 %.

All the two-phase curves are intended taken at the same suction pressure level, when not specifically stated.

Each time the test rig is operated, the formal test procedure is followed. After verifying the equipment integrity and switching on the electrical and signal connections, the pump is started at low speed for some minutes. For performance testing, the pump is run at constant speed for around 30 minutes, until a stable bearings oil temperature is reached. After the operating conditions are varied and the parameters get stable, the data are recorded for 30 s.

As stated earlier, the different test procedures affect how the unstable conditions are approached.

The outcome of the performance tests is reported in Ch. 6, while the accurate study of characteristic operating conditions is the main focus of Ch. 7.

5.2 Test matrix

The test matrix is summarized in Tab. 4.

Parameter	Range
Gas Volume Fraction, *GVF*	0 – 35 %
Nominal flow rate, Q_{nom}	125,6 m^3/h at 1800 rpm
Relative Volume Flow Rate, q^*	30 – 110 %
Rotational Speed, n	600 – 2400 rpm
Inlet Pressure, p_i	1,0 – 2,0 – 3,0 – 4,0 bar(a)
Density Ratio at Inlet, δ_i	840 – 420 – 280 - 210
Impeller Tip Clearance	Three Levels

Table 4 – Test matrix

When the effect of a parameter is studied, depending on the specific investigation, the input value is varied at the regular steps specified in Tab. 5.

Parameter	Common Step
GVF	2 or 5 %
q^*	5 or 10 %
n [rpm]	200
p_i [bar]	1

Table 5 – Test parameters steps

However, when a particular operating condition is the main focus of the investigation, as the approach to the surging point, the considered parameter step is progressively refined towards the point of interest.

Visualization tests are started with little air content, around 1 % in volume, in a passive tracer fashion, to study if the flow mechanisms at single-phase operation are already responsible for flow field modifications.

5.3 Flow visualization

5.3.1 Apparatus description

The test facility has been specifically designed to allow flow visualization in multiple locations. Direct visualization of multiphase flows provides a very detailed description of the flow structures and mechanisms. The use of a stroboscopic light constitutes a reasonably cheap technique. Along with a High Definition camera, it allows to identify the flow regimes and the air accumulation

zones, and to capture interesting pictures of tip leakage and cavitation streaks. Since the flow phenomena involved in this study present a broad range of spatial and temporal scales, and the flow field needs to be studied at different locations too, multiple tools are useful in the analysis; visual investigations already provide a good insight into the low-frequency, broad flow field oscillations. This technique finds, however, a limit in the unsteady and irregular fluctuating nature of the flow mechanisms here considered; therefore, the succession of sharp individual photographs of the flow structures, provided by high-speed imaging, is needed.

For these investigations, in order to provide a spatial reconstruction of the flow field, the fast-response pressure sensors are placed at the same location of the high-speed camera. The visualization window is shown in Fig. 19. Figure 20 shows the visualization equipment set-up: the high-speed camera is combined with a 400 W tungsten light bulb projector.

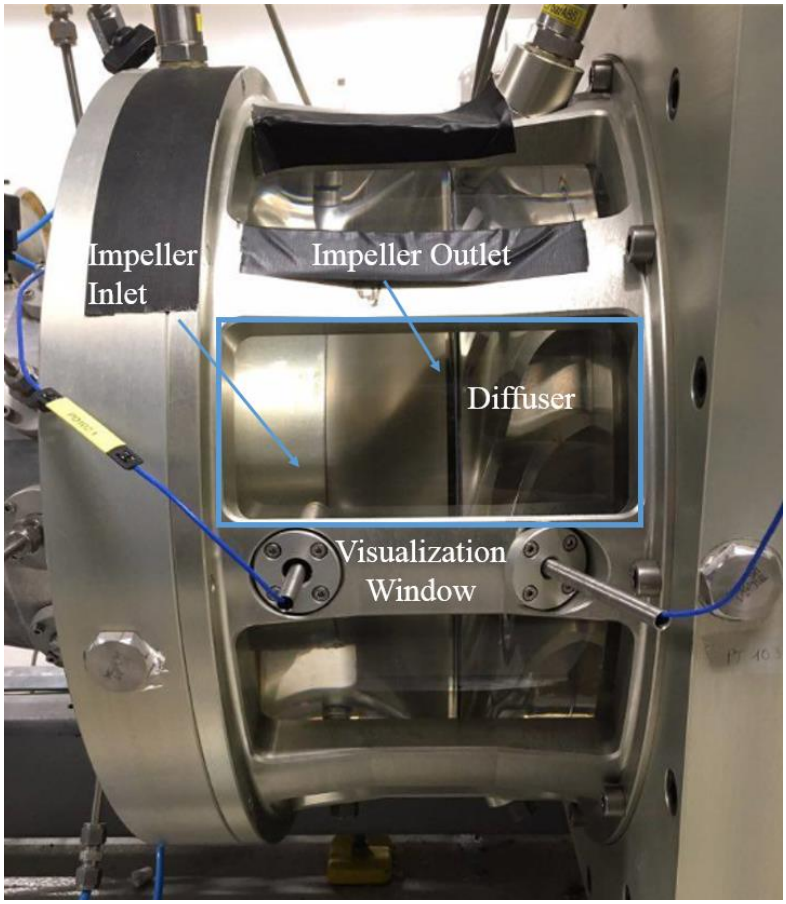

Fig. 19 - Visualization window and corresponding pressure sensors location

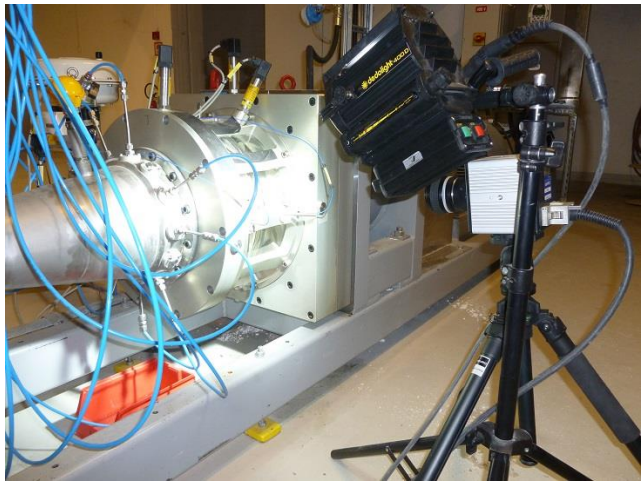

Fig. 20 - Visualization setup: high-speed camera and light focused on the visualization window

In order to find the proper visualization setup, the lighting and camera positioning and the combination of their settings had to be tested extensively. An intense light is needed to obtain sharp pictures, but, due to the reflection by the metallic parts, it produces a glare which immediately saturates part of the picture. No opaque painting or taping resulted helpful, so the installation of a polarized filter on the camera lens and a prismatic light diffuser allowed to avoid a direct beam into the visualization window, getting rid of the glare while still producing an intense but diffuse lighting. The light needs to be properly fed in order to avoid flickering, and not generating too much heat.
The factors to be considered involve the camera, the lighting, and the overall setup.
The main camera parameters are:

- number of shots per second, or framing rate, described by the frames per second value (fps), representing the temporal resolution of the investigation;
- shutter speed, expressing the exposure time in fractions of second, starting from 1/fps and below, for sharper pictures;
- picture resolution, in pixels
- record duration, in s; since the camera memory is limited, a compromise between temporal and spatial scales description is needed;
- triggering – different trigger modes are available;
- characteristic values of the objective – distance from the window, focal length, aperture, shutter time. Once the light intensity is fixed, a necessary compromise between the aperture and shutter time is needed to obtain the desired depth of field, as the blade channel radii are different between inlet and outlet
- the overall sensitivity depends on the size of the pixel, the fill factor, the sensor architecture;

- governing and processing software.

In addition, specific features as the dual slope shutter (preventing over exposure) and the pixel depth (related to the dynamic range) improve the camera capabilities when a very broad grey scale needs to be covered.

It should be remarked that multiphase flow complicates finding the proper lighting and camera settings, as the moving interfaces among the phases act as mirrors and introduce multiple reflections and refractions of the light. Tests involving very different *GVF* values and bubble distributions require an adjustment of the combination of the lighting system and the optical settings.

In Tab. 6, the specifications of the high-speed camera are reported.

Model	**Photron PCI 1024**
Maximum Resolution	1024 x 1024 pixel at 1000 fps
Set Resolution	384 x 352 pixel
Set Frame Rate	1500-6000 fps
Focal length	50 mm
Objective aperture	f/4.0
Depth of Field	18 mm
Shutter time	140 μs
Record time	1,5-6 s

Table 6 – Specifications of the high-speed camera; optical specifications relative to the investigations on the impeller channel

The shutter time is quite long since, to obtain a sufficient depth of field to focus over the whole channel with the same framing, a limited aperture is needed. This slightly affects the picture sharpness at the impeller outlet, where the flow velocities are higher.
The PMMA index of refraction is around 1,49.
The movies are alternatively saved in AVI (8 bit grey levels) or MRAW formats.

5.3.2 Image processing and bubble tracking

The outcome of flow visualization and high-speed imaging provides a good insight into the flow structures and mechanisms; however, it is not directly suitable to the implementation of image-based metrology techniques, needed to perform a statistical analysis of the bubbles shape, size and distribution, and their motion, for example to determine a velocity-size profile. As mentioned before, bubble clusters and the alternation of gas and liquid phases introduce reflections and disturbances complicating the detection of the interfaces. In addition, bubbles wobbling and more in general a continuous variation in their shape require a specific interface tracking algorithm. In

order to reduce these effects, research efforts have been made; representative results, among them, are due to these authors:

- Nishino [59] introduced a technique, based on stroboscopic background illumination and stereo imaging, to track and size spherical glass dispersed in water. The result showed that stereo imaging helped reduce the depth of field distortion, but the uneven light distribution seemed to reduce the tracking capability
- Zaruba et al. [60] improved the illumination using an LED array and reduced the superimposed bubbles using a flat column
- Honkanen et al [61] proposed algorithms to recognize highly overlapping ellipse-like bubble images.

Each single image needs to be converted into a data structure through a sequence of actions, corresponding to a series of matrix operations, involving compensation of uneven lighting (through morphological opening), histogram equalization, contrast enhancement, filtering (to remove noise), sharpening, edge detection, thresholding (for example through the Calzado-Acuna algorithm), segmentation. The bubbles can now finally be isolated.

In order to properly perform a bubble shape and motion tracking analysis, some resolution requirements need to be satisfied; as a representative value, Perez [62] indicates in 35 pixels/mm the minimum spatial resolution. For the current application, a compromise among framing rate, picture size, record length and spatial resolution and the current camera capabilities limits the possibilities of performing bubble tracking below a limited speed. The high-speed camera employed for this research study, with the set framing rate needed to capture the bubbles movement, allows to reach a resolution of 5 – 10 pixels/mm.

Owing to the different channel wall inclination and curvatures, and the limited depth of field due to the relatively long objective focal length, if the camera focus is set over the whole stage, it is not possible to properly record the flow field and thus the analyses have been performed focusing on three key areas: the approaching flow before the impeller inlet, the flow in the rotating channel, the flow in the diffuser.

5.4 Conclusion

Despite the complex pump casing surface, the optical access to the flow is satisfactory and no major image distortion occurs. The available camera settings have been extensively tested in order to fully exploit its capabilities and assess the desired features for an upgrade of the equipment, also taking into account the evaluation of the needs of advanced visualization techniques; the application of these is among the future plans.
A more detailed study of the flow field, in order to guarantee a good spatial resolution of the pressure fluctuations, would benefit from the installation of more fast-response pressure sensors, at least at two radial and two axial locations, allowing to perform instabilities analyses.

Chapter 6
Test Results

The main objectives of this research study, as listed in the previous chapters, comprise:

- exploration of the pump gas-handling capabilities
- sensitivity study of the main machine, flow and fluid parameters influence on performance and stability
- definition of the safe operating zone
- experimental study of the characteristic flow patterns and understanding of the originating mechanisms
- relation between outer measurements and flow visualization.

As to performance curves, the test data are presented in terms of the differential pressure: Δp vs q^* curves are obtained.
The calculation of the pump head requires the specification of the fluid density; in case of two-phase mixtures, different definitions have been proposed, depending on the location where this parameter is calculated and how the phases are averaged. The isothermal reference process with the density calculated at the inlet section has been used. The isothermal two-phase work is calculated as:

$$Y_{isot,SP} = \frac{\Delta p_t}{\rho_w}$$

$$Y_{isot,TP} = (1-x)\frac{\Delta p_t}{\rho_w} + x\ R\ T\ ln\frac{\Delta p_t + p_i}{p_i}$$

When the parameters affecting the fluid properties (as T and p) are not involved in the sensitivity study, the results presented in this chapter are expressed in terms of differential pressure instead.

When a single parameter is varied to perform a sensitivity study, in order to isolate the effect of the single parameter, the curves are presented at constant volume flow rate and increasing GVF, and the pressure production at each point is divided by the corresponding value in single-phase operation.

Hereafter, the expressions for the pressure and head multipliers:

$$f_\psi = \left.\frac{Y_{isot,TP}}{Y_{isot,SP}}\right|_Q$$

$$f_{\Delta p} = \left.\frac{\Delta p_{TP}}{\Delta p_{SP}}\right|_Q$$

The test campaigns performed during this study have covered a broad test matrix; the most representative comparisons, relevant for the discussion of the flow mechanisms, are presented in the following sections, starting from a sensitivity study on the effects of the main operating parameters on performance.

6.1 Effect of the tip clearance

In order to allow flow visualization, the tested pump features an open impeller. The blade tip leakage flow causes periodical vortex separation and channel obstruction and energy losses due to the interaction between the leakage and the main flow.
In this specific application, tip clearance effects strongly affect the machine operation as the blade chords are long and nearly tangentially oriented, making the secondary flow oppose the main one. The blade aspect ratio is very low, differently from typical axial turbines and pumps, therefore the leakage flow can interest a considerable part of the channel in the spanwise direction, especially in the central chord section where the blade loading is higher.
The tip clearance has been varied at small steps, by progressively axially moving the impeller towards the casing. The representative value, measured at the mid-chord section, has been reduced starting from 1500 down to 410 μm.
A variation in the tip clearance, which has proved to affect very sensitively the machine performance, can occur for different causes:

- the blade tip or casing erosion by the presence of some particles
- during operation, a minimal axial movement of the shaft, especially in the small clearance allowed in the roller bearings, due to a reversal in the thrust force, as a result of start-up or surging conditions
- the expansion of a component, due to overheating after a prolonged working interval processing a high *GVF* mixture.

The test matrix comprises three levels of the tip clearance, varied by axially moving the shaft, in order to improve flow visualization, study the effect of the leakage flow on performance, stability and the main flow mechanisms leading to degradation and blockage. The measured values at the mid-chord location are 550, 480 and 410 μm, referred to as I, II, and III in the graphs, respectively. Later, the study of the effect of the other operating parameters is performed at the minimum tip clearance level.

In general, once the gap size is increased, the pump performance is severely affected due to a reduction in the blade loading - by the gap flow acceleration and the missing contribution of the wall shear - and in the portion of the blade effectively transferring work to the fluid.

In Fig. 21, the performance curves resulting from tests at three tip clearance levels are presented.
The increased value of tip clearance gap strongly affects the pump performance over the whole operating range.

A variation in the curve slope is evident in the reduced clearance case – this can correspond to a modification of the flow field due to the switch to another leading flow mechanism. This is particularly interesting for the study of the machine instabilities under two-phase operation, since flow field modifications at single-phase operation, which can be studied in the CFD tool with reasonable accuracy and effort, can be responsible for them and thus allow to evaluate design improvements.
For the tested impeller, a reduction in the tip clearance height, as expected, improves the machine performance, and, below a threshold value, the open impeller performance matches the shrouded one; considering the absence of front sidewall gap leakage, which would generate a disturbance secondary flow too.

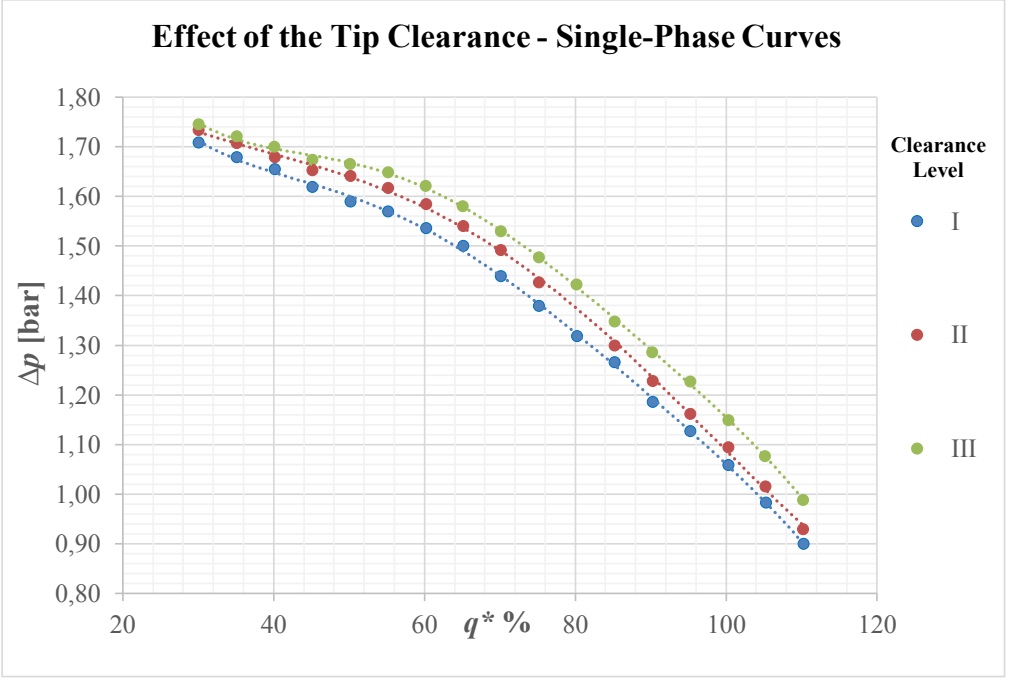

Fig. 21 - Effect of the tip clearance level on single-phase operation, n = 1200 rpm and p_i = 1 atm

Although they affect the differential pressure production in single-phase operation, additional gaps, as the clearance between the outer casing and the blade tips, can positively improve the two-phase performance, introducing secondary flows, fostering phase coupling, and mixing, reducing the bubble size and increasing the turbulence level.
As it can be seen in Fig. 21 and 22, a variation in the tip clearance causes opposing trends in single-phase and two-phase operation.

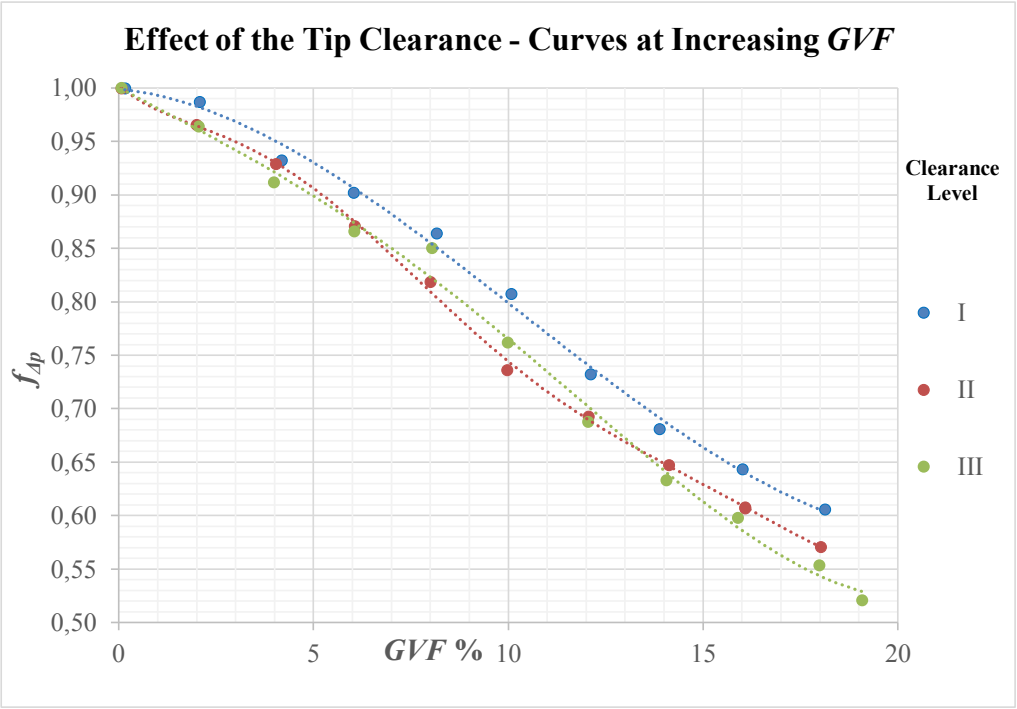

Fig. 22 - Effect of the tip clearance level on two-phase operation, n = 1200 rpm and p_i = 1 atm

The test results indicate that optimal operation should include manifold considerations over a broader range of values, differently from the traditional design-point approach. A higher tip clearance, while slightly impairing the absolute performance, might provide an extended components life and reduce the mechanical stresses due to flow instabilities.

6.2 Effect of the rotational speed, *n*

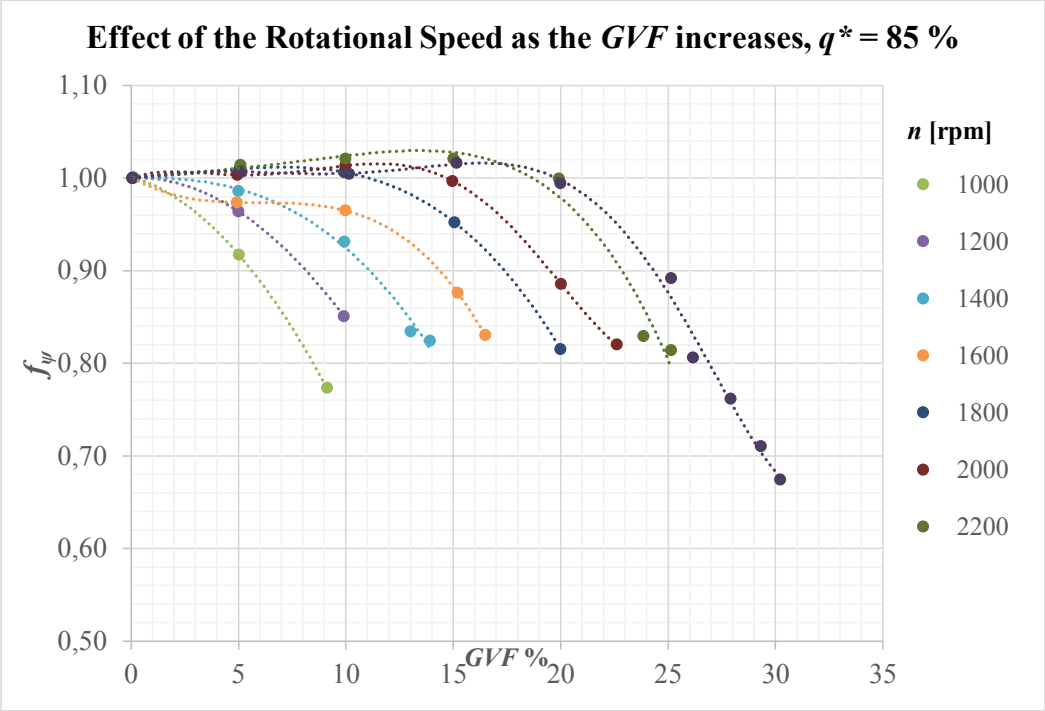

Fig. 23 – Effect of the rotational speed, q = 85 % and p_i = 1 atm*

This test is performed at atmospheric suction pressure. For each curve, the rotational speed is increased at steps of 200 rpm. Three main effects are observed as the rotational speed is increased: the gas handling capability is improved, the performance degradation factor presents higher values, the range of almost no performance deterioration is extended. Regarding this last, it should be noted that the pump experiences some light cavitation in the channels over 1800 rpm, this impairing the reference performance at single-phase operation. The values of f_ψ overcome 1 in the range *GVF* = 5 – 15 % for the combined effect of cavitation and gas phase compression at the impeller outlet, which makes the stage operating at a lower effective volumetric flow rate, as it will be explained later in the suction pressure effect section.

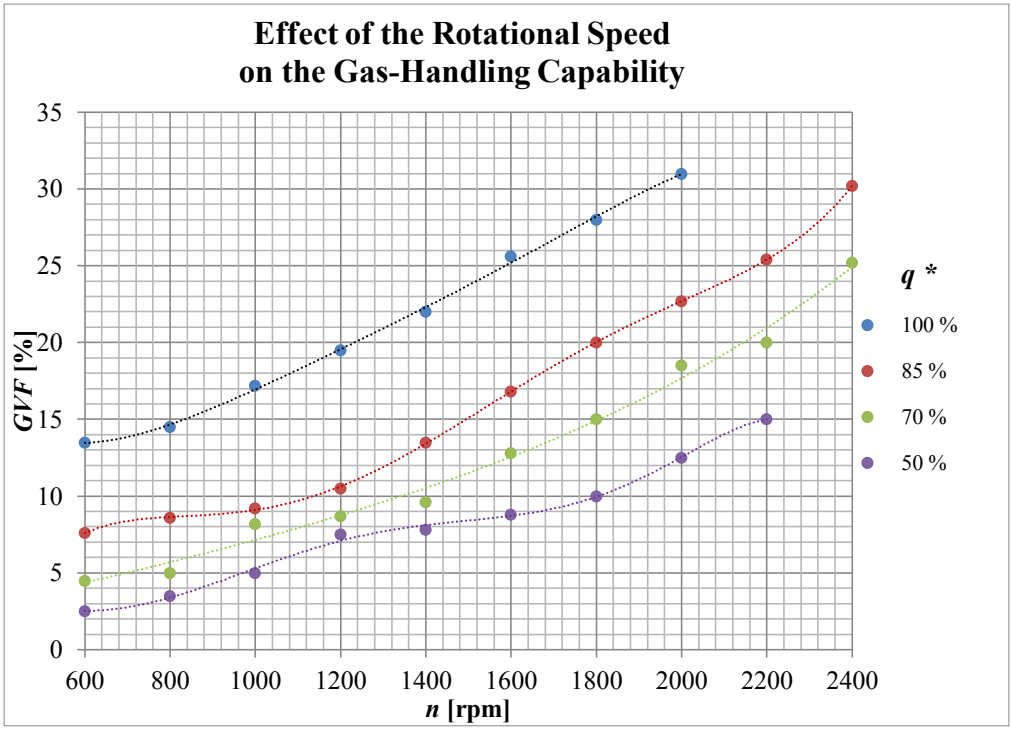

Fig. 24 - Effect of the rotational speed on the gas-handling capability, p_i = 1 atm

As explained above, the rotational speed strongly affects the gas handling capability at any value of the relative flow rate. The last points at the two highest values of the rotational speed are missing due to limitations in the air flow meter capacity at q^* = 100 % and in the maximum pressure at q^* = 50 %.

6.3 Effect of the relative flow rate, q^*

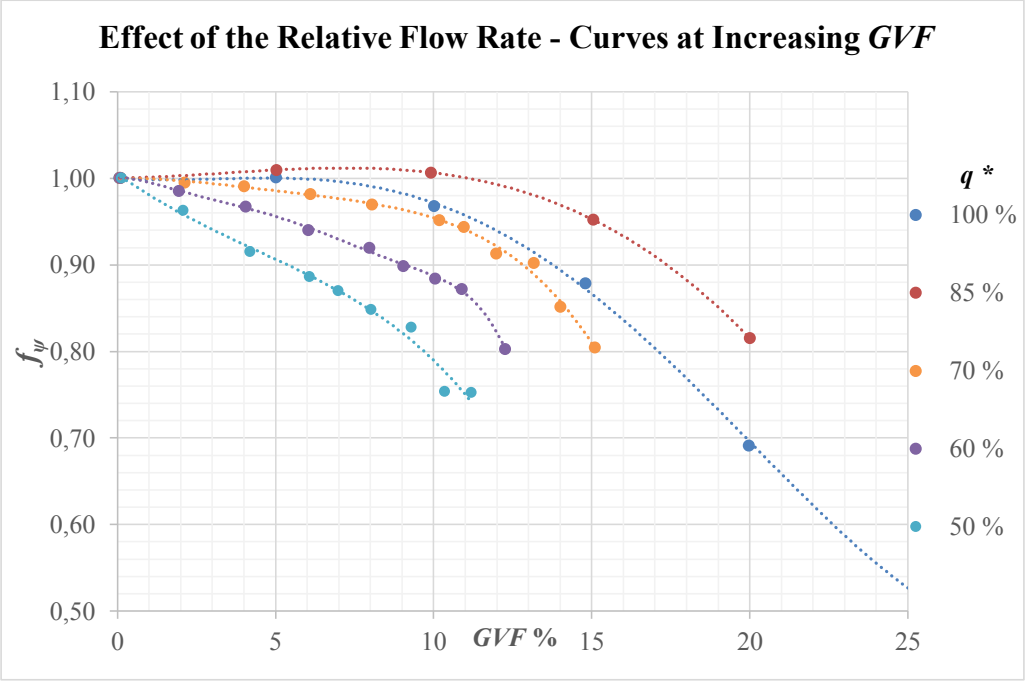

Fig. 25 - Effect of the relative flow rate, n = 1800 rpm and p_i = 1 atm

The relative flow rate plays a major role in determining the performance degradation and pump two-phase capability, as both the flow velocity and the residence time strongly affect the balance of forces in the channels and lead to the development of secondary flows. High flow velocities maintain a significant drag, which guarantees that the liquid phase successfully carries a well dispersed gas phase, resulting in a considerable gas-handling capability. As the flow rate is reduced, despite the ideal flow path is no longer maintained, the increased cross-streamline turbulent motion enhances the coupling between the phases, reducing the bubble size. The two-phase performance is thus enhanced, suggesting that the definition of the optimal operational range of a multiphase pump should take into account manifold considerations, besides the traditional design condition of flow angles matching the blades.

When the gas content is further increased, accumulations form and the performance is severely affected. Under part-load operation, these gas pockets cause strongly unsteady modifications of the flow field, which result in the characteristic phenomenon named surging, described in detail in Ch. 7.

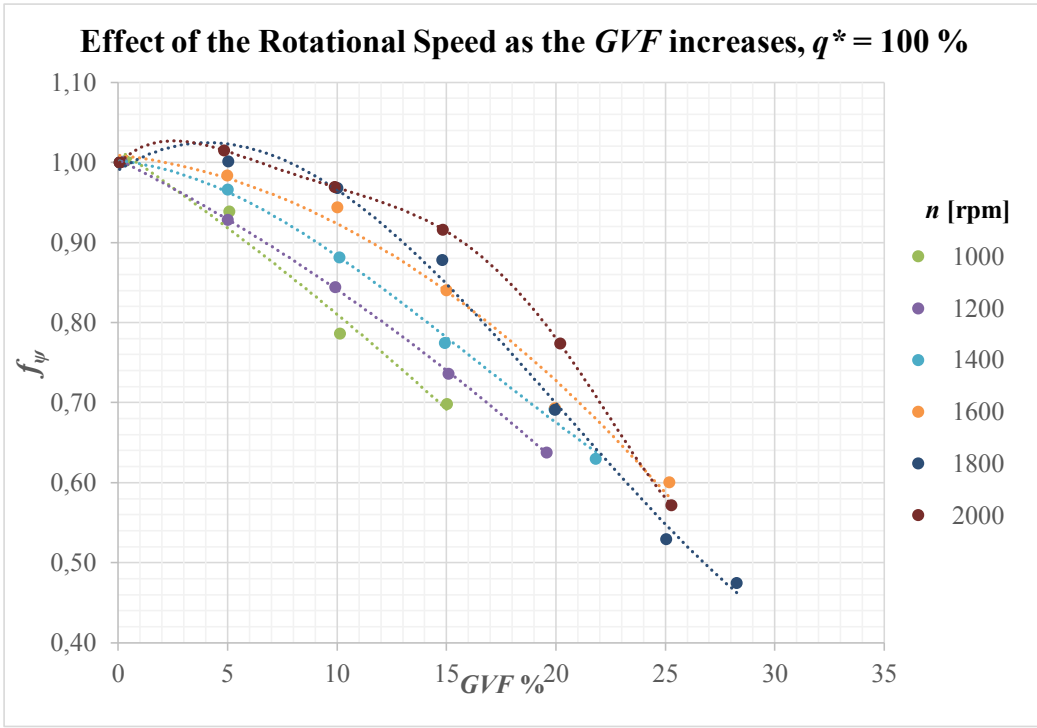

Fig. 26 - Effect of the rotational speed, q = 100 % and p_i = 1 atm*

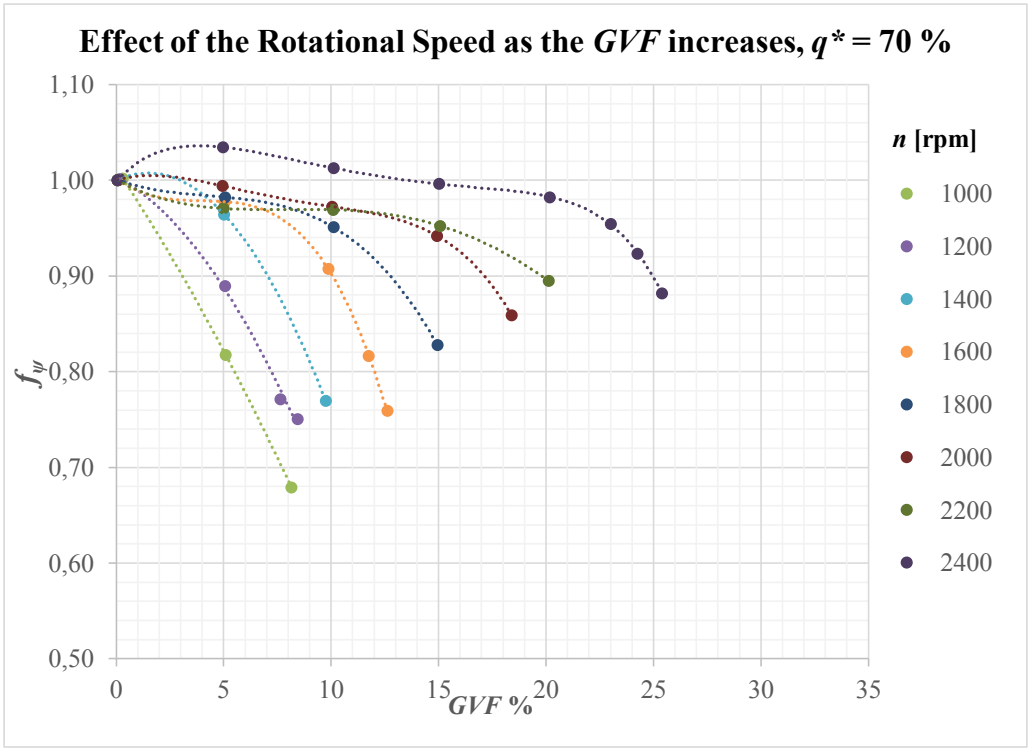

Fig. 27 - Effect of the rotational speed, q = 70 % and p_i = 1 atm*

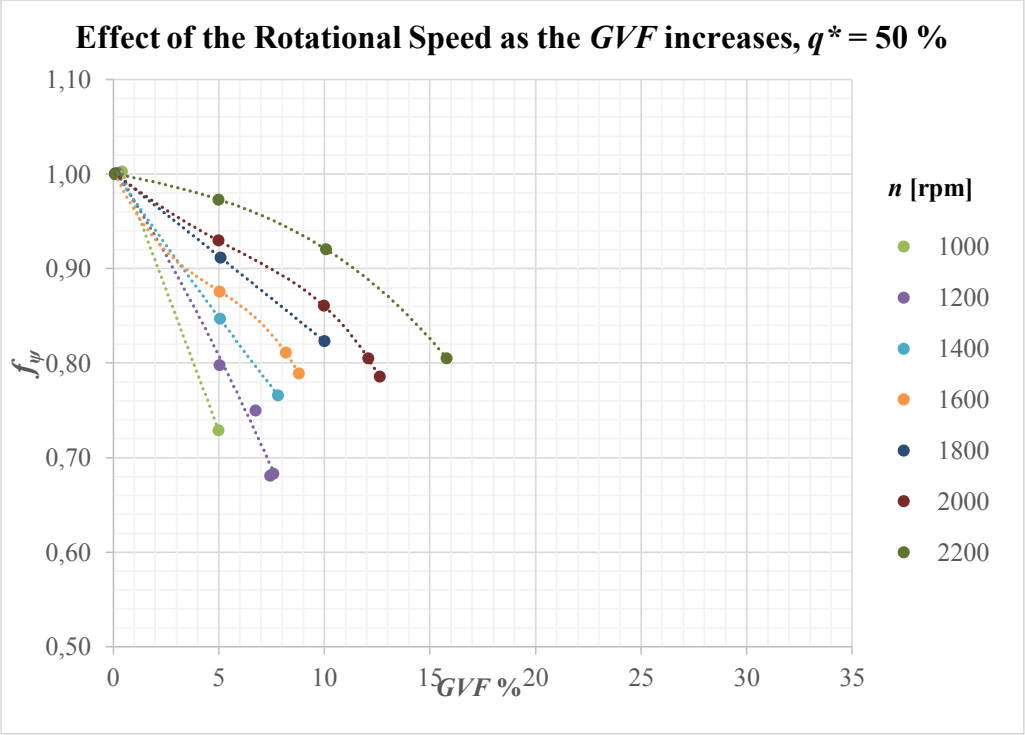

Fig. 28 - Effect of the rotational speed, $q^* = 50$ % and $p_i = 1$ atm

6.4 Effect of the volumetric gas content, *GVF*

As the injected gas fraction increases, the flow field is significantly modified and the pressure production progressively affected. In the previous curves, the following main zones are recognized:

- A mild performance deterioration zone, corresponding to the almost flat zone in the curves at constant total volume flow rates and varying *GVF*, while in the performance maps the curves present the same shape and curvature as the single-phase ones but they seem translated. Performance degradation is limited to some percentage values. The extent of this zone strongly depends on the rotational speed and relative flow rate. At high rotational speed values and in the range $q^* = 75$ - 90 % performance is almost unaffected by the air presence.
- A performance deterioration zone: both the curves at constant q^* and increasing *GVF* and the performance curves change their slopes when entering this zone. Gas accumulations develop and expand; their location depends on the relative flow rate, while their size expands as the gas fraction is increased.

- As the gas fraction is further increased, the flow field becomes highly unstable and the pump enters the surging zone, especially at part-load. This operating condition is explained in detail in the corresponding chapter.

6.5 Effect of the suction pressure, p_i

Tests at different suction pressures confirm some of the expected trends: as this parameter is increased, the gas-handling capabilities are improved, both in terms of reduced performance degradation and maximum *GVF*. Unfortunately, due to the equipment pressure limitations, the suction pressure can be varied only within a limited range, this restricting the performance variations; additional disturbing effects might have introduced different trends and a scatter in the data too.

Tests on the full-size machine, performed between 10 and 50 bar (a) at the inlet, confirm the general trends, but also show some interesting deviations from the expectations, as explained later.

Test results are plotted through the isothermal two-phase head multiplier, calculated with the density at the inlet section. In this case, the choice of the isothermal process as the reference one is reliable, since, for low- to mid- gas volume fractions, the high water thermal capacity absorbs the heat produced by the gas compression. The polytrophic calculation, on the other hand, is needed when multistage pumps performance at high gas contents is analyzed.

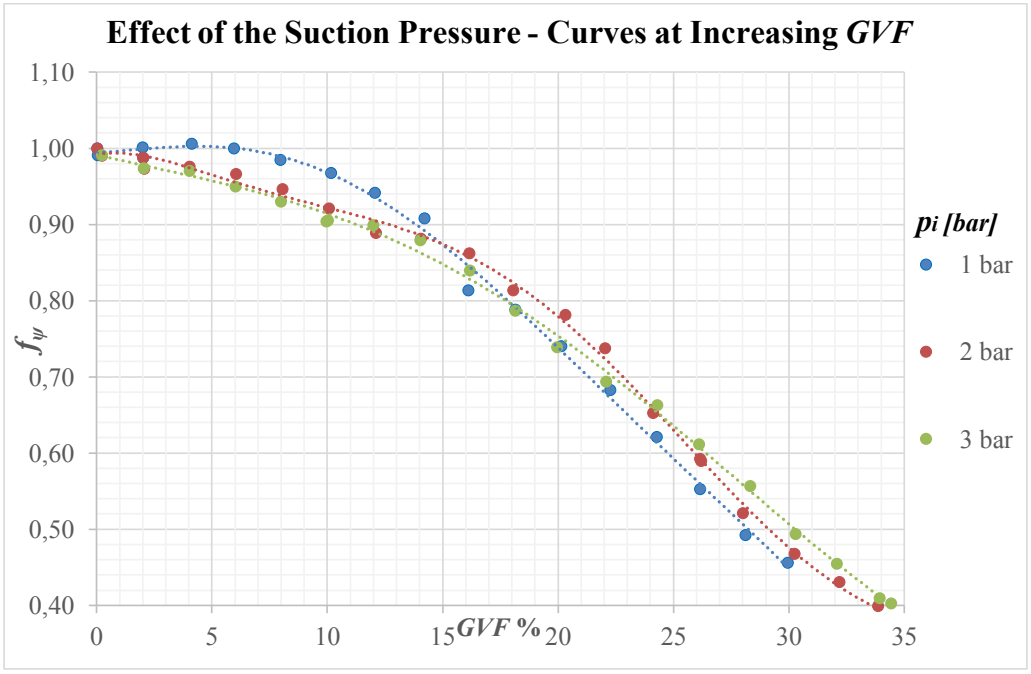

*Fig. 29 – Effect of the suction pressure, n = 1800 rpm and q * = 100 %*

For low gas contents, the performance degradation is higher when the suction pressure is increased. The comparisons are made in relation to inlet *GVF*; in the low inlet pressure cases, especially at the higher rotational speed levels, an explanation might be that the air experiences a significant compression, improving the performance as the bubble size decreases. In addition, the compression of the gas phase makes the pump work at an actual volume flow rate which is lower than in the higher inlet pressure case, and the liquid phase accelerates too. Moreover, as explained in an earlier paragraph, when operated at p_i = 1 bar, the pump experiences a light cavitation, which reduces the single-phase performance, which is later used as the reference value for the two-phase performance degradation calculation.

Possible ways to compensate for the first effect are plotting against the mass flow rate, the gas mass fraction, x, or at least the *GVF* referred to the average stage parameters. The following figures present the results with the mixture composition expressed in terms of gas mass fraction, which remains constant along the stage. In addition, when the goal is to find representative points for comparison, the pressure ratio across the stage needs to be included as a scaling parameter.

Tests at p_i = 4 bar could only be performed at q^* = 85 %, due to limited capacity in the air flow meter at full-load tests and too high pressure at part-load.

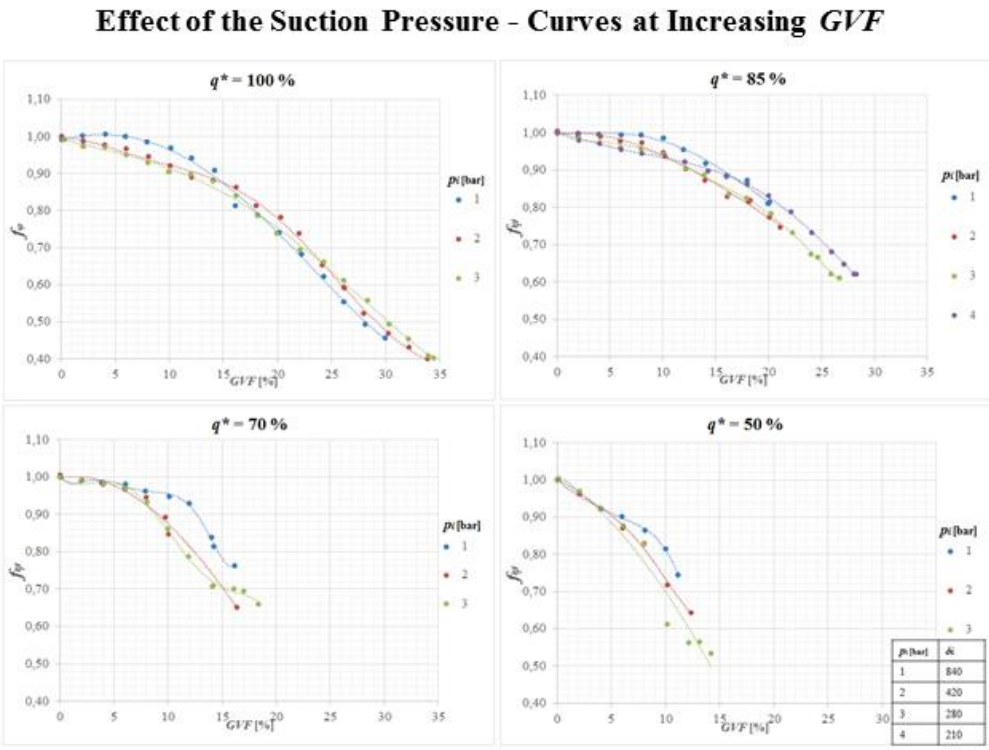

Fig. 30 - Effect of the suction pressure, curves at increasing GVF and different levels of the total volumetric flow rate; isothermal head multiplier plotted against the GVF at the inlet, n = 1800 rpm

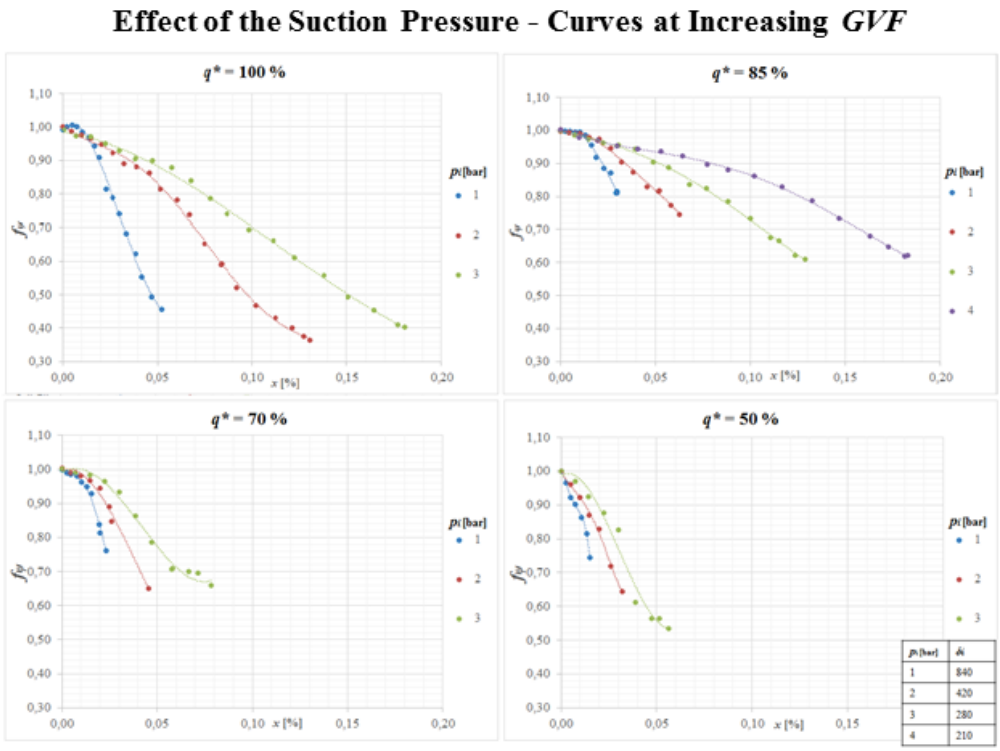

Fig. 31 - Effect of the suction pressure, curves at increasing GVF and different levels of the total volumetric flow rate; isothermal head multiplier plotted against x, n = 1800 rpm

6.6 Operational boundaries

When it comes to the definition of the safe operating zone, as stated in Ch. 2, the performance curves are bounded by upper and lower limits of the flow rate, corresponding to too little pressure production and too unsteady flow field, respectively. In addition, part-load operation features a major flow field unsteadiness. The dashed lines link the points presenting relative variations in the delivered pressure of 5, 10 and 15 %, respectively, in the zone $q^* = 45 – 80$ %. A discussion about the threshold value to define the surging onset is reported in Ch. 7.

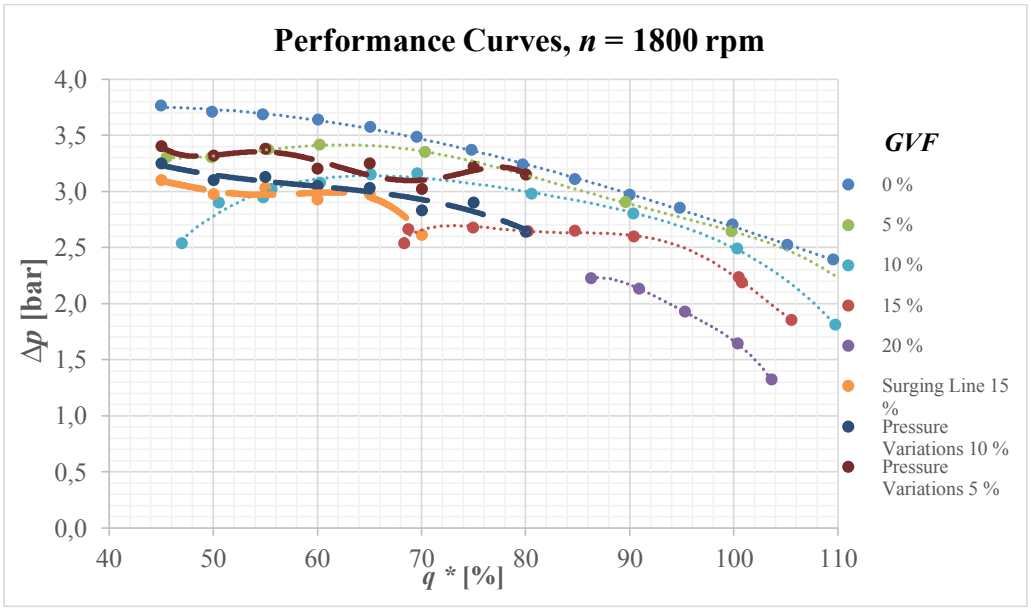

Fig. 32 – Performance curves at n = 1800 rpm and p_i = 1 bar; the dashed lines represent the relative variations in the delivered pressure

As stated before, the flow through the tested pump presents an intrinsic unsteadiness, due to turbulence, rotor-stator interaction, and two-phase flow. This complicates the identification of the originating flow mechanisms, as even in stable operation, when all the machine and flow parameters are balanced, stochastic variations occur. The pump channels, at nominal operating points, already present an irregular gas content.
The flow can be described as unsteady all along the performance curves, but specific conditions as part-load and relatively high air content may cause severe oscillations in the flow field. Despite this, the machine is still operating stably, with periodical fluctuations around average values.

Real working conditions, however, involve variations in the operating parameters which can force the machine into cycles similar to the surge experienced by compressors and eventually block it.

In order to evaluate the machine performance in these conditions and its response to a sudden variation in the main parameters, the effect of the surrounding system needs to be included. The pipes, valves and other devices response to the flow field variations plays a key role in the evolution of machine instabilities.

The accurate fine time-scale flow visualization allowed by high-speed imaging helps to perform some transient tests, in which just one of the parameters is varied, to enhance its effect on the related flow mechanism. For the time being, only a qualitative outcome of these results can be presented. The whole measurement chain cannot assist these tests properly (a fast-acting valve on the pressurized air line would be required too) and the response of the surrounding components during transient events has to be carefully evaluated before drawing conclusions on the pump transient behaviour.

Some representative transient tests, aided by flow visualization, have been performed and the results are reported in [63]. Variations in n, q^* and GVF are taken into consideration, and tests are performed at $n = 1200$ rpm, as the lower blade loading limits the tip leakage, improving, thus, flow visualization. However, analogue trends are observed at higher speed too.

6.7 Uncertainty in the experimental data

As stated in the project objectives, the main research focus is the recognition of the flow mechanism characterizing the different operating zones and those originating unsteady modifications of the flow field. Therefore, the careful evaluation of the measurement accuracy does not play a key role. However, when a sensitivity study on the effect of a parameter is performed to define trends or a comparison with numerical simulations is needed, the uncertainty associated with a certain value needs to be calculated.
According to the Standard, in the Type B case the overall uncertainty value of a parameter resulting from a measurement chain is evaluated considering the contribution of each of the single variable uncertainties, calculated with the specific formula depending whether the variables are correlated or not. For each of the considered variables, the main random (repeatability, thermal stability, resolution) and systematic (accuracy, hysteresis, linearity) uncertainties need to be considered and combined. In addition, the uncertainties connected to the electrical signal transducer, conditioner, amplifier, filter, analog to digital converter and finally computerized data acquisition need to be taken into account: the main sources are gain accuracy, stability, linearity, noise, quantization. Additional uncertainties arise when an optimal matching of the range of the instruments in the system sequence is not achieved.

An alternative approach, named “Type A” in the Standard, is based on the statistical analysis resulting from the collection of the test data. Data are acquired for 30 s (which correspond to 301 data samples at 10 Hz) and the arithmetic mean and standard deviations are calculated. The pressure measurements present a relative error which is within 0,5 – 1 % at nominal flow, with any air content, and the flow rate ones even much lower values, making them respect the Standards

requirements, as reported in Tab. 3. When it comes to the effect of the presence of the gas phase, it should be remembered that air dampens the pressure field small fluctuations. Only when operating at part-load approaching the surging condition, the unsteady flow field presents larger variations.

6.8 Conclusions

An extensive experimental campaign has been necessary as the way the different phenomena affect the pump performance strongly depends on the pump geometry.

The influence of the operating parameters - pump speed, flow rates, mixture composition, suction pressure - on the machine performance and operating range has been extensively studied.

The test results confirm most of the expected trends: an improved phase coupling, due to the pump speed or to secondary flows, mitigates performance deterioration and delays the instabilities inception. However, tests at increased values of n, p_i and GVF, possible with a future update of the equipment, will help to approach realistic operating values.

The accurate study of the flow field through high-speed imaging helps detect the flow mechanisms responsible for performance degradation and instabilities and is presented in detail in Ch. 7.

Chapter 7
Flow Phenomena and Operating Conditions

7.1 Methods and analyses

The recognition of the unsteady flow mechanisms responsible for performance degradation and instabilities, representing the objective of this Chapter, requires an analysis tool able to provide a properly refined temporal and spatial description of the flow field. The approach followed in this research is based on:

- flow visualization related to fast-response pressure signals
- evaluation of frequency and time-frequency analyses.

In order to do so, the high-speed camera is focused on the same window where two fast response pressure sensors are installed; the exact locations are shown in Fig.19.
The video recording is started at the same time as the signal log system.

The main tool employed in the study of the flow mechanisms and their relation to the pressure measurements is the analysis of the correspondence between the short time-scale pressure variations and high-speed camera recordings.
Due to limitations in the sensors response time, the low frequency pressure signals are acquired at 10 Hz to capture large time-scale variations, as those occurring at surging. The high-frequency ones are acquired at 1500 Hz, high enough to avoid aliases in the signal analysis and to relate well to the camera shots, which are taken at a framing rate from 250 to 6000 fps, depending on the studied phenomenon and the memory possibility at the considered resolution. Both the pressure signal and the movie are imported in the software National Instruments DIAdem: if the movie is played at very low speed, a fine time-scale study is possible. As the playback speed is increased, the overall evolution over different areas in the machine can be studied.
This tool provides a valuable input to assess the validity of the machine instabilities inception and evolution analyses usually performed in the frequency and time-frequency domains.

As regards the analysis of the pressure field oscillations, in both the Fourier and Wavelet Transforms, inner products quantify the similarity between the measured signal and a family of reference analyzing functions, which are complex exponentials for the Fourier one, windowed complex exponentials for the short-time Fourier transform, and wavelets for the Wavelet transform. It should be noted that these analyses present some intrinsic limitations: care should be taken when choosing the analyzing function, which might ease the detection of specific features or match a certain behaviour. In addition, the Uncertainty Principle imposes a compromise on the temporal and frequency resolutions. The two extremes are the measured signal (absolute precision in time) and the Fourier Transform (absolute precision in frequency). The Wavelet transform, on the other hand, once accepted a certain compromise in the resolution, is suitable to perform analyses on unsteady signals and, thus, promises to allow a detection of instabilities precursors and evolution.

7.2 Investigation of the main flow phenomena

7.2.1 Bubble size and shape evolution

As to the bubble size, this investigation is of key importance, not only since this parameter plays the most important role in phase interaction, through its effect on the drag and lift forces, and on performance degradation, due to flow obstruction, but also because of the study and validation of the numerical codes modelling capabilities. This tool can take into account the compression of the gas phase through a pressure-dependent bubble size expression, but it cannot properly and effectively model the complex real bubbles distribution and their interaction.

The main forces acting on the bubbles are surface tension, drag, lift, shear stresses and the added mass; the accelerating flow field and turbulence introduce further complications. These forces affect the bubbles shape and dimensions, which are governed by coalescence and breakup. In general, the dominant force promoting fission is shear, while the one opposing it is surface tension.

As discussed in Brennen [21], the identification of a criterion describing the transition among flow patterns requires the specification of the bubble size, which is however determined by a mutual influence between the flow and the bubble itself.

Bubble size statistics and characterization is a complex analysis, outside of the scope of the current investigation; however, typical trends are:

- regions of high shear stress, as vortices and boundary layers, present the smallest bubbles
- higher bubble sizes once the *GVF* increases
- finer bubbles and more homogeneous phase distribution as the flow velocity, and consequent drag, increases as a result of a higher rotational speed; coalescence is less frequent as the residence time is shorter.

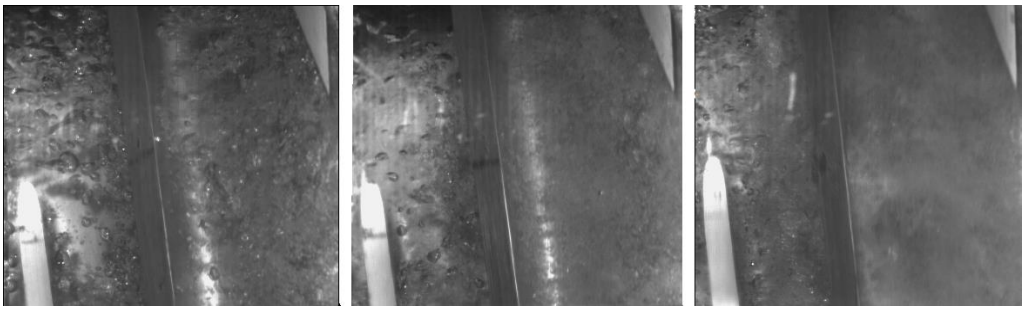

*Fig. 33 – Bubble size evolution in the impeller channel; q * = 100 %, GVF 5 %; from left to right: n = 900, 1200, 1800 rpm*

- when the relative flow rate decreases, the secondary flows and increased turbulence level compensate the lower flow velocity; the bubbles are now very fine and form a foam following

the same trajectories as the leakage flow and tip vortex. In Fig. 34, it can be observed that the average bubble size is smaller at $q^* = 100$ than at $q^* = 85$ %.

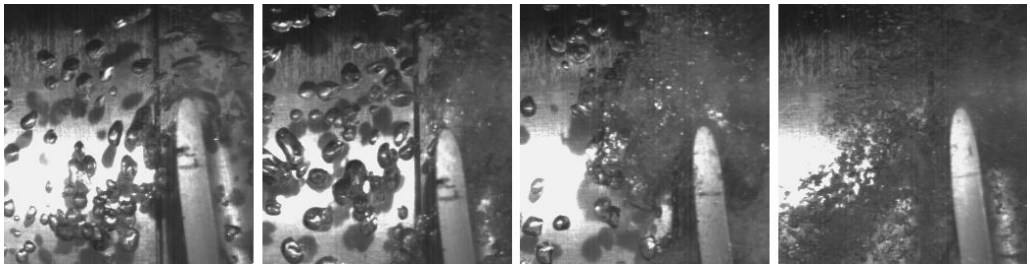

Fig. 34 – Bubbles at the impeller inlet; n = 900 rpm, GVF = 5 %; from left to right: q = 100, 85, 70, 50 %*

The high-speed camera software, Photron Fastcam Analysis®, allows to perform bubble tracking, providing information about the particle movement, velocity and acceleration. However, this is made difficult by the variation in bubble shape and size, resulting from the complex forces system in the channel. The boundary detection becomes challenging; in addition, wall contact plays a key role as a breakup mechanism.
In addition, as explained later, in the identified surging mechanisms a combination of flow structures is involved, but bubbles characterization is not the most relevant investigation for the overall understanding of the phenomenon.

7.2.2 Rotating stall and irregular blade channel filling

As a first approach in the study of this phenomenon, the suction pressure is lowered to detect low-pressure zones and enhance the obstruction and deviation phenomenon; in single-phase operation, the Tip Leakage Vortex (TLV) appears. The mechanism and the main features are shown in Fig. 35. As the relative flow rate is reduced, the blade loading close to the leading edge increases and the inlet flow incidence angle becomes incorrect; a low pressure zone forms on the blade suction side at the entrance and the tip leakage flow, after accelerating through the gap, suddenly expands, cavitating. The disturbance extends ahead of the impeller channel and, due to its intermittency too, causes uneven sucking conditions for each blade channel. This might eventually result in the development of rotating stall.

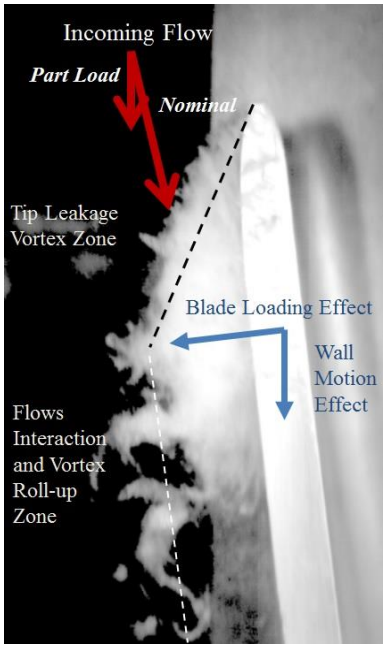

Fig. 35 – Tip Leakage Vortex mechanism

The fluid in this area mixes with the incoming main flow and a vortex is formed, usually called tip leakage vortex. The balance between the leakage and main flow is very unstable and it results in the intermittent character of the TLV, also due to the unsteady vortex shedding.

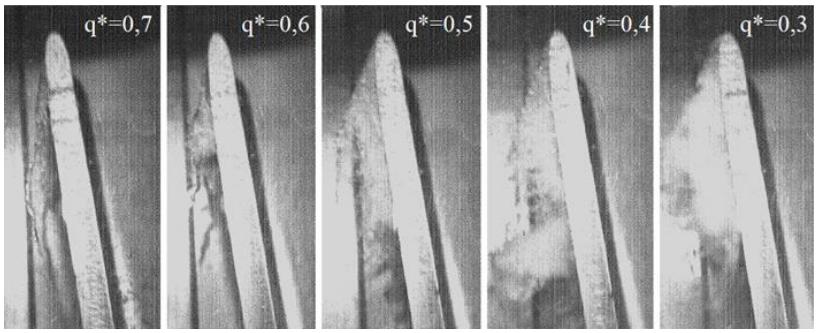

Fig. 36 – Tip Leakage Vortex extension depending on the relative flow rate, n = 1800 rpm

The accurate characterization of the cavitating vortex is not among the scopes of the current investigation, but the tip leakage flow affects the machine performance through additional losses,

channel obstruction and rotating stall, which are the typical resulting phenomena and can significantly affect the stability in two-phase operation too.
In [64], waterfall plots of the pressure signal at the impeller inlet are included; a distinct subsynchronous peak can be noticed below $q^* = 60$ %, simultaneously to the appearance of the tip vortex, and it is related to rotating stall.

7.2.3 Pump blockage

A characteristic phenomenon experienced by multiphase pumps occurs over a threshold *GVF* value, at high gas fractions or low flow rates, when a certain amount of gas accumulates in the channels and the machine can no longer suck in the regular flow rate; normal operation can only be recovered if the inlet air flow is stopped and the multiphase pump is fed by another pump which helps circulate the liquid phase.

According to the available literature, the main hypotheses involve the occurrence or combination of these phenomena:

- gas accumulation
- leakage back flow
- sonic blockage
- alternating channel obstruction.

Experimental observations have shown the concurrence of some of them; different physics, depending on the operating conditions, can play a key role. A discussion is reported in [63].

As the blockage mechanism at nominal flow, the main flow is strong and the blade loading relatively limited, this helping to carry on the gas phase and avoid cross-channel gradients. However, at high gas contents the gas phase cannot overcome the pressure gradient at the trailing edge; this trailing edge, suction side accumulation progressively extends towards the opposite channel wall as *GVF* is increased, eventually reaching the wall at gas lock, as shown in Fig. 37.

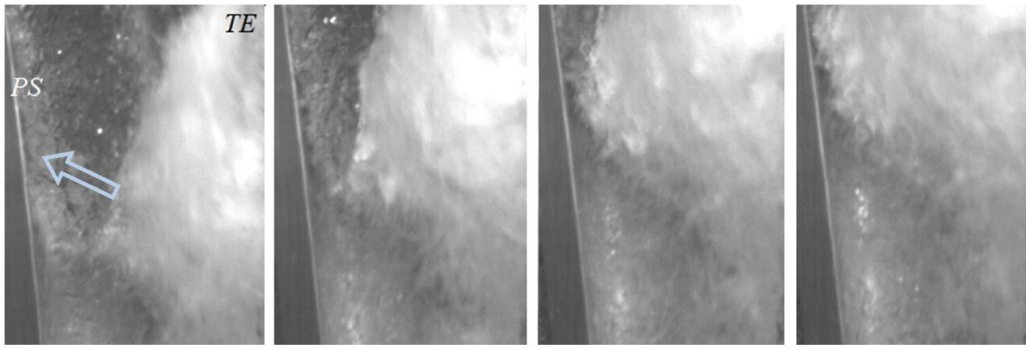

Fig. 37 - Pump blockage from nominal flow operation, n = 1200 rpm, lowest tip clearance level

The part-load blockage mechanism at surging has been identified as follows: in this case, a very unsteady gas pocket at the pressure side, mid chord; it obstructs part of the channel and interacts with the TE accumulation, finally blocking the passage.

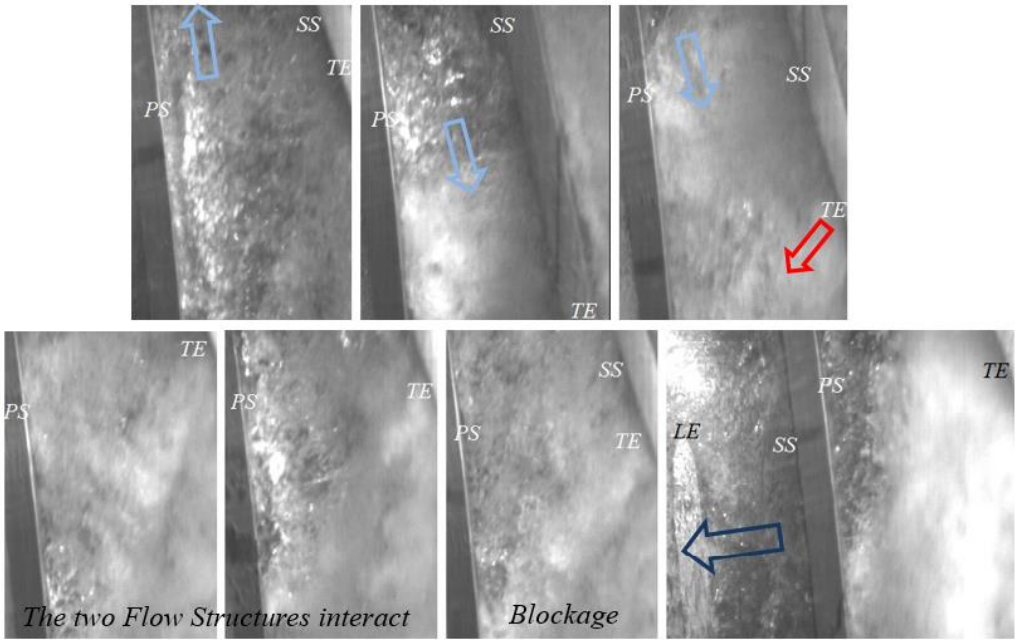

Fig. 38 - Pump blockage at part-load

In the following graph, the change in slope of the curve is related to the appearance of the gas pocket on the pressure side.

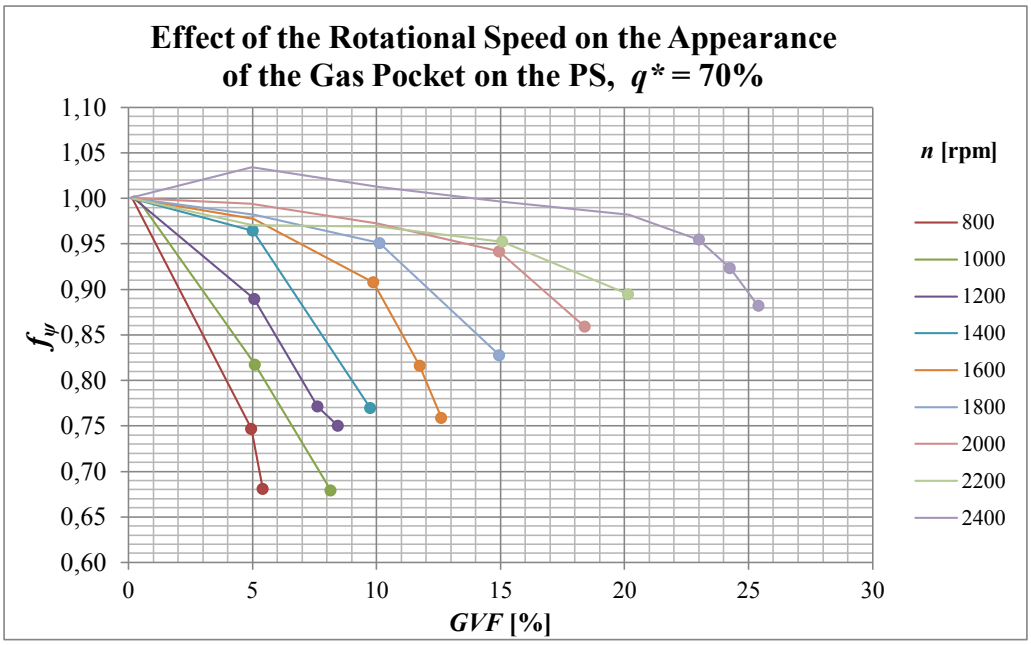

Fig. 39 – Effect of the rotational speed on the appearance of the gas pocket on the PS, q = 70 %; the dots correspond to the presence of the gas pocket in the high-speed videos*

Increased values of the rotational speed delay the formation of the gas pocket, thanks to the higher flow rates and interfacial stresses, limiting the bubble size.

7.2.4 Surging

In Ch. 2, the hypotheses previously formulated by other researchers have been presented. Tests have proved that surging is a complex phenomenon, involving multiple flow mechanisms; however, the earlier hypotheses of forces balance resulting in a static bubble are not valid for this specific case, due to a very different hydraulic design and operating conditions when compared to those typical of multiphase pumps. Flow visualization confirms that surging corresponds to the transition to a complex flow pattern, with gas accumulation, and instabilities at the interfaces, and is associated with strong and irregular oscillations in the flow field variables. A quantitative reconstruction of the flow field would allow the measurement of the phase slip, which plays a key role in the analytical treatment of two-phase flow.

Inlet

This irregular flow at part-load arises from the asymmetric conditions already observed when rotating stall is studied, without any gas injection.

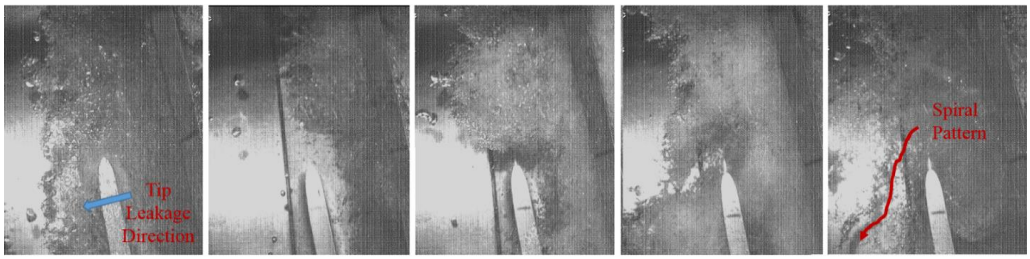

Fig. 40 –Irregular flow at surging in the inlet section, n = 1200 rpm

Channel

As to the surging mechanism inception and evolution, the following sequence of processes has been identified:

- an irregular gas pocket forms at the PS, triggering unsteady variations in the flow field, due to its irregular location and shape and instabilities at the gas-liquid phases interface;
- depending on the flow rate, the gas pocket can either interact with the gas accumulation on the SS or grow further approaching the opposite blade wall, resulting in increased channel obstruction and eventually blockage;

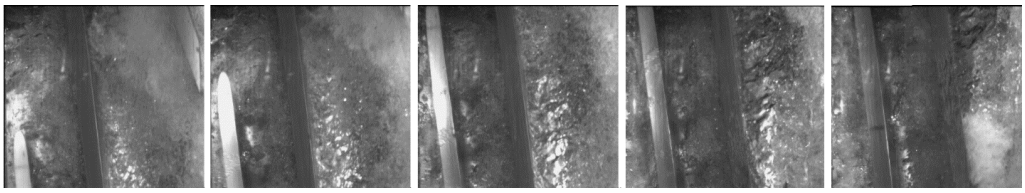

Fig. 41 - Gas pocket expansion at surging, n = 1200 rpm, q = 70 %*

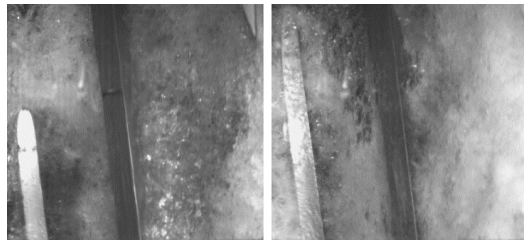

Fig. 42 - Gas pocket interaction and resulting channel blockage and backflow, n = 1200 rpm, q = 70 %*

- the incoming flow finds an obstructed channel and is deviated to the following one, which is entered with an incorrect angle; due to the accumulated gas present in the channel, some

liquid, which has just entered or was already present in the channel, flows back through the tip clearance, driven by the pressure gradient due to the blade loading.

The sequence of these mechanisms is irregular; however, in some specific cases the deviation due to channel blockage sums with the tip clearance effect eventually producing a very strong flow resulting in “empty from gas channels”, which helps to flush down the trapped gas.

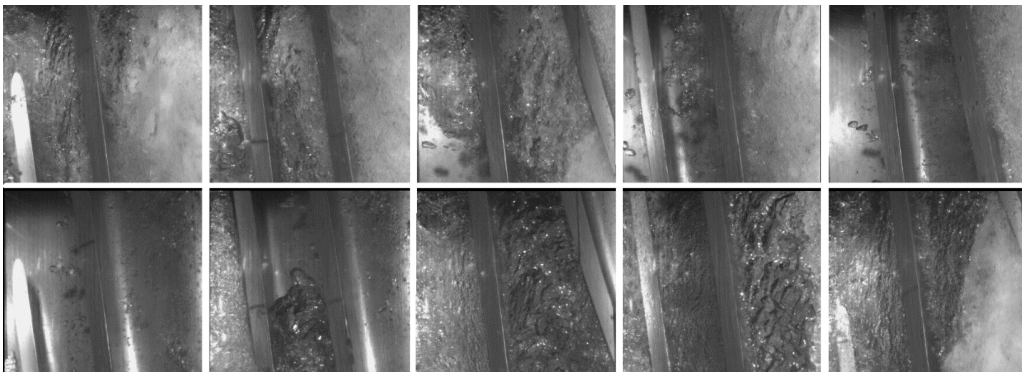

Fig. 43 - Surging condition at n = 900 rpm and q = 70 %: the framing rate corresponds to 25 pictures per blade passage; one every 10 pictures is shown (all but the last one); the succession of gas-filled, liquid back-flow and only liquid channels is presented*

For the n = 900 rpm and q^* = 70 % case, this alternate blade channel blockage is quite regular and occurs every third and fourth blade passage; it would be desirable to detect its inception and axial-radial evolution in a similar fashion as done for surge and rotating stall in compressors, by the use of frequency and time-frequency analyses of the signal, but tests prove that air filled structures dampen the pressure pulsations by compressibility. Figure 44 shows the outcome of the measurements; the static pressure signal is on the right side, while the fast-response one on the bottom. A correspondence has been found at n = 1200 rpm too.
A quantitative assessment of the liquid velocity is needed to validate the inlet flow deviation and channel obstruction hypotheses.

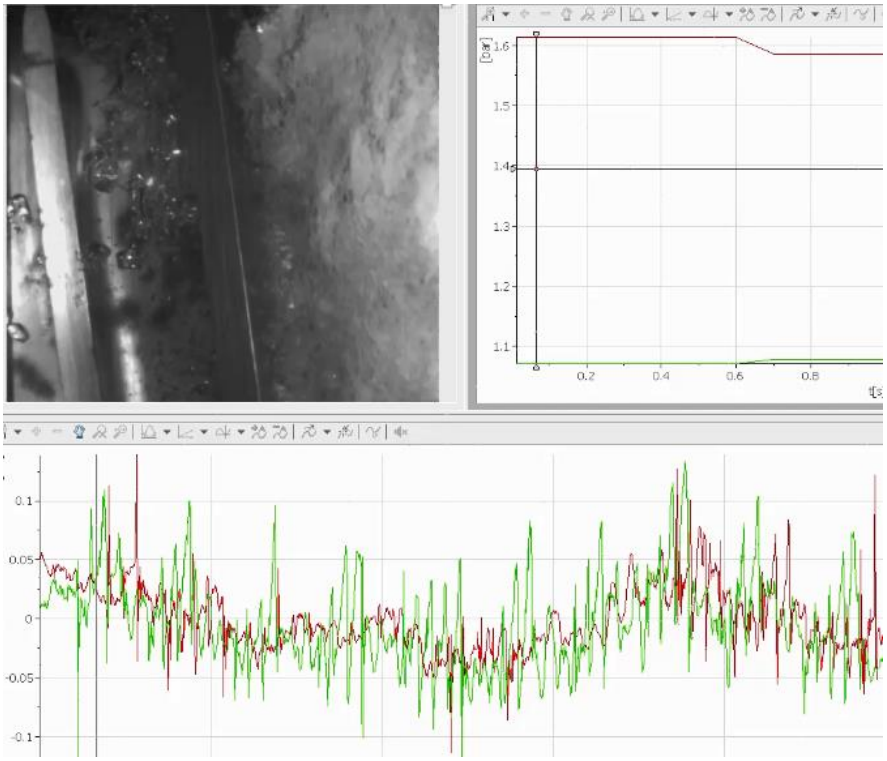

Fig. 44 - Blade passing pressure peaks damping by air compressibility; test at n = 900 rpm, q = 70 %, p_i = 1 atm, GVF = 6,8 %; green signal - impeller inlet, red signal – impeller outlet*

Concerning the measurements which can be implemented on a real machine in order to detect surging initiation, the experimental research has provided some valuable insights. This operating condition features strong oscillations in the measured pressure; a threshold value can be identified to try to recover normal operation once it is approached.
Figure 45 shows the typical low-frequency pressure oscillations at surging.

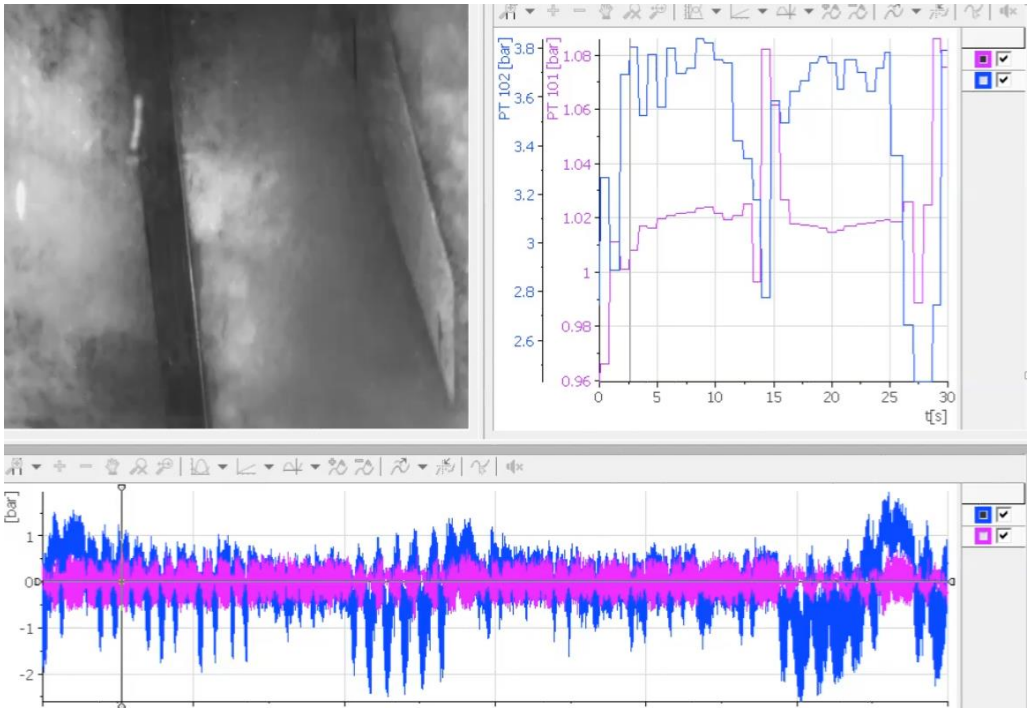

Fig. 45 - Pressure oscillations at surging; test at n = 1800 rpm, q = 50 %, p_i = 1 atm, GVF = 10,0 %; rose signal - impeller inlet, blue signal – impeller outlet*

It should be noted that, however, due to the reduced rotational speed and suction pressure, the transition between the stable operation and surging is often quite quick, making it challenging to perform transient tests with progressively varied values of the input parameters.
The detection of the formation of a gas pocket on a high rotational speed, shrouded impeller is not feasible, while more promising is the study of the dynamic pressure signal modifications introduced by the presence of air accumulation, which dampens the regular pressure peaks. For example, a control on the pressure peaks at the blade passing frequency can show if some blade passages present a gas accumulation. Further analyses are needed to properly relate the pressure peak damping and the evolution of the flow instabilities in the machine.

Diffuser

As explained in [65], the flow in the diffuser presents a considerable recirculation, due to the sudden expansion and resulting flow deceleration; in addition, the absence of the following rotating stage enhances this phenomenon. When a two-phase flow is processed, the air fills the low-pressure and low-velocity zones, helping to visualize the vortex location and evolution. Experiments have

shown that, when surging is approached, the main vortex core moves back and forth at a frequency below the blade passing one; this corresponds to the strong intensification of the pressure oscillations in the frequency spectrum. A further analysis of the flow instabilities evolution through the spatial reconstruction of the pressure pulsations signal, requiring the installation of more sensors to perform cross-correlation analyses, will allow to identify the origin of this intermittency. Figure 46 shows the different flow areas and the vortex location, while the sequence of pictures in Fig. 47 shows the flow mechanism.

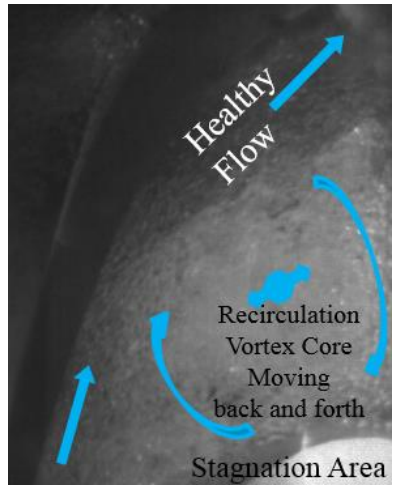

Fig. 46 – Recirculation at the diffuser outlet - flow mechanism

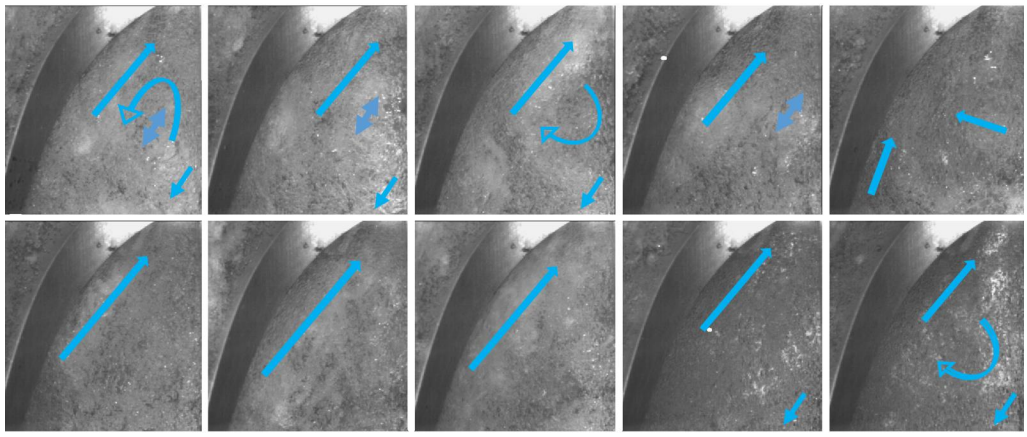

Fig. 47 – Irregular mechanism of the recirculation at the diffuser outlet at surging, n = 1800 rpm, q = 50 %, GVF = 10 %*

As explained by Gülich [10], the pressure recovery in the diffuser when operating a two-phase mixture is limited and depends on the gas-liquid distribution; in case of a well dispersed flow pattern, it is almost determined by the density of the carrier fluid, while if the phases separate, the diffuser becomes very inefficient and the pressure recovery is limited by the gas density - in this case the kinetic energy of the liquid is dissipated.
In general, the pressure recovery capabilities of the diffuser are strongly dependent on the flow rate and degrade severely over the nominal capacity.

A correspondence between the intensification of the flow field unsteadiness and the characteristic pressure oscillations as surging is approached has been observed.

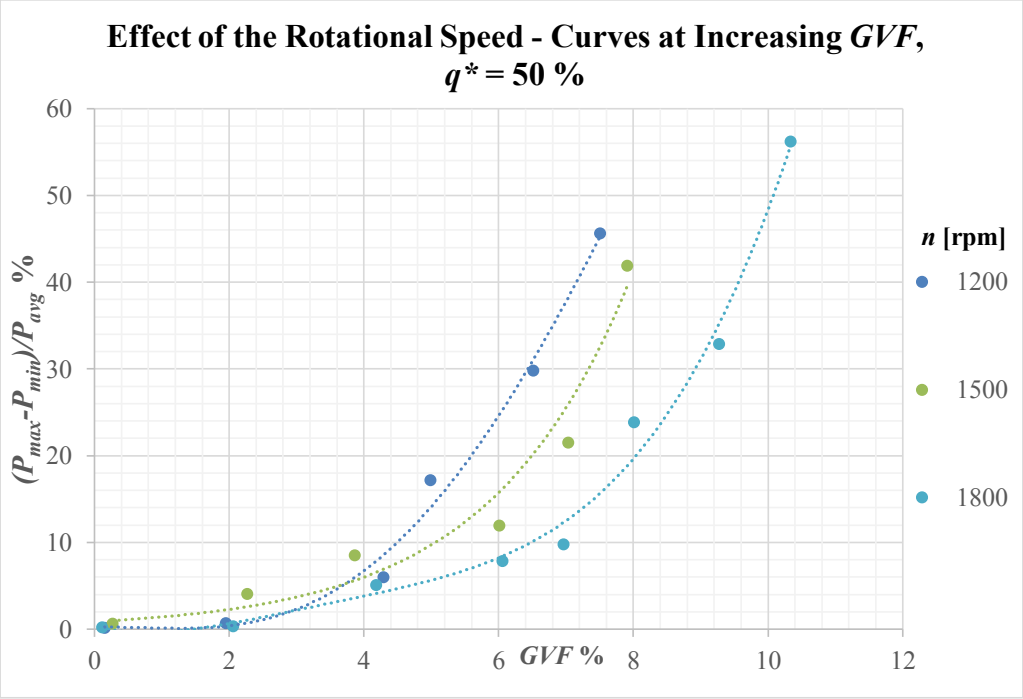

Fig. 48 – Effect of the rotational speed on the maximum relative variation in the delivered pressure

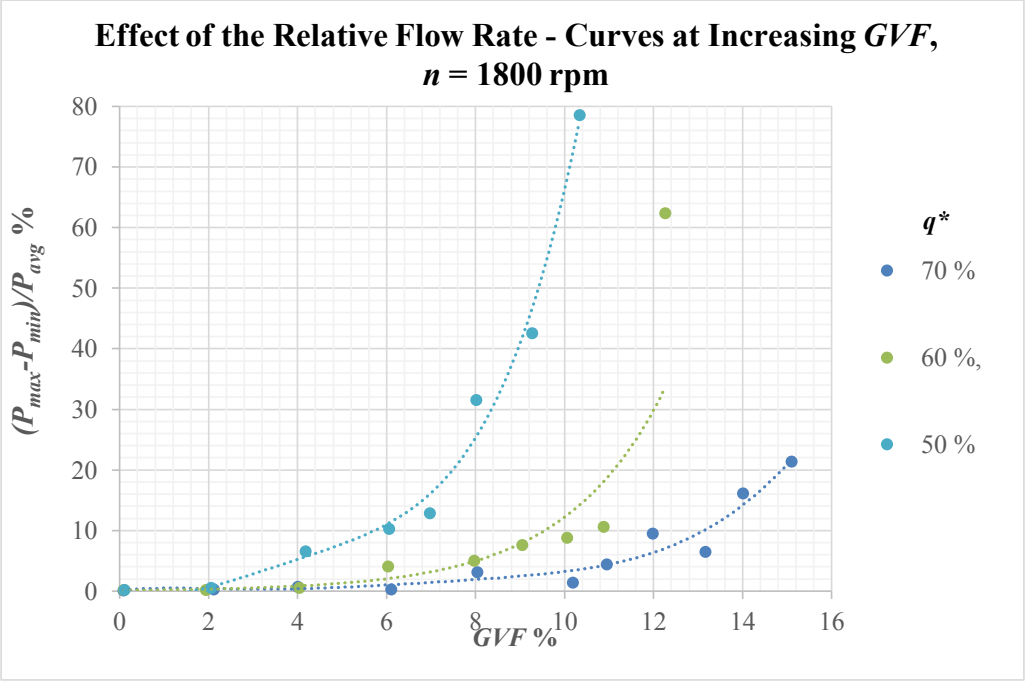

Fig. 49 - Effect of the relative flow rate on the maximum relative variation in the delivered pressure

The pressure at the pump outlet is taken as the reference value, since this location presents the strongest variations and it is related to the head delivered to the system and components installed downstream, which is the main purpose of the machine. The value in the curves above is calculated as the maximum variation in the pressure divided by its average value.

It should be noted, on the other side, that the most burdensome value of the thrust force, acting on the bearings, is related to the variations in the pressure difference across the pump stage, but the evaluation of this value is not so relevant, as other measurements giving a direct indication of the stresses on the shaft are rather required.

Figure 32 shows a level map of the relative variations in the pressure at the pump outlet.

According to the test results, an indicative threshold value to be used to monitor when this operating condition is approached can be within the range 10 – 16 %.

7.2.5 Flow pattern switch related to a performance curve change in slope

As discussed earlier, when switching among different operating conditions, the change in the flow pattern or the shift in the leading flow mechanism is progressive, but it can be accompanied by an intensification of the variations in the flow field variables. Figure 50 refers to the performance curve at n = 1200 rpm and a constant *GVF* value of 5 % reported in Fig. 9 of [77]. As it can be

observed, in the range between q^* = 70 % and q^* = 50%, the delivered pressure presents strong variations, which correspond to a variation in the flow pattern: the gas pocket forming on the blade pressure side interacts with the wake at the trailing edge, obstructing part of the channel. As the flow rate is decreased below q^* = 50 %, a gas pocket forms again at a lower streamwise location. The pressure oscillations have become now much lower; this can be also due to the contribution of the stronger tip leakage which contributes to mix the flow. This trend was confirmed when tests at higher settings of the tip clearance were performed.

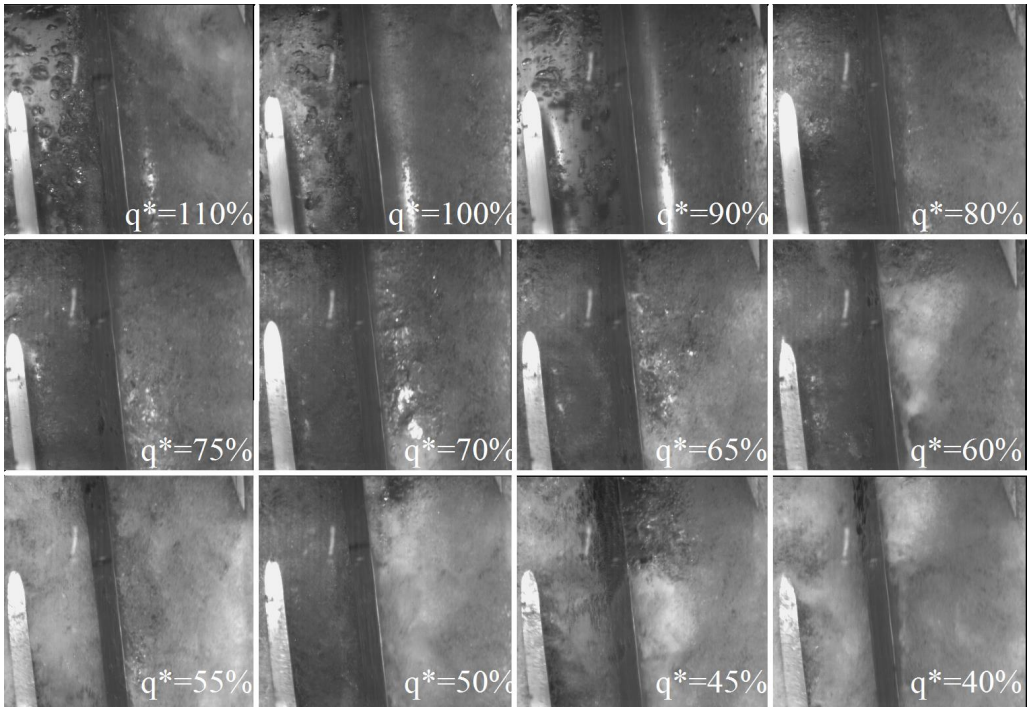

Fig. 50 - Flow pattern switch while decreasing the relative volumetric flow rate; test at n = 1200 rpm, p_i =1 atm, GVF = 5 %

7.3 Conclusions

The flow in the rotating channels presents an intrinsic unsteadiness which requires highly sensitive instrumentation to capture the low-scale temporal and spatial variations. Characteristic phenomena as the tip and recirculation vortices, and the formation of wakes and gas pockets, can still be clearly distinguished by visual investigations; however, a proper recognition through signal analysis, especially of their formation and related instability inception, is challenging, as the disturbances they introduce are quite irregular.

The analyses performed in the current work have allowed to understand their mechanisms and relate them to the outer measurements; this is useful to develop a control strategy, which can be implemented in real machines.
As a recommendation for further work, a thorough evaluation of the time-frequency analyses, once additional sensors are installed, is necessary.
In addition, advanced visualization techniques, promising to provide a quantitative reconstruction of the flow field, will be implemented once their feasibility in this specific application has been carefully evaluated.

Chapter 8
Computational Fluid Dynamics

The main objective of the project is to gain a deeper understanding of the flow fundamentals so as to improve the machine design. Multiphase flow operation involves a variety of additional phenomena which introduce a broad spectrum of disturbances in the flow field. The main investigation tool is, thus, direct flow visualization of the hydraulic channels, but Computational Fluid Dynamics provides a powerful tool to preliminarily assess the feasibility and improvement given by design modifications, once its reliability and fidelity to the real physics are proved. Unfortunately, as stated earlier, the characteristic phenomena due to the tip clearance and two-phase flow interaction often arise in locations where the mesh topology changes, for example near the blade leading edge, therefore making the simulation stability and success extremely demanding and sensitive to the space and time discretization.

8.1 The numerical flow simulations

In the last two decades, the marked increase in computational power and memory has made the use of numerical simulations reasonably affordable both at the design and performance analysis stages, and it currently covers a widespread range of applications; accurate calculations are performed on the whole machine stage. Nowadays, Computational Fluid Dynamics is extensively employed in the design and analysis of rotating machines. However, many secondary flow phenomena have a local inception and intermittent character requiring very fine spatial (grid) and temporal (time-step) discretization scales. This especially concerns the flow through small gaps, as the tip clearance in open impellers, the vortices generated by the sudden expansion of the leakage flow and their interaction with the main one, and the flow through the diffuser, which is governed by boundary layer effects and turbulence. General suggestions for the choice of the turbulent model and the near wall treatment are possible but the success mostly relies on the user's care in choosing the models which are supposed to reproduce the best fidelity to the real physics. These predictions need an accurate experimental validation, and, despite this, the model would still difficultly claim for general validity. When operating two-phase flows, the numerical simulation becomes very challenging, due to the phase interaction, bubble coalescence, momentum exchange; in addition, the bubble size varies along the flow path, and an incorrect choice of this parameter and the related models might strongly affect the prediction validity.

8.2 Modelling issues

There are no available models able to accurately describe the previously presented phenomena, which could be efficiently implemented in a turbomachine numerical simulation, so some simplified models are employed; the main goal then becomes a reliable modelization of the flow phenomena, possibly providing realistic results, close enough to experimental measurements, and still respecting the main features of the real physics.

A sensitivity study of the effect of these simulation settings is therefore needed to improve the capabilities and reduce the discretization errors.
The main investigation areas, with the relative parameters involved, are:

- tip clearance flow
- steady and unsteady simulations
- spatial and temporal discretization: mesh refinement and time stepping
- effects of simulating only separated components
- turbulence model
- interface between rotating and static part when the entire machine is included
- bubble size setting
- bubble accumulation and coalescence
- two-phase flow simulation model

Hereafter, a short overview of the modelling challenges is presented.

- Turbulence

The flow in the pump channels is intrinsically turbulent, thus a thorough evaluation of the models physics and limitations is of key importance. A common or separate turbulence treatment for the phases is possible.
Each of the turbulence models presents different capabilities and succeeds in specific areas but it presents limitations when applied to the whole machine. Besides the models adherence to the considered phenomenon, their applicability is related to both convergence issues and computational time. The proper meshing for an LES simulation, for example, would require extremely refined isotropic grids, but the general recommendation of grid lines orthogonal to the wall is difficult to be fulfilled due to the low impeller blade angles. In addition, a smoothly varying mesh size close to the zones where strong field variables gradients occur, increases the discretization cells number.

- Effect of simulating only separated components

Separate unsteady calculations of components, as the single rotating impeller, allow the use of refined meshes, required by more demanding turbulence models, which can give a more accurate description of the generation of the tip vortex and related unstable phenomena, mainly useful to reveal the effect of the geometry on the local velocity field. However, the flow in the diffuser is intrinsically unsteady, especially at part-load, and the rotor-stator interaction exerts a strong influence on the impeller pressure field. A proper analysis of the machine performance and stability requires, therefore, whole stage simulations.

- Domain Interface

When the entire machine is included, the interface between the rotating and static part can be handled with in different ways:

- Mixing plane technique: an average of the flow field is calculated at the interface and provided as an inlet condition for the following component; this way, the transient interaction between the following blade rows is not correctly taken into account;
- Frozen rotor setting: the interface is static, and the flow field values are transferred at each point between the two domains. To include the dependence on the angular position, a series of steady state simulations needs to be carried out;
- Sliding mesh principle, when unsteady calculations are performed: in this case, the required computational resources increase considerably;
- Transient Blade Row method: an attempt to reduce the computational efforts is simulating only a fraction of the geometry: the transient blade row technique, through some specific transformations at the rotating - static interface, allows to apply a transient simulation to only some blade channels. However, the transfer of the solution from the rotating to the static domain involves a complex transformation, affecting the prediction accuracy.

A careful evaluation of the validity of these techniques with a two-phase flow is needed.

- Domain Extent

The investigation of the machine stability should take into account the effect of local geometrical variations as curvatures and obstructions before and after the stage and the unsteady contribution of the flows through gaps and seals; the domain should reasonably extend upstream and downstream, in order to include the effect of the auxiliary components and let the flow develop, this adding further complexity to the simulated model.

- Multiphase Models

In this section, the theory behind homogeneous and in-homogeneous models is shortly presented in regard to the numerical implementation, highlighting the limitations and fidelity to the simulated physics the choice of the model entails.

The homogeneous model is based on the assumption that the phases share a common flow field, thus excluding any possible velocity slip and phase separation. A single equation for each of the transported quantities is solved, using an average density for the two-phase mixture. The equation of state for the gas phase compressibility and a constraint on the volume fractions (i.e. their sum being equal to 1) complete the equations system. It models evenly distributed very small bubbles carried away by an infinite drag force.

The in-homogeneous model allows phase separation solving two equations for each of the transported variables. Different formulations are available and the main parameters involved are the bubble diameter and its regime, both directly influencing the drag coefficient. The bubbles are assumed to be spherical and the Schiller-Naumann and Newton expressions are used, depending on the actual Reynolds number. The limitations of this model lay on the dispersed flow assumption, preventing a proper description of gas accumulation. This is, however, still valuable to describe the phases tendency to separate and accumulate.

The mixing model improves the modelling capabilities in the air accumulation areas, considering that the water phase becomes dispersed in these areas; this is taken into account through a switch in the interphase interaction terms once a threshold value of the void fraction is overcome.
It should be noted that, for relatively limited gas contents, the Eulerian-Lagrangian approach, with improved correlations, can be considered too.

8.3 Previous analyses related to the main phenomena involved

In the available literature, many investigations performed on turbomachines are available; hereafter, some representative results dealing with the challenges encountered in this specific research are presented.

Falcimaigne et al. [33] performed CFD analyses in Fluent®, investigating the areas of gas accumulation and loss sources models. The two-phase flow model is Eulerian. The hyphotesis is a low volumetric fraction of the dispersed phase, neglecting the mass transfer between the phases. A thin area of gas concentration is observed on the blade suction side.

Kim et al. [66] reported the performance and design optimization of a scaled single-stage helico-axial pump, through CFD and an experimental facility presenting similar operating values to the one considered in this study. The analysis is focused on a single blade passage and a stage average condition between the rotating and static parts is used. From numerical and experimental observations, water flowing on the outer ring and air accumulation on the blade suction side are reported. The numerical calculations predict more air accumulating on the blades, thus leading to higher losses than in reality. The authors considered the momentum transfer mainly due to the drag force and used a Grace model to determine the drag coefficients from experimental correlations. Non-drag forces are considered to exert a little influence.

Lucius and Brenner [67] performed a comparison of the SST and SAS approaches capabilities to the unsteady simulation of a centrifugal pump under part-load operation. While providing a reasonable agreement with regard to pressure rise, the SST model presents limitations in the resolution of turbulent velocity fluctuations, this according to the model formulation, which tends to include all the unsteadiness in turbulence. The SAS mode succeeds in capturing the dominant frequency of the rotating stall phenomenon at a cost of a longer computational time due to the spatial and temporal discretization refinement. Nevertheless, to properly perform an FFT analysis, extremely short time steps would be required, which are beyond the current calculators capability.

Posa et al [68] performed an LES of a mixed-flow pump under off-design conditions, employing an immersed boundary methodology along with a structural cylindrical coordinate solver; a discussion of the different flow physics under design and off-design conditions is presented.

Kochevsky [69] described the capabilities of the numerical simulation of two-phase flows in centrifugal pumps using a commercial CFD software. Two main cases are distinguished: limited content of gas/solid particles (presenting the various approaches to describe the different fractions)

and high gas content; in this case, the pump performance is affected by gas cavities (originated by merging gas bubbles), rupturing the fluid continuum. Different approaches are evaluated:

- Free Surface Flows: phases do not intermix. A homogeneous model is used, featuring a common set of Navier-Stokes equations and an equation of transfer of the fill function, expressing the concentration of liquid in gas;
- Mixture model: appropriate when none of the phases has dominant influence on the flow pattern. Equations for each phase and heat and mass transfer among them are used. Other physical phenomena described are compressibility (simulated using the energy equation), buoyancy and surface tension;
- Turbulence modelization: usually, the same model for both the phases is used
- Transient effects

Caridad et al. [70] carried out an investigation on a single impeller from an ESP, then compared to experimental data, making use of a two-fluid model for the flow field, while an extended version of the k-ε for turbulence modelling was employed. Different bubble sizes were simulated and a gas pocket on the blade pressure side was found. The set bubble size was 300 μm.

Marsis et al. [71] in order to improve the performance of an ESP, used CFD to compare the feasibility and effect some diffuser design modifications have; they simulated the entire stage, with a sliding mesh interface and transient simulations over a whole rotation. The set bubble size was 10 μm.

8.4 Software and workstation

The numerical simulations are performed using the software ANSYS CFX® 15; the blade geometry is prepared using ANSYS BladeGen® and the meshing in ANSYS Turbo Grid®. The calculations are carried out on a dedicated workstation featuring a 6 cores, 3,5 Mhz Intel® Xeon® central processing unit, with a 32 GB DDR4 RAM memory.

8.5 Test cases

The current experimental investigations comprise the effect of the impeller tip clearance on performance and stability and the two-phase flow mechanisms. An open impeller design has been chosen in order to allow direct visual access to the hydraulic channels. Unfortunately, the numerical simulation of the tip leakage flow is very demanding, requiring to limit the simulation to only one part of the machine.
To reduce tip leakage effects and to ease visualization, the rotor, which can be moved axially, has been positioned so as the tip clearance of the impeller-casing is the minimum possible (taking into account rotodynamic issues and thus limiting the rotational speed). This setting is meant to validate the numerical predictions of the shrouded version of the impeller.
As regards the choice of the test points, the values are limited by the test rig safety issues; the rotational speed is set at 1200 rpm. Tests are performed over a broader test matrix, which is

however not included in the current CFD analysis, as higher values of the speed and a higher density ratio (due to a lower inlet pressure), would cause a less homogeneous bubble size spatial distribution, and favor phase separation, making the simulation of the machine even more challenging. An accurate modelization involves parameters and coefficients which fit specifically a restricted phenomenon, so the fidelity to the real physics requires the pressure and velocity fields not to present strong variations along the machine, this especially applies to the bubble size; for this reason too, the machine rotational speed is limited, otherwise strong gradients would occur at the impeller-diffuser interface.

8.6 Geometry and mesh

As to the domain extent, the simulated model comprises an annular ring before and after the pump stage, extended enough in order to let the flow develop and not be influenced by the averaged imposed boundary conditions, but not too long to prevent the flow from separating.
When simulating separated components, the choice of the domain extent presents additional issues. Specific issues are the unknown turbulence field, back-flow zones, velocity field at the boundaries. The outcomes of a sector instead of the full 360^{O} simulation have been compared: no relevant difference justifying the increased solver efforts, for performance validation purposes, was found.
The grid topology is hexaedral and features around 200 nodes in the blade to blade direction, 50 in the hub to shroud one and 100 in the streamwise one. Figure 51 shows the grid refinement around the leading edge, while Tab. 7 reports the main mesh features.

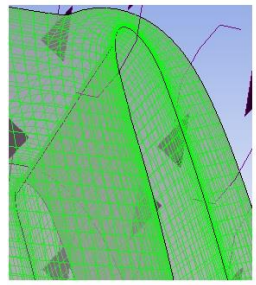

Fig. 51 - Mesh around the leading edge, shrouded version of the impeller

Parameter	**Value**
Number of Nodes	1017000
Target y^{+}	1
Min Ort. Angle	22,9 °
Exp. Factor	8
Asp. Ratio Max	13253

Table 7 - Shrouded impeller channel: mesh specifications

The simulations of the open impeller have proved to be more demanding due to the thin tip gap.
A progressive mesh refinement is required to assess the influence of the spatial discretization resolution, until the increase in mesh nodes does not entail any longer a relevant improvement on the control values results. In order to approach the target experimental value, the mesh should be refined well beyond the 1 million nodes of the shrouded impeller case, and the trend is not yet asymptotic. The number of cells covering the tip gap is specified and varies from 20 to 30 in the most refined cases. A meshing with 1,5 million nodes has been chosen as a good compromise between proximity to the experimental value and required computational resources.
A different topology and refinement in key areas seems not to affect significantly the overall flow field results; a quicker residuals reduction and no backflow areas at the inlet occur with a more homogeneous meshing.
A further mesh refinement, especially in the vicinity of the walls, needs to be performed when transient simulations with more accurate turbulence models are performed, in order to catch the local inception of typical intermittent phenomena as recirculation and tip vortex formation and shed, characteristic of part-load operation and open impellers.
It should be remarked that, once the mesh is well refined approaching a y^+ value of 1 to solve the boundary layer, the laminar – turbulent transition and the boundary layer detachment introduce oscillations in the solver residuals, which slow the convergence and complicate the two-phase model evaluation.

8.7 Simulation and solver settings

The following boundary conditions have been set:

- average reference pressure at the impeller inlet, along with the mixture composition
- bulk mass flow rate at the diffuser outlet.

A reversal of these boundary conditions has shown to ease mass conservation when introducing the two-phase flow, avoiding imbalances between inlet and outlet; afterwards, they have been set again as stated above.
A medium intensity turbulence level has been specified as 5 % of the average velocity; this setting, along with the turbulent model choice (SST for the water phase, and a laminar assumption for the air one), in this case, might exert a significant influence on the multiphase flow behaviour; increased turbulent flow conditions are beneficial for the interfacial momentum transfer between the phases. Part-load operation requires the specification of higher turbulence levels.
Proper periodicity conditions and symmetries are set to simulate only a sector of the machine.
For the interface between the rotating and static stages, the frozen rotor method is used for the steady state simulations, while the transient blade row technique allows to transfer the flow field values when unsteady calculations are performed. In this case, an accurate specification of the time-steps is required to ease convergence, usually involving a progressive reduction of this parameter: initially very little, to ease stability and smooth the flow field variations, after some hundreds of iterations, increased to quicken convergence.

In case of two-phase flow simulations, the flow model, the mixture properties and the interface terms parameters are specified. The usual method to approach a two-phase flow operating point is starting with a single-phase simulation at the desired volume flow rate, then introducing the two-phase mixture through the homogeneous model to provide an initial solution for the in-homogeneous simulation. A low initial bubble size, corresponding to the very high drag case, helps to obtain a converged solution. This parameter can then be progressively increased until a realistic value is reached.
When the whole performance curve needs to be simulated, the calculations start at the nominal flow value and the other points are obtained using the higher flow simulations results as the initial condition, at steps of usually $q^* = 10$ %.

8.8 Results

A thorough sensitivity study helps to choose the best simulation settings and reduce modelization errors; however, to assess the reliability of the numerical analyses, experimental validation is needed.

Hereafter, the results of the numerical investigations are reported.
In Fig. 52 and Fig. 53, the operating points below $q^* = 80$ % are obtained through a transient simulation making use of the transient blade row model.

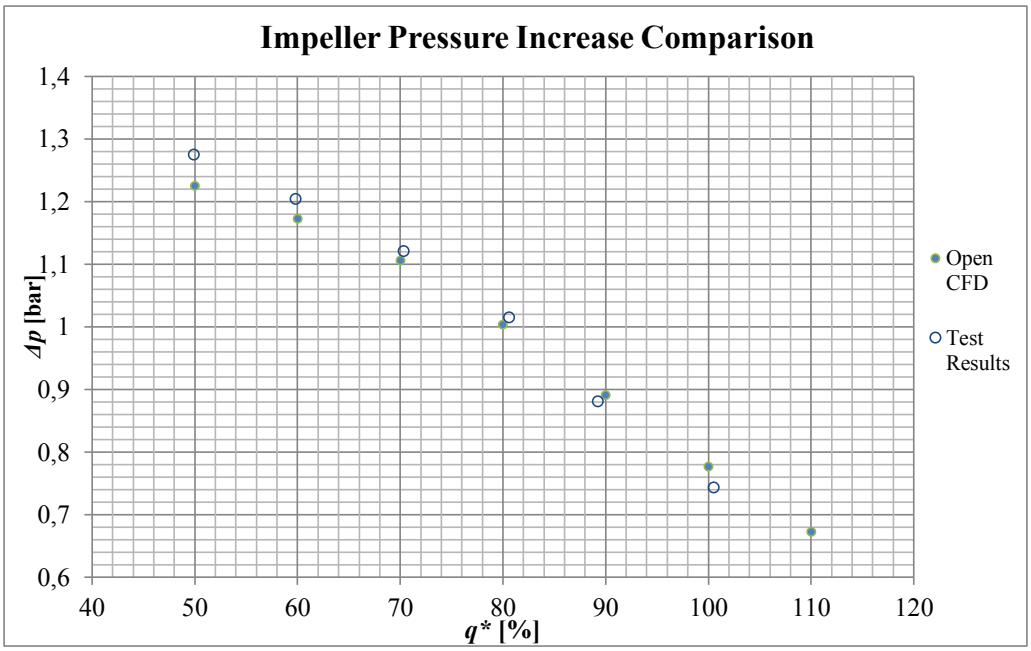

Fig. 52 - Impeller pressure increase – comparison at single-phase operation, open impeller case

In Fig. 53, the test results at very low tip clearance are compared with the simulation of the whole pump stage, shrouded impeller and diffuser. The contributions to the pressure increase by the two components are presented separately. The steady state simulations are performed on a single channel with the frozen rotor interface technique, while the transient ones use the blade row method.

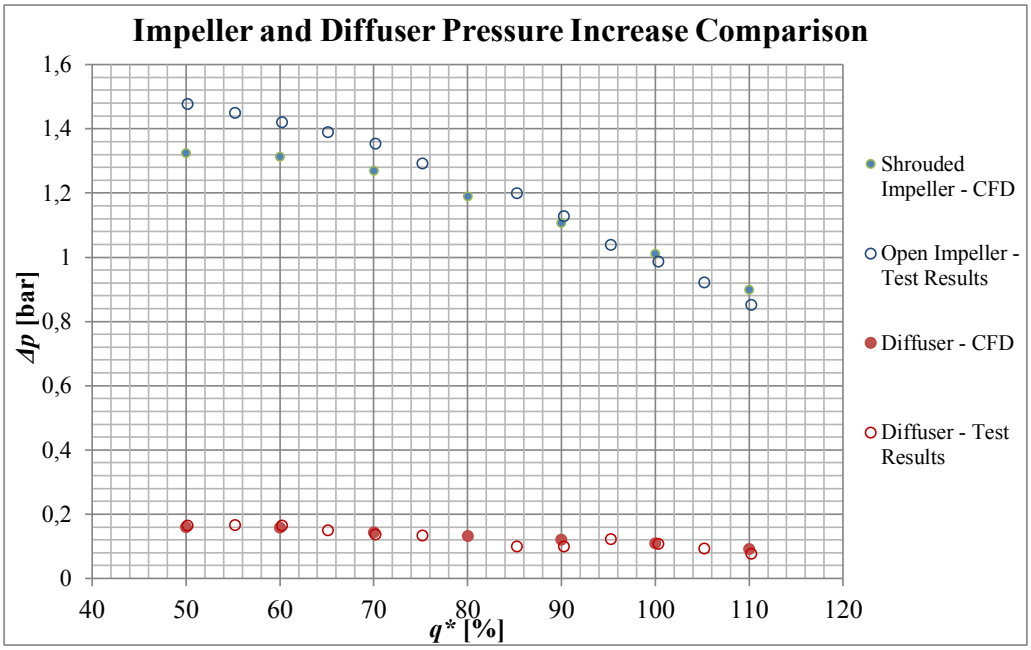

Fig. 53 - Impeller and diffuser pressure increase – comparison at single-phase operation, shrouded impeller case for the numerical simulations and low tip clearance case for the experimental one

Figure 54 shows the complex flow field at the diffuser outlet.

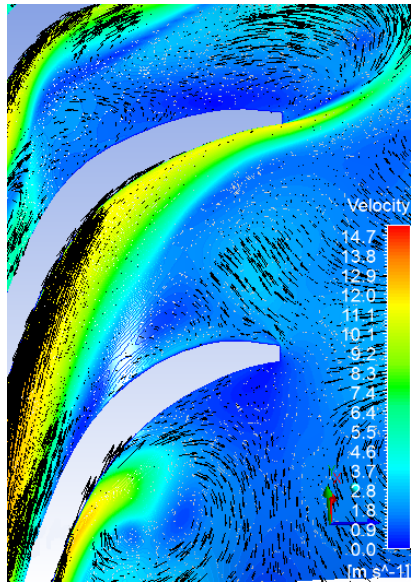

Fig. 54 - Recirculation at the diffuser outlet, from a single-phase simulation at q = 0,55*

8.9 Conclusion

The numerical simulation software ANSYS CFX® has been considered to:

- evaluate the capabilities of the currently available numerical simulation tool in single-phase operation, through comparison with experimental measurements
- understand the fundamentals, requirements and limitations of the available two-phase flow simulation models which can reasonably be implemented for this specific application.

Steady state models without a complex grid refinement, despite not capturing local phenomena, produce reliable overall performance prediction data under nominal conditions, and are still useful to provide a map of the velocity and pressure distribution useful for design optimization and evaluation of different concepts.
Unsteady simulations are essential to model the rotor-stator interaction, which produces pressure pulsations, and for all the cases in which the flow field presents a characteristic transient behaviour.

The averaging plane for the pressure calculation between impeller and diffuser coincides with the interface between these simulation domains, but the location of the real static pressure sensors slightly differs, being placed at the diffuser entrance, and their alignment is in accordance with the outer casing inner surface.
As reported before, a major cause of discrepancy between the model calculation results and the test measurements, which, apart from uncertainties, are taken as reality, is the influence the whole system exerts on the flow parameters, especially the pressure pulsations.

The numerical calculations of the machine operation in the part-load zone are reliable, but the accurate instability onset prediction remains a challenge.
Very demanding is the simulation of the diffuser flow, especially at part-load; a statistical description of the wall effects fails to predict the onset of recirculation as this phenomenon arises locally and only the simulation of the flow field can properly describe it.

The much easier convergence and the little dependence on the modelling settings of the homogeneous model do not compensate the intrinsic limitations it presents when attempting to model the two-phase flow through a rotating machine, especially if high gaseous fractions are simulated – in this case phase segregation plays a key role in performance degradation.
The intrinsic unsteadiness of multiphase flow complicates the analysis as, for example, a fundamental phase-interaction parameter as the bubble size presents a very broad distribution and variation along the hydraulic channel. In addition, the study of flow visualization has not shown a univocal bubble motion regime in the different areas and conditions, and typical phenomena as bubble breakup and coalescence, along with instabilities at the gas pocket interface, occur continuously.

8.10 Further investigations

Turbulence modelling for the tip leakage effects and two-phase flow needs further investigation.
The SST model is the most widely employed: despite it provides reliable performance results with still reasonable computational resources needs, a turbulence resolving model promises better adherence to reality. In this case, powerful calculators are required, and the modelling fidelity to reality and success rely on the correct choice of the threshold value for the length scale dividing the simulated from the modellized scales.
The Detached Eddy Simulation model interprets this concept; however, grid induced separation might occur, depending upon the settings, so no general rules of validity are available.
The more recent SAS mode, constitutes a good compromise between computational requirements and less sensitivity to the user's settings. It is based on an additional term reducing the excessive eddy viscosity introduced by Reynolds Averaged Navier-Stokes models, allowing to adapt the length scale to the local morphology.

Concerning Eulerian-Eulerian multiphase models, if the time scales to reach the equilibrium slip velocity are small, simplified models are available to compute the velocity of the dispersed phases, as performed in the Algebraic Slip Model.
Desirable and interesting further investigations are the choice of a reliable bubble size correlation and the implementation of a bubble size expression variable with the local flow field values. The inclusion of the Population Balance Model can take into account the bubble size distribution. In the MUSIG Model, the dispersed phase is divided into a number of size groups since the interfacial forces strongly depend on the bubble size.

Chapter 9
Conclusions

The experimental investigations, thanks to a detailed preliminary literature review and a careful consideration of the most suitable analysis tools, have allowed to accomplish the main research objectives, gaining a deeper understanding of the flow mechanisms responsible for performance degradation and instabilities. This, along with the evaluation of the different analysis tools capabilities, constitutes the original contribution of this work. The effect of the operating parameters on the onset and evolution of these phenomena has been studied relating flow visualization to performance measurements.
However, the thorough definition of a flow regimes map, as performed for the traditional cases of horizontal and vertical pipes, would require the knowledge of the individual phase velocities; these values can be provided by either image-based metrology or CFD.

The most challenging area, for both the signal analysis and numerical simulations, is to capture the local inception and to model the dynamic evolution of the two-phase flow instabilities, which has a fundamental role in pump performance degradation. More in general, as the bubbles coalesce and form a gas pocket, a very refined mesh is needed at the solid-liquid-gas interfaces. High-speed videos show that the liquid phase acts on the gas-accumulation zones mostly through shear stresses at the interface rather than by exerting a drag on its frontal area, trying to flush it downstream. In addition, the recirculation at the diffuser outlet causes troubles in ensuring mass balance between inlet and outlet.

The injection of small air contents has proved to reduce the noise emission and mitigate the effects of tip cavitation.

As regards the rotodynamic aspects, an already available two-axes vibration sensor has been placed on the bearings pedestal; however, due to the hub and casing arrangement, these data do not provide the necessary information to properly perform a thrust force and radial stresses analyses, which would rather benefit from the installation of magnetic bearings.

The experimental campaigns have confirmed most of the expected trends: conditions guaranteeing a higher shear among the phases, due to the pump speed or to secondary flows, improve the pump performance and delay the instabilities inception. However, how the different phenomena combine strongly depends on the pump geometry, so the definition of the operational boundaries and of a proper control strategy still relies on extensive experimental tests.

The traditional turbomachines design strategy aims at providing the maximum efficiency around the nominal operating point, with the minimum losses and the flow optimally matching the blade angles. The higher head production at lower flow rates, however, shows that recirculation can provide a different energy transfer method, sometimes even more effective in case of two-phase flow operation, where it fosters phase mixing, making the flow pattern more similar to dispersed

than separated flow. Therefore, in the design of a multiphase pump, manifold objectives need to be included: the optimal operating range should be targeted considering the effect of the operating parameters on efficiency, stability and reliability.

Tests over a broad range of operating conditions have shown that the typical flow structures occur at different operating parameters, but they present very similar features. Operation at low rotational speed and suction pressure has resulted in higher performance degradation than the values typical of operation under normal field conditions, but the performance curves shape, the surging inception zone and oscillations at surging are similar.

Turbulence and the flow unsteadiness due to phase interaction make the numerical simulation very challenging, giving flow visualization through high-speed imaging a great value for a further understanding of two-phase flow phenomena. However, in specific conditions, some flow phenomena as the tip leakage, might hide what happens below it, in the blade channel. In addition, it is difficult to assess local flow field parameters values as even bubble tracking is complicated by the continuous bubbles change in shape and size and coalescence.

Chapter 10
Further Work

A reconstruction of the entire flow field, with properly refined temporal and spatial scales, is desirable to improve the understanding of the flow mechanisms and validate the numerical simulations predictions.
Alternative techniques, as conductivity and optic fiber sensors, can already be used [62] to measure individual bubble velocity and size, and proved to be successful even up to α = 30 %, but bubble trajectory and bubble interaction cannot be detected.
On an electrical submersible pump application, Pirouzpanah et al. [72] made use of Electrical Resistance Tomography to investigate the flow field inside the diffuser. The technique is based on the different electrical properties of the two phases.
Advanced flow visualization experiments are reported in the open literature: the investigations mainly make use of laser-based optical diagnostics methods, either intrusive (i.e. tracer-based techniques: PIV, LDV) or non-intrusive (i.e. both Doppler-shifted and Time-of-flight methods).
According to [73-74], PIV and LDV techniques are useful to track fluid motion, but shadows generated by bubbles make it difficult to track accurately the fluid motion, and the technique is limited to low values of the dispersed phase volume fraction [75].
However, the application of these methods to the particular test conditions of this test facility, especially due to the broad range of scales introduced by the two-phase flow, requires a careful assessment. Some specific researches have focused on two-phase flow metrology, as PIV and X-ray imaging. The latter, thanks to the small beam size, can provide a fine resolution and can be based on X-ray absorption, related to material properties, or alternatively X-ray phase contrast, related to interface detection. These investigations are usually performed on very thin experimental sections assuming symmetry in depth; in the multiphase pump considered in this study, the flow field can present significative differences in the spanwise direction; in addition, due to the strong gradients in the boundary layers, the bubbles are smaller close to the walls.

It is desirable, for the development of the analytical approach describing the bubble motion and the two-phase flow evolution, that the correlations describing the switch among different flow regimes are experimentally validated for this specific application. Other two-phase flow non-dimensional numbers can be useful to complete the analysis; among them, Bond, Euler, Galileo, Kapitza, Knudsen, Kutateladze, Laplace, Stokes are of interest.

Future plans include an update of the laboratory setup to allow testing at higher rotational speed and suction pressure levels. When the tested *GVF* values overcome the range 50 – 80 %, the polytrophic reference transform and calculation procedure should be used instead. This requires accurate temperature measurements; multiphase flow, however, strongly affects their validity and accuracy. The main factors involved are: flow pattern, kinetics involved in the heat exchange,

thermal equilibrium, dynamic response behaviour due to transient phenomena and unsteady mixture composition, formation of a liquid layer on the sensor tip.

Further analyses are needed to properly relate the pressure peak dampening and the evolution of the flow instabilities in the machine, also making use of cross-correlation analyses which can provide a spatial reconstruction of the instabilities evolution, both in the axial and radial directions.

As a suggestion for a design improvement, the introduction of additional gaps on the blades should be considered in order to destroy gas accumulation; tests have shown that this would be helpful especially at the hub section and at mid-chord. The vane split design, as applied in [9], can be beneficial too.
An interesting further development, the contra-rotating rotors concept, as in [76], promises to avoid the recirculation at the diffuser outlet and allows an additional control through the rear rotor rotational speed.

References

[1] Falcimaigne, J., Decarre, S., *Multiphase Production*, 2008, Editions Technip

[2] Bratu, C., *Two-Phase Pump Transient Behaviour*, 1995, SPE Paper NO. 30660, pp. 247-261

[3] Pessoa, R., Prado, M. G., *Two-Phase Flow Performance for Electrical Submersible Pump Stages,* in *SPE Production & Facilities Journal*, vol. 18, no. 1, Feb. 2003, pp. 13-27

[4] Barrios, L. J., *Visualization and Modeling of Multiphase Performance Inside an Electrical Submersible Pump*, 2007, PhD Thesis, The University of Tulsa

[5] Gamboa, J. and Prado, M. G., *Visualization Study of Performance Breakdown in Two-Phase Performance of an Electrical Submersible Pump*, 2010, International Pump Users Symposium, Houston, TX

[6] F. Trevisan, M. Prado, *Experimental Investigation of the Viscous Effect on Two-Phase-Flow Patterns and Hydraulic Performance of Electrical Submersible Pumps,* in *Journal of Canadian Petroleum Technology,* vol. 50, no. 4, Apr. 2011, pp. 45-52

[7] Gamboa, J., Prado, M., G., *Review of Electrical-Submersible-Pump Surging Correlation and Models*, in *SPE Production & Operations Journal*, vol. 26, no. 4, Nov. 2011, pp. 314-324

[8] Gamboa, J., Prado, M., G., *Experimental Study of Two-Phase Performance of an Electric-Submersible-Pump Stage,* in *SPE Production & Operations*, vol. 27, no. 4, Nov. 2012, pp. 414-421

[9] Morrison, G., Pirouzpanah, S., Kirland, K, Scott, S. L., Barrios, L. J., *Performance Evaluation of a Multiphase Electric Submersible Pump*, 2014, OTC Conference Paper 25080

[10] Gülich, J. F., *Centrifugal Pumps*, 2nd edition, Springer, New York

[11] Furuya, O., *An Analytical Model for Prediction of Two-phase Flow Pump Performance*, 1985, *ASME J. Fluid. Eng*., 107, pp. 139-147

[12] Caridad, J., Kenyery, F., *Slip Factor for Centrifugal Impellers Under Single- and Two-Phase Flow Conditions*, 2004, ASME *J. Fluids Eng.,* vol. 127, no. 2, pp. 317-321

[13] Cooper, P., Schiavello, B., de Marolles, C., de Salis, J., Prang, A. J., Broussard, D. H., *Tutorial on Multiphase Gas-Liquid Pumping*, in *13th International Pump Users Symposium*, 1996

[14] Weber, M. E., Clift, R., Grace, J. R., *Bubbles, Drops and Particles*, 1978, Academic Press, New York

[15] Bhaga, D., Weber, M. E., *Bubbles in viscous liquids: shapes, wakes and velocities*, 1981, *Journal of Fluid Mechanics*, vol. 105, pp. 61-85

[16] Hinze, J. O., Fundamentals of the Hydrodynamic Mechanism of Splitting in Dispersion Processes, 1955, *Jl of AlChE*, Vol. l(3), pp. 289 - 295

[17] Spelt, P. D. M., Biesheuvel, A., *On the Motion of Gas Bubbles in Homogeneous Isotropic Turbulence*, 1997, *J. Fluid Mech.*, vol. 336, pp. 221-244

[18] Magnaudet, J., Eames, I., *The Motion of High-Reynolds-Number Bubbles in Inhomogeneous Flows*, 2000, *Annu. Rev. Fluid Mech.* 2000, 32, pp. 659–708

[19] Minemura, K., Murakami, M., *A Theoretical Study on Air Bubble Motion in a Centrifugal Pump Impeller*, 1980, *J. Fluid. Eng.,* 102(4), pp. 446-453

[20] Sterrett, J. D., *An experimental and analytical investigation into the performance of centrifugal pumps operating with air-water mixtures*, 1994, Ph.D. Thesis Auburn Univ., AL

[21] Brennen, C. E., *Fundamentals of Multiphase Flow*, 2009, 1st edition, Cambridge University Press

[22] Patel, B. R., Runstadler, P. W., *Investigation into the Two-Phase Flow Behavior of Centrifugal Pumps*, 1978, *ASME Symp. Polyphase Flow in Turbomachines*

[23] Sekoguchi, K., Takeda, S., Kanemori, Y., *Study of Air-Water Two-Phase Centrifugal Pump by means of Electric Resistivity Probe Technique for Void Fraction Measurement*, 1983, *Trans. Jpn. Soc. Mech. Eng.*, Vol. 49, pp. 1859-1868

[24] Kim., J. H., *A Formulation for Two-Phase Flow Dynamics in Centrifugal Pump,* 1984, *ASME Cavitation and Multiphase Flow*, pp. 58 - 60

[25] Sato, S., Asano, Y. and Furukawa, A., *Studies on Air-Water Two-Phase Flow Performance of a Centrifugal Pump with Open Impeller*, 1995, *Bulletin of Tsuyama National College of Technology* (in Japanese), no. 37, pp. 11-15.

[26] Chisely, E. A., *Two Phase Flow Centrifugal Pump. Performance*, 1997, Doctoral Thesis at the Idaho State University

[27] Kosyna, G., Suryawijaya, P., Friedrichs, J., *Improved Understanding of Two-Phase Flow Phenomena Based on Unsteady Blade Pressure Measurements*, 2001, vol. 2, no. 1, pp. 45 - 52

[28] Lea, J. F., Bearden, J. L., *Effect of Gaseous Fluids on Submersible Pump Performance*, 1982, *Journal of Petroleum Technology*, Vol. 34(12), pp. 2922-2930

[29] Poullikkas, A., *Two Phase Flow and Cavitation in Centrifugal Pump: A Theoretical and Experimental Investigation*, 1992, Loughborough University of Technology

[30] Thum, D: *Untersuchung von Homogenisierungseinrichtugen auf das Förderverhalten Radialer Kreiselpumpen bei Gasbeladenen Strömungen*. 2007, *Diss. TU Kaiserslautern* (in German)

[31] Gaard, S., *Modeling of Two-Phase Bubble Flow in Centrifugal Pumps*, 1992, Doctoral Thesis at the Norwegian University of Science and Technology

[32] Estevam, V., *A Phenomenological Analysis about Centrifugal Pump in Two-Phase flow Operation*, 2002, Campinas: Faculdade de Engenharia Mecanica. PhD Thesis, Universidade Estadual de Campinas

[33] Falcimaigne, J., Brac, J., Charron, Y., Pagnier P. and Vilagines, R., *Multiphase Pumping: Achievements and Perspectives*, in *Oil & Gas Science and Technology - Rev. IFP*, vol. 57, no. 1, 2002, pp. 99-107

[34] Zhang, J., Cai, S., Li, Y., Zhu, H., Zhang, Y., *Visualization Study of Gas-liquid Two-phase Flow Patterns Inside a Three-stage Rotodynamic Multiphase Pump*, 2015, in *Elsevier Journal of Experimental Thermal and Fluid Science*, vol. 70, pp. 125-138

[35] Cappellino, C., Roll, D., Wilson, G., *Design Considerations and Applications Guidelines for Pumping Liquids with Entrained Gas Using Open Impeller Centrifugal Pumps*, 1992, 9th International Pump Users Symposium, Houston, TX

[36] Turpin, J. L., Lea, J. F., Bearden J. L., *Gas-liquid Flow Through Centrifugal Pump – Correlation of Data*, 1986, Proc 3rd Interntl Pump Symp, Texas A&M, pp 13-20

[37] Chan, A. M. C., Kawaji, M., Nakamura, H., Kukita, Y., *Experimental study of two-phase pump performance using a full size nuclear reactor pump*, 1999, Vol. 193, pp. 159 - 172

[38] Korenchan, J. E., *Application of Analytical Centrifugal-Pump Performance Models in Two-Phase Flow*, 1984, MS Thesis at MIT

[39] Leporcher, E., Taiani, S., *Multiphase Pumping: The Lessons of Long-Term Field Testing*, 1995, SPE Conference Paper 30661

[40] Vangen, G., Carstensen, C., Bakken, L. E., *Gullfaks Multiphase Booster Project*, 1995, Offshore Technology Conference

[41] Ramberg, R. M., *Multiphase Pump Performance Modelling*, Doctoral Thesis, NTNU, Trondheim, 2007

[42] Beltur, R., Prado, M., Duran, J., Pessoa, R., *Analysis of Experimental Data of ESP Performance Under Two-Phase Flow Conditions*, 2003, SPE Conference Paper 80921

[43] Zhang, J., Zhu, H., Wei, H., Peng, J., *Performance Test of a 5-Stage Helico-axial Multiphase Pump*, 2011, *Applied Mechanics and Materials,* Vols. 52-54, pp 399-404

[44] Zhang, J., Cai, S., Zhu, H., Qiang, R., *Characteristic Analysis of Pressure Fluctuation in a Three-Stage Rotodynamic Multiphase Pump*, 2014, Proceedings of the ASME 2014 International Mechanical Engineering Congress and Exposition, ASME Paper IMECE2014-36092

[45] Mikielewicz J, Wilson D, Chan T, Goldfinch AL. *A Method for Correlating the Characteristics of Centrifugal Pumps in Two-Phase Flow,* 1978, *ASME J. Fluids Eng*, 100(4):395-409

[46] Bratu, C., *Rotodynamic Two-Phase Pump Performance*, in *Proceedings of SPE Annual Technical Conference and Exhibition*, 1994, pp. 555-567

[47] Zakem, S., *Determination of Gas Accumulation and Two-Phase Slip Velocity Ratio in a Rotating Impeller*, 1980, ASME Polyphase Flow and Transport Technology Symposium, pp. 167 - 173

[48] Manzano-Ruiz, J.J., *Experimental and Theoretical Study of Two-Phase Flow in Centrifugal Pumps*, 1980, Ph.D. Thesis, Massachusetts Institute of Technology

[49] Sachdeva, R., Doty, D. R., and Schmidt, Z., *Multiphase Flow Through Centrifugal Pumps*, 1992, University of Tulsa

[50] Sun, D., Modeling Gas-Liquid Head Performance of Electrical Submersible Pumps, 2009, Lambert Academic Publishing,

[51] Coste, P., Vilagines, R., *Use of the Cathare 1D Pump Model to Predict the Two-Phase Characteristic of a Pump for Petroleum Fluids*, 1993, Proceedings of the European Two-Phase Flow Group Meeting in Hannover, Germany

[52] S. Cao, G. Peng, Z. Yu, *Hydrodynamic Design of Rotodynamic Pump Impeller for Multiphase Pumping by Combined Approach of Inverse Design and CFD Analysis,* in *Journal of Fluids Engineering,* vol. 127, Mar. 2005

[53] Cirilo, R., *Air-Water Flow Through Electric Submersible Pumps*, 1998, MS Thesis at the University of Tulsa, Oklahoma

[54] Romero, M., *An Evaluation of an Electric Submersible Pumping System for High GOR Wells*, 1999, MS Thesis at the University of Tulsa, Oklahoma

[55] Minemura, K., Uchiyama, T., *Three-Dimensional Calculation of Air-Water Two-Phase Flow in Centrifugal Pump Impeller Based on a Bubbly Flow Model*, 1993, J. Fluids Eng, vol. 115(4), pp. 766 - 771

[56] Esson, A. L., Cohen, D. J., *The Development of a gas-handling Downhole Pump*, ImechE, 1996

[57] Grüner, T. G., *Wet Gas Compression*, Doctoral Thesis, NTNU, Trondheim, 2012

[58] Ishii, M., *Scaling Laws for Thermal-Hydraulic System Under Single Phase and Two-Phase Natural Circulation*, 1984, *Nuclear Engineering and Design*, Vol. 81, pp. 411 - 425

[59] Nishino K., Kato H., Torii K., *Stereo Imaging for Simultaneous Measurement of Size and Velocity of Particles in Dispersed Two-Phase Flow*, 2000, *Measurement Science and Technology*, Vol. 11(6), pp. 633-645

[60] Zaruba, A., Krepper, E., Prasser, H.-M., Reddy Vanga B.N., *Flow measurement and Instrumentation*, 2005, Vol. 16, pp. 277-287

[61] Honkanen, M., Saarenrinne, P., Stoor, T., Niinim, J., *Recognition of highly overlapping ellipse like bubble images*, 2005, *Meas. Sci. Technol.,* Vol. 16, pp. 1760-1770.

[62] Perez, C. A. A., *Measurement Techniques to Characterize Bubble Motion in Swarms*, 2007, PhD Thesis at the McGill University, Montreal, Canada

[63] Serena, A., Bakken, L. E., *Flow Visualization of Unsteady and Transient Phenomena in a Mixed-Flow Multiphase Pump*, 2016, *Proceedings of the ASME TurboExpo 2016*, Seould, South Korea, Paper No. GT2016-56581

[64] Serena, A., Bakken, L. E., *Investigation of the Blade Tip Clearance Effects on Performance and Stability of a Mixed-Flow Pump: High-Speed Camera Recordings of the Flow Structures, Local Measurements and Numerical Simulation*, 2015, *Proceedings of the ASME IMECE 2015*, Houston, TX, Paper No. IMECE2015-50398

[65] Serena, A., Bakken, L. E., *Experimental Characterization of the Flow Instabilities of a Mixed-Flow Multiphase Pump Operating Air and Water Through Local Visualization and Analysis of Dynamic Measurements*, 2015, *Proceedings of the ASME IMECE 2015*, Houston, TX, Paper No. IMECE2015-50396

[66] Kim, J-H., Lee, H-C., Kim, J-H., Choi, Y-S., Yoon, J-Y., Yoo, I-S., Choi, W-C., *Improvement of Hydrodynamic Performance of a Multiphase Pump Using Design of Experiment Techniques*, 2015, *ASME Journal of Fluids Engineering*, vol. 137, pp. 1-15

[67] Lucius, A., Brenner, G., *Unsteady CFD Simulations of a Pump in Part Load Conditions Using Scale-Adaptive Simulation*, 2010, *International Journal of Heat and Fluid Flow*, vol. 31, pp. 1113-1118

[68] Posa, A., Lippolis, A., Balaras, E., *Large-Eddy Simulation of a Mixed-Flow Pump at Off-Design Conditions*, 2015, *ASME Journal of Fluids Engineering,* Vol. 137(10), 101302

[69] Kochevsky, A. N., *Capabilities of Numerical Simulation of Multiphase Flows in Centrifugal Pumps Using Modern CFD Software*, 2005, ARXIV, eprint arXiv:physics/0509193

[70] Caridad, J., Asuage, M, Kenyery, F., Aguillon, O., *Characterization of a centrifugal pump impeller under two-phase flow conditions*, 2008, *J. Petrol*, Vol. 63(1), pp. 18-22

[71] Marsis, E., Pirouzpanah, S., Morrison, G., CFD-*Based Design Improvement for Single-phase and Two-Phase Flows Inside an Electrical Submersible Pump*, 2013, ASME Paper FEDSM2013-16060

[72] Pirouzpanah, S., Gudigopuram, S. R., Morrison, G. L., *Flow Characterization in an ESP Pump Using Conductivity Measurements*, 2016, *Proceedings of the Joint US-European Fluids Engineering Division Summer Meeting*, Paper No. FEDSM2014-21611

[73] Deen, N. G., Hjertager, B. H., Solberg, T., *Comparison of PIV and LDA measurement methods applied to gas-liquid flow in a bubble column*, 2000, 10th Int. Symp. on Appl. of Laser Techniques to Fluid Mech., Lisbon, Portugal

[74] Buwa, V., Ranade, V., *Dynamic of gas-liquid flow in a rectangular bubble column: experiments and single/multi-group CFD simulations*, 2002, *Chemical Engineering Science*, Vol. 57, pp. 4715-4736.

[75] Deen, N.G., Westerweel, J., Delnoij, E., *Two-Phase PIV of Bubbly Flows: Status and Trends*, 2002, *Chem. Eng. Technol.*, Vol. 25, pp. 97-101

[76] Shigemitsu, T., Furukawa, A., Watanabe, S., Okuma, K., *Air/Water Two-Phase Flow Performance of Contra-Rotating Axial Flow Pump and Rotational Speed Control of Rear Rotor*, 2005, *Proceedings of the ASME 2015 Fluids Engineering Division Summer Meeting*, Paper No. FEDSM2005-77002

[77] Serena, A., Bakken, L. E., *Experimental Study of the Influence of the Operating Parameters on the Performance and Capability of a Mixed-Flow Multiphase Pump*, 2016, *Proceedings of the ASME TurboExpo 2016*, Seould, South Korea, Paper No. GT2016-56576

[78] Rothe, P. H., Runstadler, P. W., Jr. and Dolan, F. X., *Pump Surge Due to Two-Phase Flow*, in *Polyphase Flow in Turbomachinery*, C. Brennan et al., Publ. H00123, ASME, New York, NY, 1978, pp. 121-137

[79] E. Schleicher, M. J. Da Silva, U. Hampel, *Enhanced Local Void and Temperature Measurements for Highly Transient Multiphase Flows*, in *IEEE Transactions on Instrumentation and Measurement*, vol. 57, no. 2, Feb. 2008, pp. 401-405

APPENDIX

Appendix I – Summary of the original contributions of previous researchers on flow visualization

Murakami and Minemura [19] – semi-open type centrifugal pump mounted in a transparent casing

- a transparent casing allows observation of the flow phenomena making use of a strobolight;
- three impellers with a different number of blades are compared at the same rotational speed: the bubble behaviour and the *GVF* at which the transition bubbly- to slug- flow occurs are affected: in the impellers with a higher number of blades, a more regular behaviour and continuous change in the performance deterioration is observed;
- this model deals with the case of few small bubbles: their motion is described through a differential equation in which the drag, pressure, buoyancy and inertia forces are taken into account;
- the performance curves are affected by an increase in the void-fraction: the abrupt flow pattern change results in curve discontinuities. The change in flow patterns is presented: at very low air content, the pump head is increased by air admission, due to the increase in the peripheral component of the absolute velocity. Air is accumulated on the blade suction side due to a strong adverse pressure gradient. A further increase in the air fraction decreases the available flow area; a discontinuity now appears, but the rate of decrease is lessened because of a compensation between higher impeller work and losses too. As the air bubbles occupy the greater part of the suction side of the blades, two abrupt changes in the flow pattern cause two other discontinuities;
- as the *GVF* is considerably increased, unstable operating conditions occur: an air filled space is observed extending from the inlet to the outlet;
- as the *GVF* is further increased, the pump recovers its performance; a large hollow space can be observed on the blade pressure side;
- four flow patterns are identified:
    - isolated bubbly flow at low *GVF*, negligible bubble interaction: pump head not affected
    - bubbly flow: very organised bubbly flow pattern, interaction among the bubbles
    - slug flow: bubbles coalesce forming an air pocket at the impeller inlet region
    - segregated flow: a large air pocket is stuck at the inlet impeller region.

Patel [22] – unshrouded centrifugal pump

- at low values of the flow coefficient, two flow regimes occur, depending on the *GVF*: when the gas content is low, homogeneous bubble mixture; when it increases, a large void forms in the upper part of the impeller;
- at high flow rate, no abrupt transition is found: bubbles flow along the SS.

Sekoguchi [23] – closed radial flow impeller

- for $\alpha < 0{,}02$, bubble flow is observed; the path is from SS at inlet towards PS at the outlet;
- at higher α, a large pocket grows at the inlet, leading to slug flow.

Kim [24] – radial pump

- identified the main mechanism of head degradation in the acceleration of the liquid phase;
- detected bubble accumulation on the blade pressure side;
- recognized that in an axial pump both the centrifugal and Coriolis forces are in the radial direction and the acceleration due to the streamline curvature is predominantly tangential, so none of these components plays a leading role in the axial direction, giving a reduced liquid phase acceleration compared to a radial pump.

Sato [25] – volute-type radial pump with vaneless diffuser

- at high liquid flow rate, air accumulation is found on PS at mid-radius, while on SS at the outlet; as α increases, the air cavity elongates reaching the trailing edge;
- at low liquid flow rate, gas bubbles flow on PS.

Chisely [26] – centrifugal pump, open impeller

- the head degradation mechanism is related to the reduction in the effective flow channel for water, causing an increase in the absolute flow velocity and the relative impeller discharge angle;
- the gas pocket starts at the suction pipe, where $\Delta p = 0$; as α increases, the air space extends to the pump inlet and through the vane.

Kosyna [27] – radial pumps

- gas accumulation is reported on PS;
- at higher rotational speeds, the critical *GVF* increases;
- measured the pressure profile: while α increases, p drops uniformly on PS.

Lea and Bearden [28] – centrifugal pump

- classified the two-phase flow stage performance into 4 categories:
    - non gas interference
    - gas interference
    - intermittent gas lock (causing low-frequency oscillations)
    - gas lock
- other factors reported as altering the performance are rotational speed, inlet pressure, free gas at inlet, impeller type.

Poulikkas [29] – centrifugal pump

- at low α, bubbles concentrate at the intake, on SS;
- at high α, the accumulation advances;
- as α is further increased, blockage occurs;
- flow separation at the discharge may occur, leading to flow deflection and outlet area reduction.

Thum [30] – centrifugal pump

- identifies four flow regimes:
  - Bubble flow: accumulation areas: PS, SS;
  - Plug flow, separation; accumulation on the upper part of the inlet pipe;
  - Slug flow: accumulation on the SS;
  - Stratified flow.
- it is remarked that this behaviour is affected by the flow structure in the inlet pipe; for the pumps used in the petroleum industry, the first impeller destroys the intake flow pattern into bubbles; their average size is a function of the rotational speed.

Gaard [31] – vertically oriented centrifugal pump with PMMA transparent casing

- performed local pressure measurements in the pump channel and visualization using a stroboscopic flash lamp;
- recorded hysteresis in the two-phase characteristics;
- the effect of the streamline curvature at low pressure is air accumulation and expansion, causing a reduction in the drag, thus bubbles can no longer overcome the pressure gradient;
- air is forced towards the outer annulus, increasing the water velocity and affecting the correct angles;
- concluded that the pump accepted the largest α at low volumetric flow rate.

Estevam [32] – radial pump

- gas accumulation on the PS is reported;
- identified two flow patterns:
  - stratified flow at the channels inlet due to a stationary bubble
  - dispersed bubble flow close to the exit
- in the suction pipe, a dispersed bubble flow regime is present;
- the size of the stationary elongated bubble at the impeller intake depends on ω, α, q^*
- it should be noted that, as there is not the hub part of the impeller, the contribution of recirculation plays a key role.

Falcimaigne [33] – helico-axial multiphase pump with transparent casing

- employed advanced measurement techniques to determine the velocity field and bubbles distribution, especially in proximity of the blade leading edge
- observed secondary flow regions as recirculation and vortices close to the tip clearance.

Gamboa et at. [5] – ESP stage with transparent acrylic casing

- different fluids are employed: distilled water + air, distilled water + sulphur hexafluoride, air + isopropyl alcohol;
- gas pocket: small and located near the front shroud, at over-load. When the liquid flow rate decreases, it firstly becomes stable (reducing the available flowing area for the liquid); at

lower flow rates, it forces the liquid to flow underneath; bubble coalescence within the impeller channel forms a gas pocket even at zero head;
- the gas density affects the critical *GVF* for the gas pocket formation; surface tension and the bubble size influence its stability;
- the mechanism triggering the gas pocket formation depends on: pump type, impeller geometry, rotational speed, liquid flow rate, *GVF*, fluid properties and intake pressure;
- performance curves with distillate water and air as test fluids are presented: the stage pressure rise mildly deteriorates as the *GVF* increases, until a sudden performance breakdown occurs;
- gas injection is performed through two injectors in different positions: surging moves to higher *GVF* as the liquid flow rate is reduced; the bubble size at the inlet region strongly affects the gas handling capability;
- using distilled water and SF_6, the effect of the gas density on the stage performance is investigated; SF_6 has a molecular weight 6-7 times higher than water and a similar surface tension;
- distilled water and isopropyl alcohol or isopropanol are used to study the effect of surface tension. A higher concentration of alcohol decreases the surface tension; surging moves to a higher *GVF*; different explanations are possible:
    - reduction in water surface tension (making a reduction in the particle size that may affect the stage performance);
    - change in bubble size polarization, creating a "non-coalescing" system within the impeller (the mechanism is related to higher interfacial repulsion force); the injection of surfactants moves surging at higher *GVF*;
- the following flow patterns are identified:
    - isolated bubbles: there is no reciprocal interaction; different shapes are found, depending on the dimensions. Bubbles change their orientation along the impeller channel (effect of gravity and liquid stream);
    - bubbly flow: the bubbles behaviour depends on their dimensions: the smallest, concentrated close to the back shroud; the intermediate ones, flowing between half of the channel height and the back shroud, can be dragged out or trapped in a recirculation; the largest ones flow close to the front shroud. Some agglomerations are observed. Bubble breakup occurs only if the intake bubble size overcomes a certain value;
    - gas pocket: around the operating point at which surging occurs. It is located close to the front shroud; not only a stationary gas pocket exists, but also a continuous gas zone in the region without a back shroud;
    - segregated gas: bursts of gas coming out from the gas pocket are broken into fine spherical or ellipsoid bubbles, some moving away quickly, others recirculating. The gas pockets behaviour at different flow rates is described;
- a pressure recovery is observed after the surging, when operating alcohol aqueous solutions. In addition, isopropyl alcohol strongly influences the gas pocket stability (because of the

interfacial phenomena between the phases), here studied at different *GVF*. In subsea applications, surfactants such as mono ethylene glycol corrosion inhibitors, may improve the two-phase performance.

Gamboa [8] – electrical submersible pump

- a performance map defining boundaries and discontinuities for the different pump regimes and how they are affected by rotational speed and intake stage pressure is presented:
    - explained the performance breakdown: the stage pressure increment reaches a local maximum; here the critical *GVF* is presented in function of q_l and q_g; as q_l increases, the critical *GVF* increases too, but Δp drops; pressure increment and gas tolerance combination suggest to design and operate close to BEP;
    - second boundary: steady stage operation after performance breakdown occurs; Δp is independent of q_l;
    - third boundary: Δp reaches a minimum value;
    - open-flow boundary: beginning of the normal pump operation mode (under two-phase flow, multiple operating conditions can satisfy this criterion). Some of these points lay over the surging initiation boundary;
- the so found boundaries, affected by the inlet pressure, are finally plotted together to make the pump performance map; 4 regimes can be distinguished:
    - mild performance deterioration, associated to bubbly flow pattern;
    - performance reverse slope related to the presence of an unstable gas pocket;
    - severe performance deterioration (stage-pressure increment insensitive to q_l) with a stable gas pocket;
    - nil performance.

Trevisan [6] – electrical submersible pump with transparent casing

- four flow-patterns are observed inside the impeller channel:
    - agglomerated bubble: a stationary bubble is present near the impeller blade leading edge, pressure side and close to the bottom shroud; using water instead of oil, an agglomeration of bubbles is observed; viscosity reduces the turbulence effects and improves bubble coalescence or stabilizes the stationary bubble;
    - gas pocket: it occupies half of the impeller-channel width; its length ranges from half to full impeller blade extension; the two-phase interface remains stable;
    - segregated gas: a secondary bubble appears at the impeller discharge; a stationary bubble close to the top shroud appears too;
    - intermittent gas: considerably large and irregular bubbles rise through the impeller entrance exiting without breaking; a gas-locking condition is reached;
- the two main effects of viscosity can be summarized as follows:
    - reduction in turbulent forces causing bubble breakup;

- increasing in drag forces acting on the gas-liquid interface, allowing the large gas bubbles to overcome the pressure gradient.

Zhang [34] – three-stage helico-axial pump with transparent casing

- classified four categories of flow patterns; as the gas fraction is increased: bubble, bubbly, gas pocket, segregated flow;
- gas pocket forms at the suction side and then moves to the pressure side;
- steep performance degradation curve in the gas pocket regime, then smooth decrease corresponding to the segregated flow region;
- bubble size and shape study: oblate ellipsoids and segments of ellipsoids and spheres are a good approximation; average and peak values are measured at different *GVF* and *n* values
- the bubbles enter the channel initially occupying the suction side, then move towards the pressure side at low span;
- detected recirculation and vortices in the diffuser.

Appendix II - Summary of the original features of the main semi-empirical models

Mikielewicz [45] (1978) – centrifugal pump

- defined the head loss ratio as the apparent loss of head under two-phase flow operation divided by the loss of head under single-phase flow. This head-loss ratio is shown to be primarily a function of α. A specific factor takes into account geometrical and flow regime factors. It is reported its validity is limited below $\alpha < 0{,}1$.

Turpin, Lea and Bearden [36] (1982) – three different pumps tested with diesel and CO_2 at different suction pressures

- an empirical model was developed. The factors controlling head deterioration are the ratio among the gas and liquid flow rates, the suction pressure and the total flow rate. A good validity is at low q_g and low p_i, and at high q_g and high p_i. A general exponential decay in performance with q_s/q_l is observed.
  Relationships are obtained to quantify the region of unacceptable pump performance.

Korenchan [38] (1982) – steam and water centrifugal pump

- obtained an analytical expression, giving realistic predictions for low α, for the Euler equation:

$$\psi_{tp} = 1 - \frac{f_{tp2}\Phi_{tp2}}{tg\,\beta_2} - \left(\frac{d_1}{d_2}\right)^2 (1 - f_{tp1}\Phi_{tp1} tg\,\gamma_1)$$

  where f_{tp} is a two-phase flow function depending on slip velocity and *GVF*.
  In the expression of the multiphase pump head, an integral calculation of the density trend (temperature dependent) through the pump is required. However, two simplifications - phases in thermal equilibrium and isothermal fluid behaviour - can allow to skip the need of an energy equation.
  The true values of mixture densities, phase velocities and thermal behaviour are not known, but implicitly included in the multipliers mentioned above.

Ramberg [41] (2007) – helico-axial pump

- modelled the head degradation with the following expression; the main factors accounting for the head drop are the mixture density and the void fraction:

$$H_{mp} = H_{sp}\left(\frac{\rho_{mp}}{\rho_l}\right)(1 + \alpha)$$

  which has proved to be valid in the range 0 - 60 % *GVF*.

Appendix III – Specific features of the different analytical models, with the reported range of validity

Zakem [47] – analytical model on straight bladed impellers

- mono-dimensional control volume method to analyse gas bubbles and liquid interaction;
- no separation and no stratification are assumed;
- equations: phases mass conservation, mixture momentum equation, bubble motion equation, Equation of State (ideal gas); the void fraction distribution in the channel is obtained and v_l, v_g through a Taylor series approximation method;
- the key values are: r_b = 1,5 mm, C_d = 0,4, $dp/ds|_f$ = 0,03.

Furuya [11] – developed and analytical model based on this last method

- incorporated pump geometry, α, phase slip and flow regime;
- neglected compressibility, condensation and losses in the volute;
- two flow-regimes depending on α are classified and each presents characteristic values of the interfacial properties:
  $\alpha \leq 0{,}3$: bubbly flow regime; r_b = 1,59 mm, C_d = 0,54
  $\alpha \geq 0{,}4$: churn-turbulent flow regime; $C_d/r_b = 0{,}11 \cdot (1- \alpha)^3$ [mm^{-1}];
- when it comes to the model validity, compared to experimental results, errors are around 30 % for $\alpha < 0{,}2$ and 50 % for $\alpha > 0{,}3$.

Manzano – Ruiz [48] – developed a two-phase flow model to investigate the slip effect

- the main assumptions are: one dimensional flow for each of the phases and spherical bubbles;
- the following phenomena are neglected: bubble disturbance on the liquid phase, gravitational effects and wall shear;
- as to the interfacial values, C_D is obtained from correlations, while r_b = 1 mm from observations.

Minemura [19] – included fluid viscosity and gas–phase compressibility

- considered energy changes in the transitional flow between impeller and volute;
- found that during the transition from bubbly to churn-turbulent flow, the interfacial and virtual mass coefficient changes linearly with α ($0{,}08 < \alpha < 0{,}14$);
- concerning the validity, the model provides a good agreement for ± 20 % of the rated flow rate.

Sachdeva [49] – starting from a one-dimensional liquid flow model, developed a two-phase flow model based on:

- 5 equations: liquid and gas phases mass conservation, liquid and gas phases momentum balance, equation of state;
- considered the pump geometry, but neglected the diffuser performance;
- solutions are found through the Runge-Kutta-Gill Method along a streamline;
- validity: the error in the Δp is around 50 %, while the one for α is less than 30 %.

More in detail, on Sachdeva's and Minemura's models
Assumptions:

- the friction loss within the impeller takes into account the losses in the stationary passages too;
- both phases follow the same one-dimensional streamlines;
- perfect gas, adiabatic compression; incompressible liquid;
- negligible mass and heat transfer between the phases;
- constant angular velocity; steady state flow in the rotating frame of reference;
- Sachdeva's model neglects channel roughness.

Different expressions and correlations are employed for:

- wall fraction, interfacial friction and virtual mass force;
- boundary conditions:
    - Minemura's: no prerotation
    - Sachdeva's: homogeneous flow at the entrance.

Sun [50] – two-phase flow streamline model for an Electrical Submersible Pump

- among the main assumptions:
    - perfect gas, adiabatic compression;
    - no interphase mass or heat transfer;
    - $p_l = p_g$;
- made use of a cylindrical coordinate system;
- the wall frictional pressure gradient is included;
- improved expressions for some terms are presented:
    - wall frictional pressure gradient; stratified flow is assumed and correction factors for rectangular flow channel, curved, rotating channel are included;
    - interfacial friction force per unit volume and new correlations for $C_d/r_{interfacial}$; definition of an interfacial Reynolds number, based on bubble size and slip velocity;
    - boundary conditions.

Bratu [46] – analytical model for the Poseidon Project helico – axial pump

- improvement of Furuya's model for the estimation of void fraction and slip ratio, on a pump model similar to the one considered in this research;
- the previous models were based on the extension of the Euler-Equation to separated two-phase flow through correlations. In addition, as those from [19,47], they need numerical integration, not enabling the study of design parameters sensitivity;
- a differential equation with the gas fraction only depending on the streamline coordinate is obtained. This equation describes the void fraction evolution along the streamline depending on $\dot{m}_l$, $\dot{m}_g$, n, flow section variation. Usually, it is solved numerically. In alternative, a first-order analytical approximation gives a simplified relation;

- considering the transversal acceleration field, the onset of stratification is predicted. In this case, two momentum conservation (applied to the two phases and the gas bubbles) equations are combined, yielding to a relation among Coriolis, centrifugal, streamline curvature acceleration, drag forces and the particle position and the transverse particle velocity; in addition, along with an expression for the gas layer thickness, a modified Froude Number is defined, providing a separation condition (transition bubbly to stratified flow);
- observed that an optimal design to avoid separation requires equilibrium between external forces and a significant drag force;
- numerical calculations are based on a two-fluid, two-component, seven equations model; mass, momentum, energy balance equations for each phase are written in a rotating frame; centrifugal, Coriolis and curvature accelerations are considered. In addition, a set of constitutive relations is adopted to account for 3D effects in the impeller;
- when it comes to the modelling validity, performances are well predicted; flow stratification and interfacial friction effects on the two-phase pressure gain are observed. The conclusion is that a one-dimensional theory including stratification effects is suitable to model the pump behaviour;
- long period performance tests are also reported. A recirculation tank was used to maintain a minimum liquid.

Coste and Vilagines [51]: comparison of an adapted version of the one-dimensional CATHARE model predictions with experimental data on a helico-axial pump model

- a set of constitutive relations to account for 3D effects is included;
- the deviation phenomenon at the outlet is neglected;
- included the phase mixing effects due to turbulence;
- singular head losses, due to separation, eddy effects in non uniform parts, abrupt changes in the velocity direction, are taken into account;
- recirculation is neglected;
- a correction factor is used to tune the interfacial friction model, as flow perturbation induces mode mechanical coupling between the phases compared to pipe flow;
- agreement is within 10% for low and nominal flow rates.

Appendix IV – Previous authors' original contributions on surging

Lea and Bearden [28] showed the dependency of the surging onset on:

- pump type, suggesting the best is the mixed-flow one;
- fluid properties: breakdown of pumping capacity has been observed at lower *GVF* for diesel-CO_2 instead of air-water;
- higher inlet *GVF* led to surge onset at higher flow rate.

Cooper [13] identified these mechanisms affecting surging and choking phenomena:

- at high α, gas bubbles concentrate at the impeller eye on SS (at part-load) and on PS (at over load); this behaviour is due to high local pressure gradients, resulting from:
    - incidence angle, positive for $q < q_{BEP}$ and negative for $q > q_{BEP}$;
    - bubbles local blockage;
- influence of the gas content on the speed of sound: at $\alpha = 0{,}1$, for example, $c_s \approx 25$ m/s, value reached by peak relative velocities around the blade leading edge under off-design conditions. c_s is a function of the density ratio and the inlet pressure.
  The main effects (especially under off-design, low p_i, high ω, small blade throat areas) are:
    - sonic blockage of the throat;
    - narrow operating range, depending on blade geometry;
    - additional shock loss.

Barrios [4] – electrical submersible pump, open type radial impeller

- tests are performed at 600 and 900 rpm;
- at the outlet, bubbles flow back in the channel up to a point where they accumulate and deviate flowing in the peripheral direction up to the pressure side; then they recirculate again to the next channel;
- recirculation vortices are observed close to the PS;
- a gas pocket forms at the inlet; incoming and recirculating bubbles coalesce;
- at higher rotational speed, the recirculating bubbles block the incoming ones.

Ramberg [41] – performance and stability study on a helico-axial pump

- the form and location of the surging line are found to be mainly function of the density ratio and *GVF* and, when surging occurs, *dP/dt* becomes negative and the onset is accompanied by typical heavy discharge pressure pulsations;
- difficulties in flow measurements are experienced, especially during transients;
- the pressure drop under the unstable operating condition is presented; during this process (10-15 s), q_l stops, while q_g is highly reduced. The flow separates inside the channels and gas accumulates at the inlet; the gas flows as a jet, while no energy recovery for the liquid phase

occurs in the diffuser, resulting in liquid build-up until the process recovers. As the inlet flow is increased, the gas is accelerated faster than the liquid;
- the flow behaviour is confirmed by visual observations made at the inlet section: q_g is higher than q_l at the minimum pressure rise. Velocity profiles, phase slip and gas accumulation are qualitatively recorded;
- increasing gas velocity causes mist formation and growing liquid waves, leading again to a two-phase mixture;
- the implementation of the following function to relate the main parameters involved is proposed:

$$\frac{d\alpha}{dt} = f\left(\frac{dQ_l}{dt}, n, P_i\right)$$

Grüner [57] – study of the aerodynamic instabilities in wet gas compression

- a frequency domain analysis of the instability inception is performed, outlining that a delayed onset occurs as the liquid flow rate increases; the test procedure featured constant water flow rate when throttling the discharge valve;
- compared to pure gas operation, a change in stall structure is observed, with in addition an amplification of the low frequencies. The behaviour is highly dependent on the liquid amount; especially at relatively high liquid contents, low frequency pulsations are amplified, this is probably related to the impact of the dynamic liquid film and droplet on the dynamic pressure sensors, making a precise identification of the instability onset more difficult;
- a gradually increasing ring of liquid at the shroud inlet is observed before surge occurs; the ring extended into the inlet pipe while the volume flow was gradually reduced until showing a completely chaotic flow path and finally a flow reversal; this suggests the installation of instrumentation detecting the liquid layer to implement a surge protection system;
- aerodynamic instabilities in compressors are mainly related to boundary layer separation, which is regarded as a stall and surge precursor. This should lead to a worse surge performance in case of liquid presence, while another explanation would give reason to the experimental results: the liquid imparts momentum to the gas flow changing the flow velocity and angle, contributing to a more favorable flow path.

Gamboa and Prado [7, 8] – investigations on electrical submersible pumps

- observed high wellhead and pump intake pressure fluctuations before gas-locking;
- the surging onset is identified with a sudden breakdown on the stage pressure increment and moves towards higher liquid flow rates as the normalized gas flow rate is increased;
- the surging condition is a function of gas fraction, suction pressure, liquid flow rate and pump geometry;
- a minimum in the constant gas flow rate curves appears for the highest gas flow rates before gas locking; the curve presents a sharp decrease before surging and this minimum, then these

curves change again their slopes to negative with less pressure and torque fluctuations compared to those experienced close to surging onset;

- the dependency on inlet pressure and surge evolution through the stages was studied;
- it was observed that, as the stage intake pressure increases along the pump, the maximum of the surging point moves upward and to the left; the lower density ratios and gas fractions make the curves become closer to the pure water case. The same effect is related to an increase in the rotational speed;
- as the gas flow rate increases, the surging condition moves progressively from upstream to downstream stages;
- regarding the pump head curve, different operating conditions and discontinuities are identified;
- a very interesting map, as usually done for the two-phase flow in pipes, plots the boundaries among the different flow-patterns, when q_l and q_g are varied. Four regimes can be identified: mild performance deterioration, performance reverse slope, severe performance deterioration, nil performance.

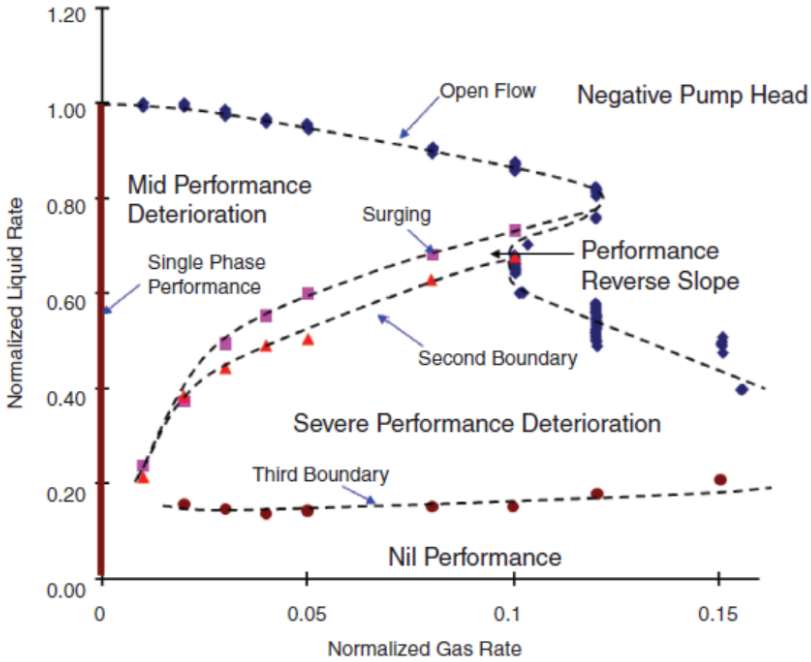

Electrical Submersible Pump operating regimes (taken from [7])

- a new correlation obtained from experimental data allows to predict the surging onset at different operating conditions (intake pressure, phase densities, viscosities, pump speed, normalized flow rates).
  To derive it, the two-phase pump performance is described relating eight dimensionless groups, some of which are not taken into account for their negligible numerical value. The pressure increment depends on gas and liquid flow rates, *Re*, density ratio and the effect of viscosity. Some further simplifications are done: the dimensionless stage pressure increment remains constant at surging initiation; the flow rates are normalized and the surface tension term is omitted; some empirical coefficients eliminate scattering noticed collecting experimental data.
  The normalized gas flow rate is thus related to density ratio, rotational speed, nominal impeller diameter, kinematic viscosity and normalized liquid flow rate according to the following relation:

$$q_{gd} = f\left(\frac{\rho_g}{\rho_l}, \frac{\omega D^2}{\nu}, q_{ld}\right)$$

- the authors concluded that surging occurs at a certain critical pressure increment independent of inlet pressure, indicating the great importance of the force balance around the bubbles for their specific application.

Appendix V – Gantt Chart and project milestones

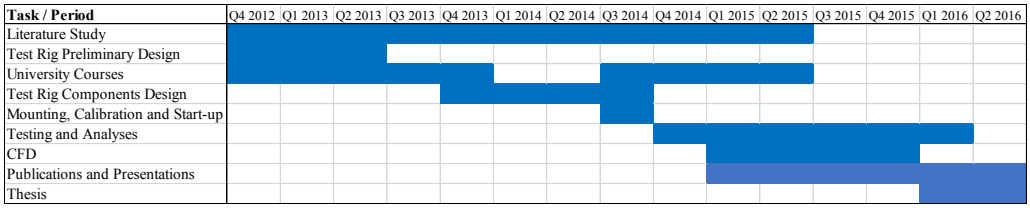

The milestones – comprising the design, commissioning and building - have been:

- 2011 - initial commitment after a discussion between Prof. Lars E. Bakken and Audun Grynning, former Aker Solutions R&D Manager
- September 2012 – PhD student enrollment and start
- Autumn 2012 to Summer 2013 – literature study of flow and machinery fundamentals and similar test facilities, compulsory courses and preliminary design
- October 2013 – start of the definitive test rig design and meetings with PTM Norway
- Autumn 2013 to Winter 2014 – components design
- Spring 2014 – preparation of the laboratory room and infrastructure; final design improvements
- Summer 2014 – first components in place in June, mechanical assembly finalized in August
- October 2014 – data acquisition system connection
- October, 22nd – first test
- December 2014 – tests over the full rotational speed range
- January, 15th – official opening
- January 2015 – high-speed imaging system in place
- January – June 2015 – tests at different tip clearance levels, study of the flow unsteadiness at part-load
- Summer 2015 – first publications and CFD calculations; design improvements of some mechanical components (bearings cooling system, connection of the centrifugal pump)
- Autumn 2015 – study of the flow mechanisms, their relation to the machine performance zones and stability, and CFD capabilities; publications writing
- Winter 2016 – publications finalized; tests at higher suction pressure
- Spring 2016 – presentations and Final Thesis

Appendix VI – Piping and Instrumentation Diagram, based on Standard ANSI/ISA S5.1 and ISO 14617-6

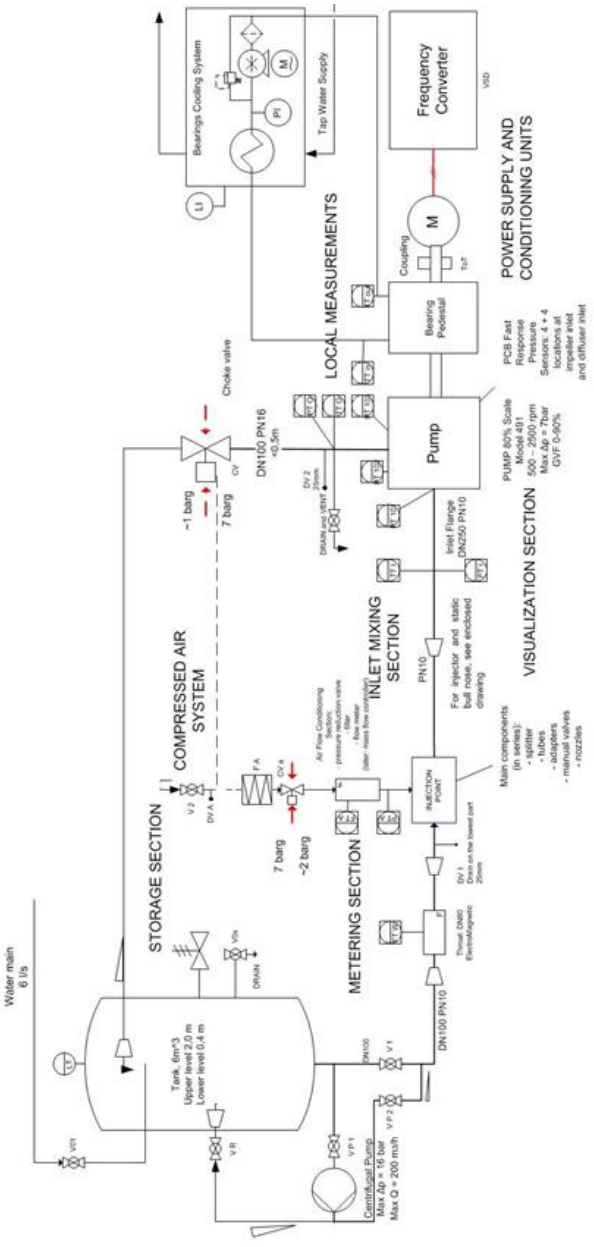

PAPER I

Is not included due to copyright

PAPER II

Is not included due to copyright

PAPER III

Is not included due to copyright

PAPER IV

Is not included due to copyright

PAPER V

Is not included due to copyright